Quantifying Physical Stressors Controlling Mangrove Seedling Dynamics

A combined observational and numerical analysis.

M. Gelderland

July 3, 2020

Cover illustration: Damsea/Shutterstock

University of Twente
Civil Engineering & Management

Master Thesis

Quantifying Physical Stressors Controlling Mangrove Seedling Dynamics

A combined observational and numerical analysis.

Marijn Gelderland
Contact: marijngelderland@gmail.com

Supervisors:
Prof. dr. K.M. Wijnberg
dr. ir. E.M. Horstman
ir. P.W.J.M. Willemsen

July 3, 2020

Preface

In front of you lays the result of 8 months of hard work on my Master Thesis in Civil Engineering, with a major in Water Engineering and a specialisation in River and Coastal Engineering. During my master I was attracted to mangroves for the first time during the Morphology course, after which my interest in modelling, fieldwork and of course mangroves only grew.

First of all, I want to thank the head of the graduation committee, Kathelijne Wijnberg, for her input during my graduation period. Next to that I want to thank both my daily supervisors Erik Horstman and Pim Willemsen. They both really helped me getting used to field work and the modelling part as well. I want to thank them both for giving me the opportunity and trust to conduct my fieldwork in Singapore, which was a life changing experience for me. Also, our meetings were always enjoyable and I especially enjoyed the time we spent together in Singapore.

Next, I want to thank my parents and my brother for supporting me over the years and especially encouraging me to do a Master.

Furthermore, I want to thank Jason Berhane Alemnu for introducing me to the Department of Geography at the National University of Singapore and for his support during my field work. Also, I want to thank the members of the Mangrove Lab by Dan Friess, and especially Jared Moore, for helping me out in the field and giving me a great time during the Friday meetings at Pasir Panjang.

During my time in Singapore I had an amazing place to stay. I want to thank Harald and Audrey for welcoming me in their family, giving me useful tips of places to visit in Singapore and inviting me to celebrate Christmas together.

Also, I want to thank my friends in both Zeeland and Enschede, my family, my roommates and my fellow graduation students for their support and their help during my whole masters.

Last, but not least I want to thank my girlfriend Iris for supporting me during my master and especially during my graduation period.

I wish everyone, who is continuing to read my thesis, much pleasure.

Marijn Gelderland,
Enschede, July 3, 2020

Summary

Mangrove forests are exposed to a wide range of physical conditions and forces, such as waves, currents, sediment supply, bed level changes, etc. These mangroves are an important ecological habitat, provide food and wood, sequester carbon and attenuate waves and surges. Vegetation in mangrove forests has an important role in attenuating hydrodynamic forces and contributes to the reduction of coastal erosion. Yet, a mechanistic understanding of feedbacks between hydro- and morphodynamical stresses and mangrove seedling dynamics is lacking. By combining field work and modelling work these processes can be analysed to understand how these processes affect the long-term development and resilience of mangrove forests and the stability of mangroves.

Firstly, the driving factors of bed level changes are determined. Waves, tides, flow velocities, seedlings and bed level changes itself have been measured in the Sungei Buloh Wetland Reserve mangroves in Singapore. Field observations show that the water depth combined with waves are the main driving factors of the bed level changes. During low waters, waves are the main cause of bed level changes. Additionally, the measured number of seedlings decrease during the whole fieldwork period. At the inland location 10 to 20 less seedlings per plot were found. However, the inland plot shows higher seedlings diameters and heights. Via a multiple linear regression (MLR), the main cause of the decrease in the number of seedlings, are bed level changes. Based on the MLR, an empirical growth formula is composed in order to simulate the growth of the number of seedlings as a function of the bed level changes.

A Delft-FM model is set-up, with a new made vegetation growth module. The model is calibrated based on the observed dynamics. Via the vegetation module, the number of seedlings is modelled for every week, using the found growth formula. Additionally, wave scenarios are set-up to analyse the effect of the increase of wave heights on bed level changes and seedling establishment. The model does represent the observed seedling dynamics, but does not show any differences as a consequences of increased wave heights. The increased waves causes erosion to happen, which is not occurring with a constant wave height of 0.02 m.

This Thesis combines fieldwork and numerical modelling to get a better understanding of seedling establishment and the effect of increased wave heights on seedling establishment. Furthermore, the new model is one of the first of its types for mangrove systems. The model, and field observations, shows that waves cause the most effects on bed level changes, which have the most effect on seedling establishment. Changes in waves cause erosion, but do not affect seedling establishment. This research contributes to modelling of mangrove seedlings using parameterizations based on observed physical processes.

Abbreviations

BMI	Basic Model Interface
DFM	Delft Flexible Mesh
ELCOM	Estuary and Lake Computer Model
FFT	Fast Fourier Transform
FM	Flexible Mesh
LWT	Linear Wave Theory
MFD	Mangrove Fringe Dynamics
MLR	Multiple linear regression
NIOZ	Royal Netherlands Institute for Sea Research
RSET	Rod Surface-elevation table
SBLM	Sungei Buloh Local Model
SBWR	Sungei Buloh Wetland Reserve
SLR	Sea level rise
SRM	Singapore Regional Model
SWAN	Simulation WAves Nearshore
TCM	Tilt Current Meter

Contents

List of Figures

List of Tables

Chapter 1

Introduction

Mangroves can be found all over the world, along (sub-)tropical waters. Mangrove systems are quite complex due to the large variations and variability in vegetation, physical conditions, area, location, etc. Furthermore, mangrove systems are exposed to a wide range of physical conditions and forces such as waves, currents, sediment supply, temperature, etc. Due to their large variations, mangroves all over the world have different properties, but their systems show similarities. Additionally, mangroves are an important ecological habitat, provide food and wood, sequestrate carbon and attenuate waves and surges (Horstman and Willemsen, 2018). Hydro- & morphodynamics of mangrove systems are currently well known. Research has shown that vegetation plays an important role in mangrove systems as they attenuate hydrodynamic forces and contribute to the reduction of coastal erosion. However, there is only a little known about the feedbacks between hydro- & morphodynamical stresses and mangrove seedling dynamics. It is unclear what drives the changes of vegetation due to waves, tides, bed level changes, etc. Knowledge of these feedbacks will help to understand how these processes affect the development and resilience of mangrove forests on the long-term development and stability of mangroves.

The prediction of the evolution of mangrove forests is complicated. Recently, the development of the Delft-FM module made it possible to include vegetation growth in hydro- and morphodynamic models. A vegetation module is in development, which can be coupled with the Delft-FM model. This module, written in Python, describes the growth, mortality and establishment of seedlings by applying growth and decay rules.

1.1 Mangrove dynamics

Mangroves are located between the ocean and the coast, in salt- and brackish environments (Furukawa et al., 1997, Van Santen et al., 2007). Different processes influence the dynamics of mangrove systems. Tides, waves, storms, sea-level rise and river discharges are forces that act on the mangrove systems (Furukawa et al., 1997). The in- and outflow of water due to different forces may cause either sediment to be deposited or eroded and thus influence the growth or disappearance of the mangrove forest. Due to their large vegetation density, mangroves are able to trap and stabilise sediments (Horstman et al., 2015). Hydro-, morpho- and vegetation-dynamics are the main subject of this thesis.

Morphodynamics is the process by which morphology affects and is affected by hydrodynamics (de Swart and Zimmerman, 2009, Friedrichs, 2012, Friedrichs and Perry, 2001,

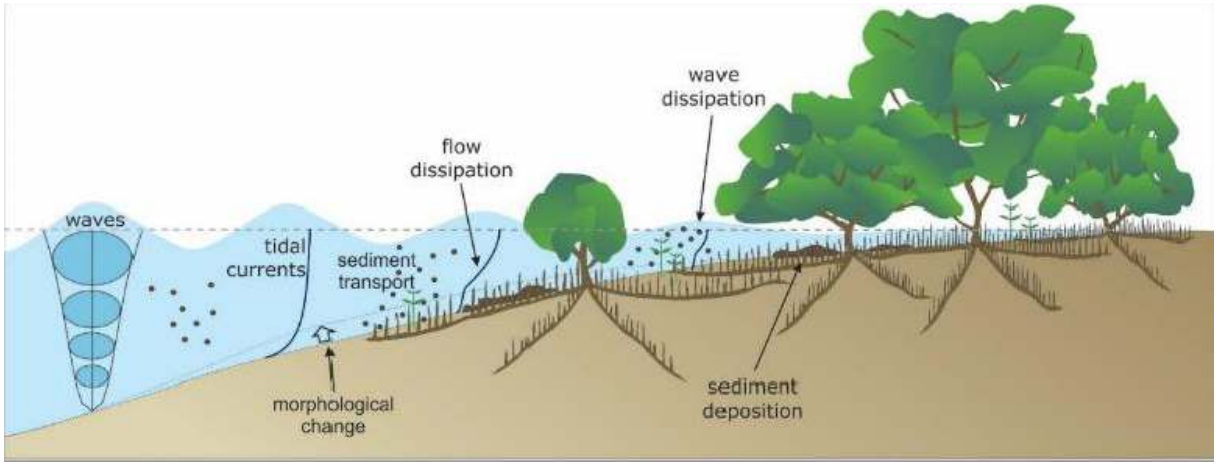

Figure 1.1: Hydro- and morphodynamics in mangrove forests (Horstman, 2019)

Wright, 1995). Morphodynamics can be caused by erosion and/or deposition. Erosion and/or deposition occur due to hydrodynamic processes, which act as a force on particles, and may cause sediment transport. The morphodynamics can be described by the morphodynamic loop (Luijendijk et al., 2017, Ribberink, 2011), which can be seen in Figure 1.2.

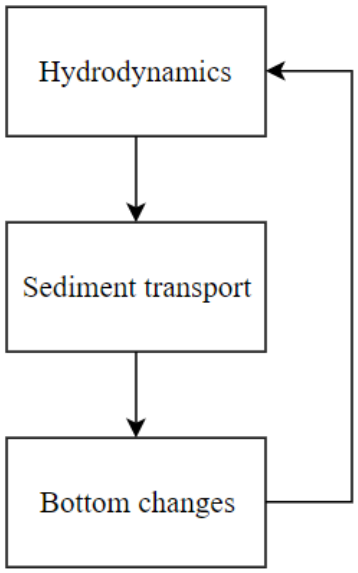

Figure 1.2: Morphodynamic loop (Ribberink, 2011)

1.1.1 Hydrodynamics

Hydrodynamics act on mangroves on different scales: turbulence (small scale), waves (middle scale) and tides (large scale). Turbulence in mangroves is in order of seconds (small), waves from seconds to hours (middle) and tides (large) have a timescale of days till months.

Water flow around vegetation results in drag, altering flow velocities and turbulence (Horstman and Willemsen, 2018). Especially the vegetation diameter, length and spacing are important length scales that affect the flow in mangrove systems. Due to the vegetation, turbulence increases through vortex shedding and wake generation (Mullarney

et al., 2017).

One of the most important conclusions on the impact of mangrove systems on waves is that waves get attenuated (Horstman et al., 2014, Massel et al., 1999, Mazda et al., 1997, Van Santen et al., 2007). Waves at the seaside boundary of mangrove systems have been compared to waves at the land-side boundaries of mangrove systems. Mazda et al. (1997) even found a wave height reduction from 1 meter (seaside) to 0.05 meter (land-side) for the Thuy Hai and Thuy Trong sites in Vietnam. An overview of the wave attenuation at different mangrove forests can be found in Table 1 of Horstman et al. (2014). Due to their wave attenuation, mangroves can even serve as coastal protection (Temmerman et al., 2013).

As mangroves get inundated during flood, the tides have impact on the mangrove systems and especially on the sediment transport within the ecosystem. An important aspect of the hydrodynamics in a mangrove system is the tidal asymmetry. Mazda et al. (1995) researched the tidal asymmetry. In this research it is concluded that the tides show asymmetry in the swamp part of a mangrove forest. The water flow in creeks consists of two components: (1) the tidal water flow without a floodplain and (2) the water flow between the creek and the swamp (Mazda et al., 1995). The velocity of the tidal water flow without floodplain is symmetric, while the water flow between the creek and swamp is asymmetric. In mangrove systems, the water flow is thus asymmetric. This tidal asymmetry is also discovered by Furukawa and Wolanski (1996) for a mangrove site in Australia. Also Mazda et al. (1995) discovered that the velocities in the creek are ebb dominated due to the phase relationship and they showed that water levels and velocities are greatly affected by vegetation. Vegetation causes drag and controls the current velocities in mangroves (Mazda et al., 1995).

On a very large timescale, sea level rise (SLR) comes into play. SLR has some effect on the hydrodynamics, affecting mangroves. First of all, the mean sea level is often the border of the mangrove forest. So, mangroves can be found above the mean sea level (Mcivor et al., 2013). Due to SLR, the mean sea level increases and thus reduces the space on which mangroves can exist. Furthermore, waves can travel further into mangroves, causing re-suspension of sediments and erosion of sediments due to bed shear stresses (Mcivor et al., 2013).

1.1.2 Morphodynamics

Sediment transport in mangroves is caused by forces due to turbulence, waves and/or currents (tides). On a short term, erosion and sedimentation mostly occurs at the forest fringe location. Generally, sediment gets transported into the mangrove due to currents, while waves further transport sediment deeper into the mangroves. On long term, sedimentation and erosion cause bed levels changes within the mangrove system, which cause different hydrodynamic conditions, which in turn impact sediment transport, see Figure 1.2.

Factors influencing surface elevation changes in mangrove can be seen in Figure 1.3 (Mcivor et al., 2013). In their research, surface processes like erosion or accretion are causes for bed level changes. However, also subsurface processes, such as root-growth and

compaction, are causes for the bed level changes. Both surface and subsurface processes also have interactions mutually. Mcivor et al. (2013) researched the mangrove surface elevation change due to sea level rise. They concluded that sea level rise (SLR) influences the hydrodynamics. The water depth increases in the mangroves and waves can travel further into the mangrove. Following the morphodynamic loop, this influences the sedimentation and accretion within mangroves. Accretion then increases the bed level, if the sediment supply is sufficient and if sediment is able to settle down. In addition, sedimentation will also increase the nutrient inflow of the mangroves, which increases plant growth and other organic processes, which then influence the hydrodynamics (Mcivor et al., 2013).

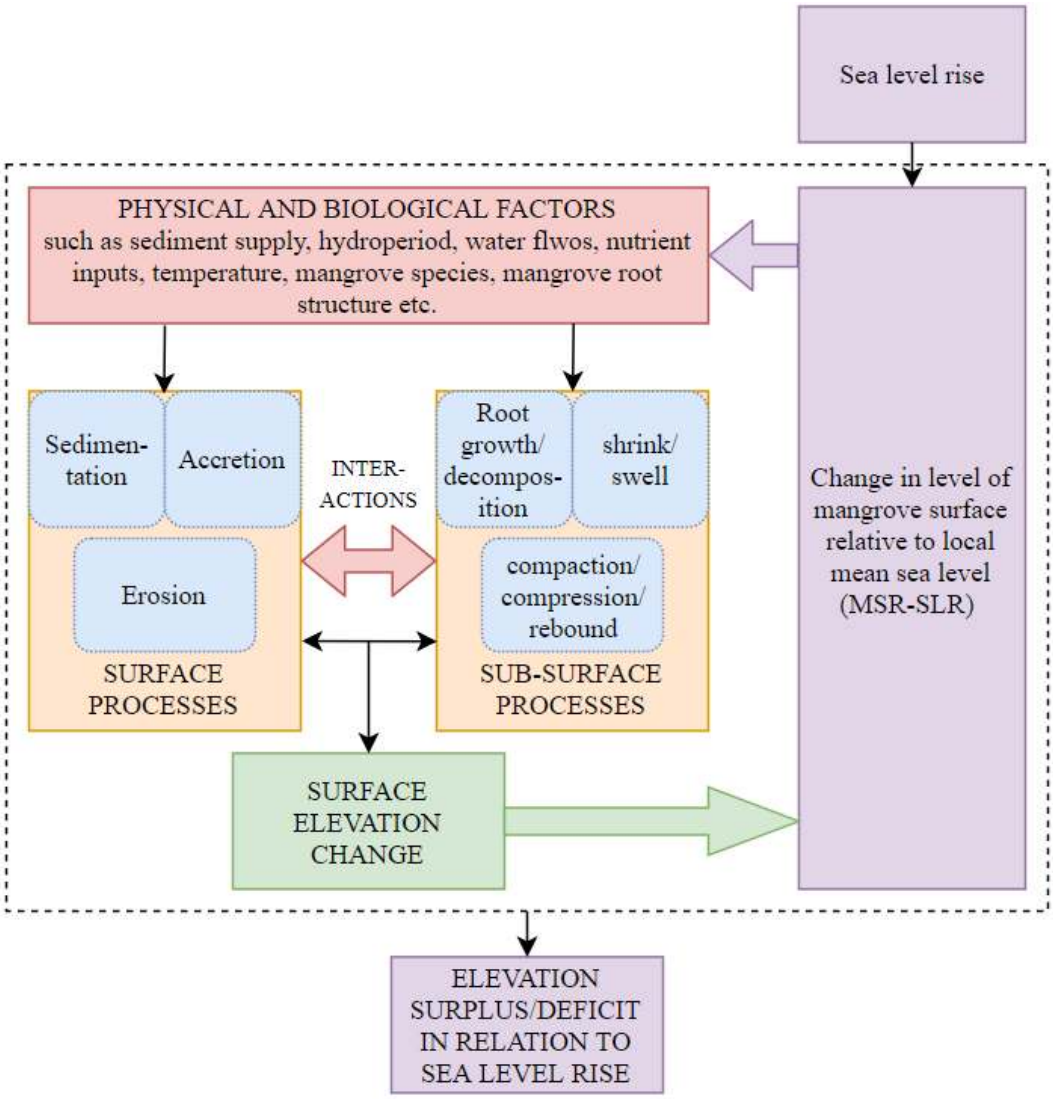

Figure 1.3: Effects of environmental and biological factors on the response of surface elevation in mangroves to sea level rise (Mcivor et al., 2013)

Long term bed level changes in mangroves are mainly measured by Rod Surface Elevation Tables (RSETs) (Ward et al., 2016). These RSETs are mainly used to understand long term bed level changes in relation with sea level rise. Short term bed level changes have been studied by Van Santen et al. (2007), Willemsen et al. (2016). These short term bed level changes do not have a high resolution. For example, the bed level changes within one inundation period for multiple days/weeks is unknown. Additionally, no relation between the short- and long-term bed level changes is known (Horstman et al., 2015).

1.1.3 Vegetation dynamics

As mentioned by Furukawa and Wolanski (1996) mangroves play an important role in trapping sediment. Due to the vegetation density, the turbulence generally reduces near the bed, which allows sediment to settle when the flow velocity reduces and causes accretion. Also, vegetation in mangrove systems can be used to attenuate waves (Horstman et al., 2014, Massel et al., 1999, Mazda et al., 1997, Van Santen et al., 2007). All in all it can be concluded that the ecology of mangrove systems is important for the biophysical interactions and the consequent biomorphological development of the system.

The establishment of propagules of the *Avicennia alba*, which is a typical mangrove colonizer, and their threshold has been researched by Balke et al. (2011). This research describes three thresholds for the establishment of seedlings. Additionally, Friess et al. (2012) studied the thresholds for mangrove growth. They found out that during the early stages of the colonisation of seedlings, drag-forces are the most important, while surface elevation changes, sea level rise and hydrodynamics are more import at later stages (long-term). An important threshold is the inundation period. According to Friess et al. (2012) different researchers came up with certain thresholds for the number of hours an area with for example *S. anglica* species can be submerged with water. However, this is saltmarsh vegetation. van Loon et al. (2007) found the same thresholds for the Can Gio mangroves in Vietnam, with for example: *Avicennia* spp. and *Sonneratia* trees can be found at an elevation of 2.44 till 3.35, with a flooding frequency of 45 - 59 times a month. For mangrove restoration projects it is especially important to plant the right species on the right locations. So, planting *Rhizophora* species at the coastal front of a mangrove, might not be the best solution for a mangrove restoration project (Samson and Rollon, 2008).

1.2 Problem definition

The hydrodynamics of mangrove systems are well known. Knowledge about morphodynamics is not complete, especially the period between short- (seconds to weeks) and longterm (years) morphodynamics is unknown. Recently, the Windows of Opportunity, which describe the physical conditions allowing for seedling establishment, have been researched (Balke et al., 2011). This research has been done for seedlings from the period of 0 to 13 days. However, it is unknown what will happen with those seedlings after that period. van Maanen et al. (2015) used the Estuary and Lake Computer Model (ELCOM) to simulate long-term morphological evolution of tidal embayments coupled to a mangrove population model. Their model only used the *A. marina* mangroves as vegetation. However, their model is schematic and can therefore not be compared to a real life study site. So, it is still unknown how physical stresses affect the growth and development of mangrove seedlings for existing mangroves. Currently, it is unclear what the thresholds for seedlings establishment are for a part of the mangrove or a whole mangrove itself (Friess et al., 2012).

Currently the link between vegetation and the long (decades)- and short (days/weeks) -term morphodynamics is missing. Long-term morphodynamics can be obtained using Rod Surface Elevation Tables (RSETs). Short-term morphodynamics however are known, but not at a high resolution (Van Santen et al., 2007, Willemsen et al., 2016). The windows of opportunity only describe restrictions and thresholds for a short time period

(Balke et al., 2011, 2013). The impacts of waves and tidal currents, including seasonal fluctuations, on bed level changes is know (Horstman et al., 2014, Van Santen et al., 2007). However, their combined effect on vegetation dynamics, is only known on a small scale (Balke et al., 2011, 2013). Especially the effects of variations within this period, as for example seasonal variations and extreme events. Studying short- and long-term bed level changes helps to understand the total morphodynamic processes and the differences between both types of processes. These processes, accretion, erosion and total surface dynamics, allow to evaluate the total morphodynamic processes in mangroves. Combining this with vegetation establishment and development will give information that can be used to develop more accurate models to predict long-term developments of mangrove systems.

The Delft3D-model can be used for hydro- and morphodynamic simulations. However, vegetation dynamics are not standard included in the model. Vegetation dynamics can be coupled to Delft3D, via an offline coupling. Currently a Delft3D Flexible Mesh (FM)-model is in development. This model can be coupled to a Python module which then can have rules about the vegetation dynamics. The Delft3D-FM model has an online coupling with the vegetation dynamics model in Python. This means that the dynamics are computed simultaneously, which strongly reduces the computation time. Nevertheless, the Delft3D-FM-model is currently in development. The Windows of Opportunity concept is modelled in Python and can be coupled to the FM-model. Parameterizations of the coupling between hydro- & morphodynamics and vegetation dynamics are still unknown for mangrove vegetation. Currently, there are mainly generalised models however, a complete biogeomorphological model for mangroves, that also simulates vegetation dynamics, has never been made, validated and calibrated. The Mandai model of Willemsen et al. (2016) is a model that is more advanced and simulates the hydro- and morphodynamic processes for the Mandai mangroves in Singapore. Only vegetation dynamics, as modelling seedling establishment, are missing in this model. A complete biogeomorphological model, that simulates vegetation dynamics, is already made for saltmarsh vegetation (Odink, 2019, Van den Broek, 2020). A biogeomorphological model, validated on field observations, with vegetation establishment, described by hydro- or morphological processes, is not yet made for mangroves.

1.3 Study area

The study area for this research is the Sungei Buloh Wetland Reserve mangroves in Singapore. An overview of the whole reserve can be seen in Figure 2.1. This patch of mangroves is the biggest on the mainland of Singapore. The reserve has an area of 202 hectares and is the first ASEAN Heritage Park of Singapore. The mangroves are already used for research purposes. For example RSETs are installed within the mangroves to see long term elevation changes. In the last few years the mangrove has expanded by the addition of the Krani Nature trail, which connects the visitor centre to the wetland centre. The park is managed by National Parks (NParks). The part at the wetland centre is the 'old' part of the mangroves. As mentioned, the Kranji Nature trail is relatively new. NParks focuses on retaining the mangroves. Recently, poles were added in front of some parts of the mangroves to protect the area due to wave action and current flows. Additionally, to stimulate vegetation growth in the new part of the mangroves, seedlings are planted. Every growth season some part of the mangroves will be used to plant new seedlings to stimulate the growth of new trees. Mainly *Avicennia* seedlings are planted.

As NParks is trying to stimulate vegetation growth, they are interested in the results of research in seedling establishment. This allows us to use our equipment in the mangroves to see the effect of hydro- and morphodynamics on mangrove seedlings. Further details of the area can be found in Chapter 2.

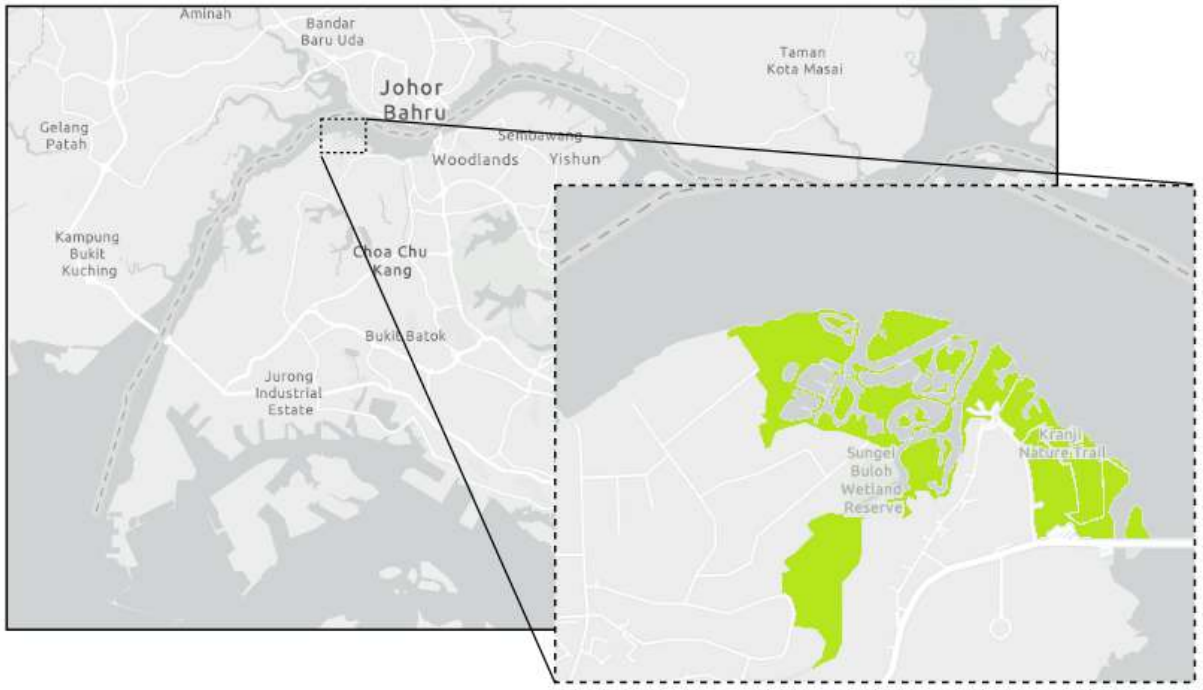

Figure 1.4: Location of the Sungei Buloh Wetland Reserve

1.4 Research objectives & Questions

This research aims to establish a mechanistic understanding of the feedbacks between hydro- and morphodynamic stresses and mangrove seedling establishment, at a short- (days) to mid- (months) term timescale, and to analyse the effect of increased wave heights on bed level changes and seedling establishment.

The first objective is to describe what the system's (study area) properties are with respect to hydrodynamics, morphodynamics and vegetation dynamics. A description of wave characteristics, inundation periods, water depths, bed level changes and seedling properties will be compiled.

The second objective is to find a relation between the hydro- and morphodynamic stresses and mangrove seedling establishment in the pioneer zone on a short- to mid-term timescale, see Figure 1.5.

Lastly, the third objective is to use the found relation between hydro- and morphodynamic stresses and mangrove seedling establishment in a model to simulate seedling establishment and to understand what the effects of an increase of wave heights are on bed level changes and vegetation establishment.

These objectives result in the following main research question:

What is the impacts of waves, over a period of months, on the bed level changes and their combined impact on seedling establishment in the mangrove forest fringe of the Sungei Buloh Wetland Reserve in Singapore?

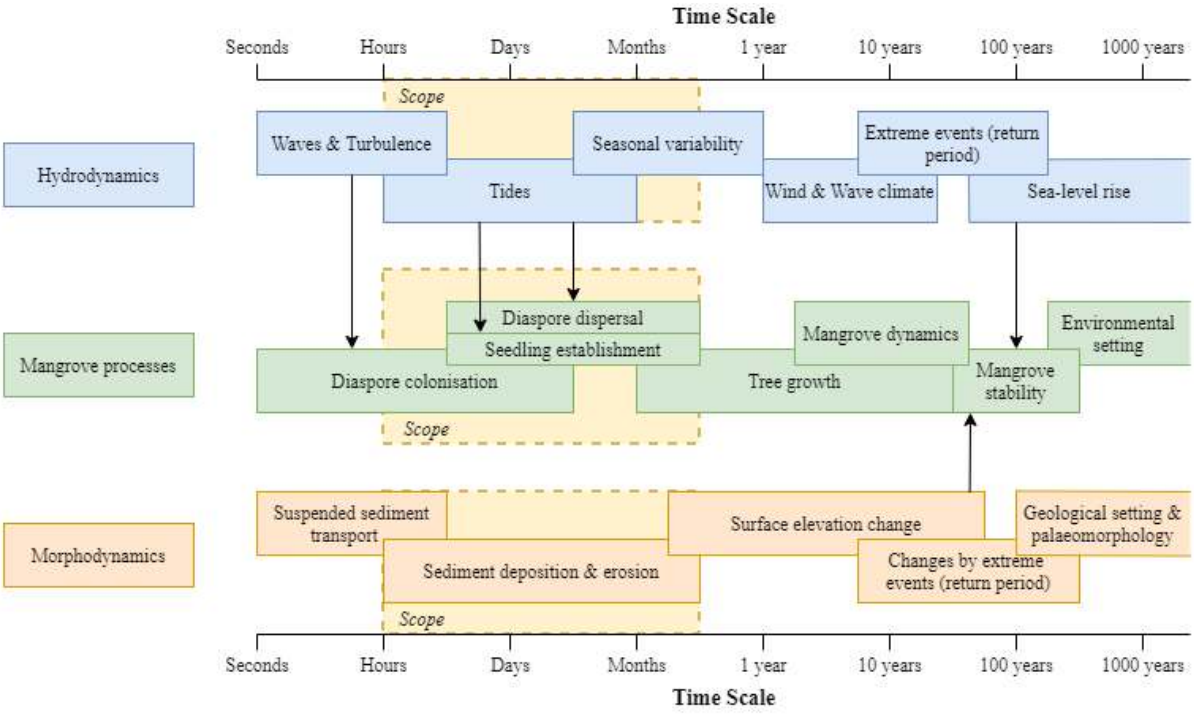

Figure 1.5: Temporal scales of mangrove and saltmarsh ecosystem processes (Friess et al., 2012)

Field research is executed in the Sungei Buloh Wetland Reserve mangroves and a Delft-FM model with a new set-up, based on the SBWR mangroves, is made in order to answer the main research question. The measurements are usefull to understand the biophysical interactions. Further methods are explained in Chapter 2 and Chapter 4.

1.4.1 Research questions

To answer the main research question, research questions have been compiled. In total four research questions are formulated. Each research question is again divided into more sub-questions (a, b, c, d).

1. What are the driving factors of the observed bed level changes in the Sungei Buloh Wetland Reserve mangroves from the 5'th of December 2019 till the 27th of February 2020?

   (a) What are the ranges and properties of the waves, tides, water-depths and bed level changes?

   (b) What is the relation between the observed tidal currents and waves and the observed bed level changes?

   (c) What are the spatial variations in the pioneer and mangrove zones regarding the observed tidal currents, waves and bed level changes?

2. What is the relation between spatial variation regarding the observed tidal currents, waves and bed level changes and seedling establishment?

   (a) What are the seedling properties at the inland and forest fringe location and how do these change during the whole fieldwork period?

   (b) What are the driving factors of seedling establishment in terms of waves, currents and bed level changes?

3. How can the relation between waves, tides and bed level changes and seedling establishment be translated to model parameterizations and be integrated with the Delft3D Flexible Mesh model?

   (a) What is the effect of the waves, tides and bed level changes on seedling establishment?

   (b) How can seedling growth and establishment be parameterized for the timescales of seconds to months?

   (c) How well does the new developed model represent the observations?

4. What are the effects on bed level changes and seedling establishment in the Sungei Buloh Wetland Reserve (SBWR) as a consequence of an increase and variable wave heights?

1.5 Thesis outline

Chapter 2 describes the methodology for the fieldwork part of this research project. It describes the methodology used to execute fieldwork and describes the use of all used instruments and how data is processed. In Chapter 3 the field observation results are shown. This chapter also contains the correlation between the observed hydro- and morphodynamics and vegetation growth. Chapter 4 describes the use of the Delft-FM model and how the model is used to simulate vegetation growth. It also includes a general description of the model. In Chapter 5 the results of the Delft-FM model are shown. This also includes the calibration and validation of the model and the effect of simulating different wave scenarios. Chapter 6 discusses the executed research. Chapter 7 shows the conclusion of this research and the answers to each research question. Recommendations for further research can be found in Chapter 8.

Chapter 2

Field data methodology

This methodology gives an overview of the location of the measurements, how and what type of measurement devices were used and how gathered data was processed.

2.1 Sungei Buloh Wetland Reserve

The Sungei Buloh Wetland Reserve (SBWR) is located in the north-west part of Singapore. Figure 2.1 shows, on the left side, the location of the SBWR in Singapore. The nature reserve has an area of 202 ha and is the first ASEAN Heritage Park of Singapore. The wetland reserve consists of mangroves, mudflats, ponds and forests. The patch of mangroves in the SBWR is the largest in Singapore.

Figure 2.1: Location of the Sungei Buloh Wetland Reserve

The SBWR mangroves were mainly used for fish ponds and agriculture. In the 1980's the SBWR was mainly used for prawn ponds. The area is an ideal place for migratory birds. Later, the ponds were abandoned and the area became a nature reserve. Paths were added to the park for tourist purposes. Mainly *Avicennia alba* trees can be found

in the mangroves. Additionally, *A. officinalis*, *A. rumphiana*, *Bruguiera cylindrica*, *B. gymnorhiza*, *Rhizophora apiculate*, *R. mucronata* and *Sonneratia alba* trees can also be found in the mangroves (Tan et al., 1997). Tides within the mangroves range between 1.5 and 2.5 m (Kurniawan et al., 2014). Waves height are small due to relative short fetch length ($<$ 1000 m) (Willemsen et al., 2016).

Within the mangrove, along three transects fieldwork has been executed; A, B and C. The transects can be seen in Figure 2.2. Transect A is a small transect, located at the Kranji Nature Trail. The transect is approximately 25 m long and consist of relatively young mangrove vegetation. Quite a lot of seedlings were found at this location $O(10^1)$ - $O(10^2)$. Additionally, a mix of tall and small trees were found. This is why the area has been chosen as field research area. Close to transect A is transect B, which has a similar length to transect A. Transect B is located approximately 20 m to the south-east parallel to transect A. Transect B is a replicate of transect A. At transect C some measurements were executed, which were outside of the scope of this thesis. Furthermore, transect A, the main field observation transect, had a row of poles at the front of the mangrove forest. So, the mudflat and the mangrove forest were somewhat separated from each other. The row of poles limits the hydrodynamic forces and somewhat traps the sediment in the mangroves itself. At the back of the mangrove forest a stop-bank is located. This stop-bank has the purpose of stopping water from flowing into the backside of mangrove and it is an elevated walkway, which is its major purpose. This part of the mangrove forest is connected to the channel, located close to Wetland Centre. The stop-bank is also used as a path. This path connects the Wetland Centre with the Visitor Centre. A close up of all transects, including frame and vegetation plot locations can be seen in Figure 2.3. An overview of some areal images can be seen in Figure 2.4.

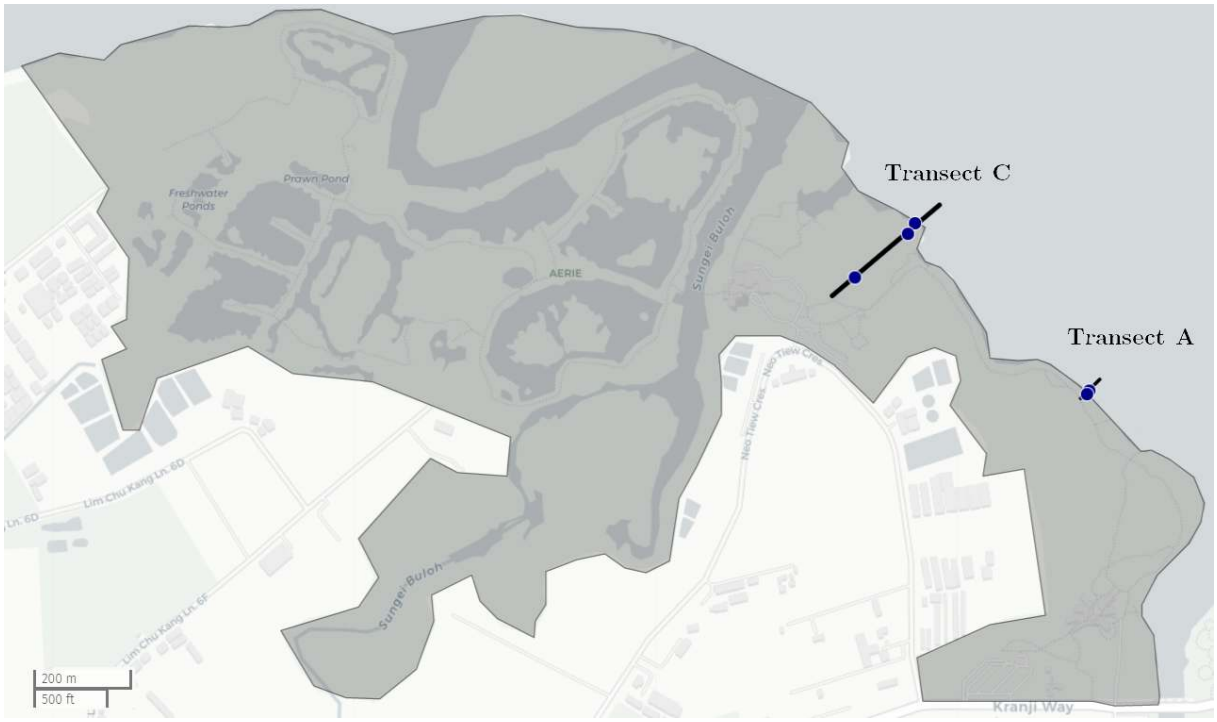

Figure 2.2: Sungei Buloh Wetland Reserve mangroves map with transect locations; the blue dots mark the monitoring stations along the transects.

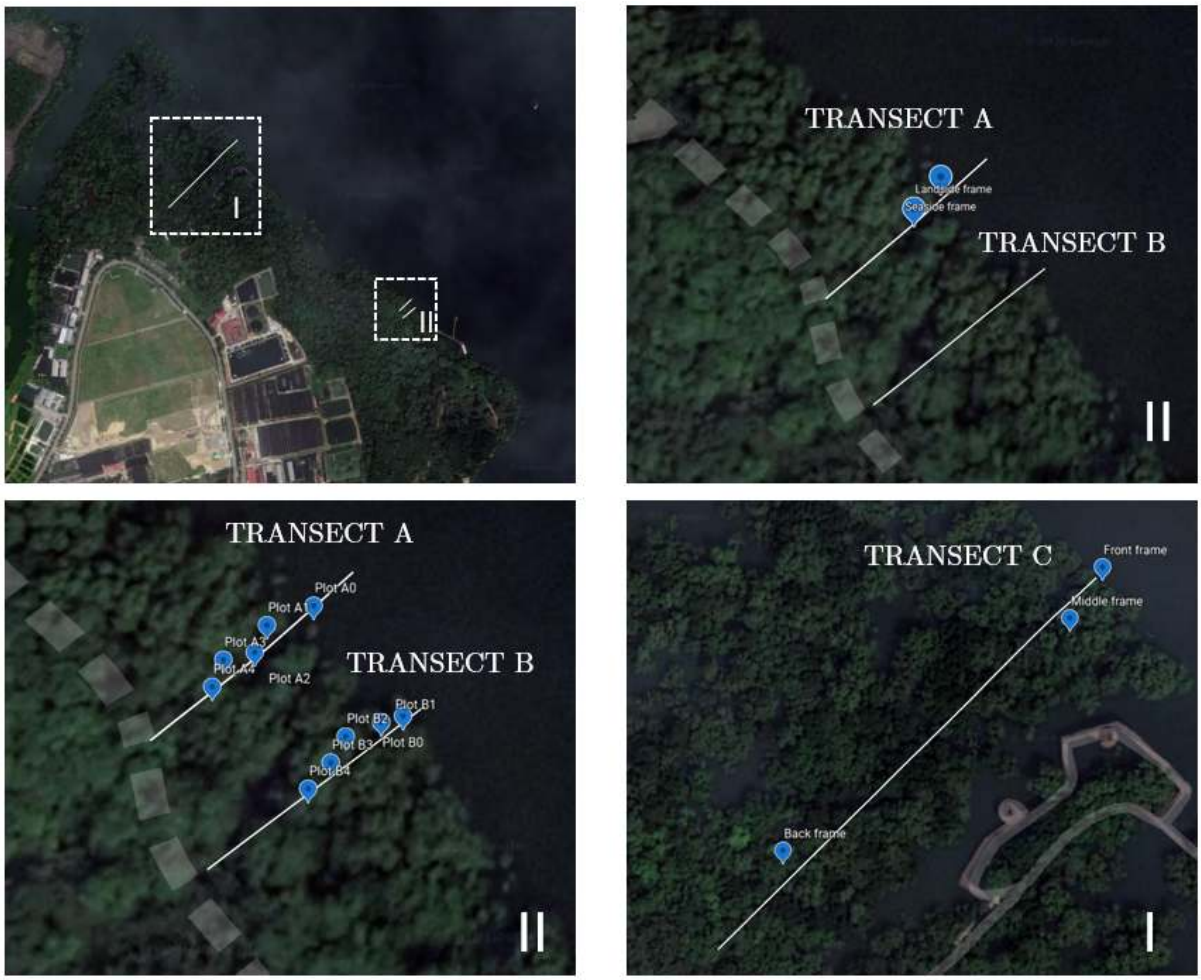

Figure 2.3: SBWR mangrove transects, monitoring stations and vegetation plots. Top left: Transect locations overview. Top right: Transect A and B close-up, with monitoring stations. Bottom left: Transect A and B close-up, with vegetation plots. Bottom right: Transect C close-up, with monitoring stations.

2.2 Measurement Method

Field measurements are used to derive the physical properties of the mangrove system in the Sungei Buloh Wetland Reserve mangroves. These measurements are useful to understand the biophysical interactions between waves and bed level changes, waves and vegetation establishment and bed level changes and vegetation establishment. Additionally, field measurements are also used to update, calibrate and validate the Delft Flexible Mesh (DFM) model.

Different measurement devices were used to collect data. Echologgers, pressure gauges, tilt current meters and a barologger are used to capture short term bed level changes, water pressure, flow velocities and air pressures respectively. Each instrument uses a different set-up and has to be set-up individually. The use and setup of those instruments will be explained in the next sections.

(a) Areal picture of transect A, with row of poles in front of transect.

(b) Picture of of area with pneumatophores and stop bank on the back.

(c) Close-up shot of new established seedling and pneumatophores.

(d) Picture of the more developed mangrove area behind the the stop-bank.

Figure 2.4: Sungei Buloh Wetland Reserve mangrove area pictures. Pictures by Hunter Calder and Erik Horstman

2.2.1 Tilt current meter

Tilt current meters are deployed in the mangroves in order to measure flow velocities in x and y-direction. Two current meters are deployed at transect A from the 30th of January till the 27th of February, see Figure 2.2. The meters are deployed next to the monitoring stations that are used for the pressure gauges and Echologgers. We positioned them close to the stations that the velocities should be similar to those at the Echologgers/pressure gauges. These meters are attached to a aluminium pipe which has been put into the soil. The meters are buoyant and tilt in the direction of the flow, when submerged. The instruments register the tilt and the bearing due to the flow, which then can be used to extract flow velocities in all directions. In Figure 2.5 the TCM-4 Tilt Current Meter, placed in the Sungei Buloh mangroves, can be seen. A schematic principle of the instrument is found in Figure 2.6. Furthermore, the instrument registers flow velocities all the time. It has no 'detect' function when submerged. Due to this, high 'flow' velocities will be detected when it is not submerged. As the instruments are not submerged, they are flat with the ground. The TCMs measure flow velocities at the bottom 25 cm of the water column. The bottom part of the water column is interesting as the height of the seedlings is similar.

Figure 2.5: Lowell TCM-4 Tilt current meter. Photographed by Erik Horstman.

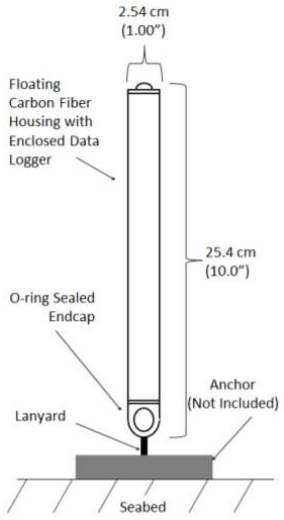

Figure 2.6: Schematic principle of Lowell TCM-4 Tilt current meter

2.2.2 Echologgers

In total three Echologgers were used to measure short-term bed level changes. The Echologgers send out acoustic signals in bursts. The signal travels through water, gets reflected by the bed, and is then received back by the transceivers of the Echologger. The Echologger measures the time it takes for the signal to travel back and forth to the device. Then, with the speed of sound in water, the distance between the sensor of the Echologger and the bed can be measured.

Two of the Echologgers were deployed at the start of the fieldwork campaign at the 5th of December 2019 at transect A, close the Kranji Nature trail, see Figure 2.2. The Echologgers are attached to frames. The loggers are placed approximately 25 cm above the bed, pointing downwards, which is based on previous field work experiences. Every 5 minutes, a signal of 10 pings is send out. This means that every 5 minutes, 10 measurements are executed. Furthermore, the Echologgers were retrieved approximately every 2 to 3 weeks in order retrieve their data. The settings for the Echologger can be found in Table 2.1. One of the two Echologgers that has been placed in the Sungei Buloh mangroves can be seen in Figure 2.7. A schematic principle of the mechanism of the Echologger can be seen in Figure 2.8. Before and after each Echologger was taken out of the frame, its height above the bed is measured. This allows to place them back at approximately the same height and to check if the produced data is correct.
The Echologgers are only able to measure when inundated. When in air, the signal can not be used to calculate the distance to the bed, so this is referred as noise. With the speed of sound in water, the measured time is used to calculate the distance. This distance then needs to be divided by two, as it travels to the bed and back to the device. The Echologger device itself calculates this distance, based on a threshold value. This distance is based on the first time the threshold, the minimum strength of the reflected signal, is exceeded, neglecting peaks before approximately 10 cm; the deadzone. The deadzone is the distance in which no signals can be measured. Furthermore, the devices send out signals every 5 minutes. This means that short term bed level changes can be detected.

Figure 2.7: Echologger EA400 placed in frame. Photographed by Erik Horstman.

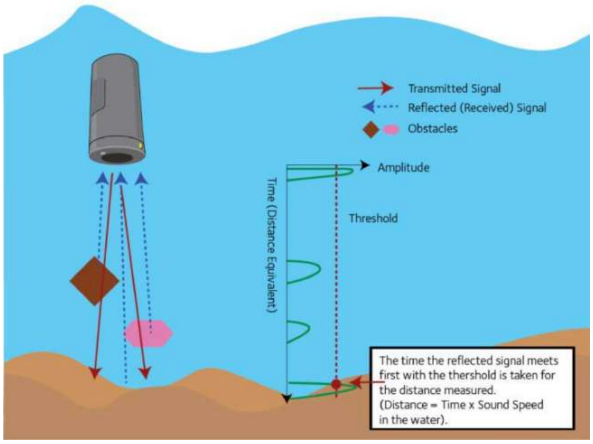

Figure 2.8: Schematic principle of EA400 Echologger.

Table 2.1: Echologger settings

Setting	Input value	Unit
Range	1	m
Tx Length	15	μsec
Period	0.1	sec
Number of pings	10	#
Interval	900	sec
Threshold	10	%
Deadzone	0.10	m
Gain	-6	db
TVG Slope	540	db/km
Sound soeed	1500	m/s
Filesize limit	4000	MB
Bluetooth module	off	-

2.2.3 Pressure gauges

Two pressure gauges were used to measure the water pressure. The pressure gauges measure water pressure at a set rate. The gauges can be used to derive water depths and waves. In order to derive waves, the measuring rate can not be too big as waves with a small period need to be detected. The gauges have a internal digital storage, which allows for autonomous measures. Two pressure gauges are deployed at the Kranji Nature Trail, transect A, at the 5th of December 2019.

At the Kranji Nature trail location, 2 RBR-Virtuoso gauges were installed for the first three field work periods. The gauges are put in a wave mode, to measure at an interval of 10 minutes. Per burst it measures at a speed of 8 Hz for a period of 256 seconds, which results in 2048 samples per 10 minutes. During the last two fieldwork periods RBR-Solos were used. These are similar to the RBR-Virtuoso, but do not output processed wave data. These devices can not be put in wave mode, but have to be put in Continuous mode. The Continuous mode measures with a sampling speed of 2 Hz. This is the maximum sampling speed of the instrument. This is sufficient to measure waves, but requires some post-processing to retrieve wave data. This will be explained in Section 2.3. The RBR-Virtuoso bursts intermittently to measure waves. Furthermore, the wave analysis is

executed by the Ruskin software itself and provides basic information about wave characteristics, as wave periods, wave heights and wave energy. In Table 2.2 an overview of the used settings for the pressure gauges can be seen.

Table 2.2: Pressure gauges settings

Setting	RBRsolo	RBRvirtuoso	Unit
Mode	Continuous	Wave	-
Speed	2	8	Hz
Duration	-	2048	Samples
Interval	-	10	min
Instrument altitude	-	0.07	m
Mean depth water	-	0.5	m
Gate	none	none	-

2.2.4 Vegetation

Trees and seedlings have been measured manually with a ruler, caliper and measuring tape. In order to model vegetation establishment and growth, the number of seedlings, heights, diameters and their number of leaves are measured multiple times. Also, the existing larger trees and pneumatophores are measured as well.

For the seedlings measurements, two transects (A and B) have been made at which plots of 1 by 1 meter have been marked out. In total 5 plots per transect were used to measure the seedlings. The plots were spread out on the transect to get a spatial representation of the seedlings. Transect A was also used for the deployment of the instruments. Transect B was very close to transect A and is replicate of transect A. In every plot the number of seedlings, their stem diameter at 1/3 of the seedling height, height and the number of leaves are measured. If the number of seedlings in a plot exceeded 20, only the average 20 seedlings are measured, but still the number of seedlings is taken into account. Per corner 5 representative seedlings for the plot were used as average. Furthermore, the seedlings are measured approximately every two weeks in order to observe their growth and the establishment of new seedlings. The seedling height is measured with a ruler, with an accuracy of 1 cm and the diameter is measured with a caliper with a 1 mm accuracy.

Established trees have been measured at the the transects. Especially *Avicennia* and *Sonneratia* were predominant. The approach of measuring these trees is similar to what Horstman did (Horstman et al., 2014). At transect A and B, the trees were measured once for the whole transect, which is approximately 25 m long and 10 m wide. The stem diameter is measured at breast height, so approximately 1.50 m, or, if too small, at a third of the height of the sapling. Next, the diameters were categorised into six groups: $0-10$ mm, $10-25$ mm, $25-100$ mm, $100-200$ mm, $200-300$ mm and >300 mm. Per category a representative tree has been selected. The diameter of this representative tree is then measured at 0.1 m, 0.5 m, 1.0 m, 1.5 m and 2.0 m height.

The pneumatophores are also measured. At transect A, where the instruments are deployed, measurements have been taken. In the previously used plots of 1 by 1 meter, the number of pneumatophores is counted. So in total five plots are used to measure the pneumatophores. This allows for spatial variability as difference in sparse or dense areas

of pneumatophores can be observed. In order to model representative pneumatophores, the height and diameter of 20 representative samples is measured as well. Again, at each corner 5 representative pneumatophores for the plot were used as an average.

2.2.5 Measuring overview

In Table 2.3 an overview of the measuring variables, devices, frequencies, etc. can be seen.

Table 2.3: Field measurements summary

Variable	Device	Frequency	Period	Location
Flow velocities	Tilt Current Meter	5 min	30-01-2020 - 27-02-2020	F.f. and inland
Water pressure	RBR Solo RBR Virtuoso	10 min	05-12-2019 - 27-02-2020	F.f. and inland
Air pressure	Solinst Levelogger	1 min	21-12-2019 - 27-02-2020	Inland
Bed level changes	Echologger	5 min	05-12-2019 - 27-02-2020	F.f. and inland
Vegetation characteristics	Hand tools	5 times	05-12-2019, 21-12-2019, 11-01-2020, 30-01-2020, 27-02-2020	Five plots at transect A and transect B

F.f. = Forest fringe

2.3 Data processing

The data, retrieved from the instruments, needs to processed before any analysis can be performed. Data from the devices will be processed in Matlab and Python to actually see what processes are happening.

2.3.1 Tilt current meters

The TCMs output flow velocity speed and direction. Flow velocities will be used to calibrate the Delft-FM model. Additionally, the pitch and roll, the rotation of the device in x- and y-direction is an output as well. This can be used to define the rotation of the instrument due to the flow, which means the direction of the flow can be determined. Also, the yaw is an output. This is the rotation of the device in z-direction. This can be used to determine if the instrument is either submerged or not. However, the TCMs still calculate the current velocities when not submerged. This is data that needs to be filtered out.

The TCM data has been filtered based on the inundation period. Via the pressure gauges the inundation period is calculated. The inundation period is then used to filter out the data when the TCM is not submerged. Then a moving mean is used to retrieve the correct current speeds. Extreme current speeds, which occurred at the start and end of each inundation period are via this way also filtered out. A moving mean window of 125 minutes has been used to get the averaged flow velocities. The moving window size is based on trial and error.

2.3.2 Echologger

The Echologgers produce a burst of data for every 5 minutes. This allows for high frequency data. In Section 2.2.2 the method of getting the data has already been explained. The measured raw signals are used to calculate the distance from the device to the bed. Firstly, the signals are burst averaged. Each burst sends out 10 signals. So, an average of 10 signals is made. Secondly, a 'window' has been created. The peak of the averaged signal should be within this window. This window represent a depth for which the signal should lay in between. So, if a manual measurement shows that the distance from the device to the bed is 25 cm, the window should be based on this value, so would approximately start at 15 cm till 45 cm. In this way, only the 'real' peak is taken into account and the 'noise' peak is neglected. Next, the derivative of the signal between the minimum value of the window and the maximum value of the window is calculated. The maximum value of this derivative is determined and gives us the point where the intensity of the reflected signal is the largest. This is the point with the highest derivative of the 'original' signal. This point is used as the representative point to calculate the distance to the bed level. The time from the start of the search window till the representative point is then calculated. Adding the time from t = 0 till the start of the search window with the previous found time gets the total time till the representative point. The time it takes for the signal to this representative point is then multiplied with the speed of sound in water, which results in a distance. This is the distance between the instrument and the bed level (height above the bed). Figure 2.9 shows the process of retrieving the representative values for each signal with time on the x-axis and the intensity of the reflected signal on the y-axis at the top plot, and the time derivative of the signal on the y-axis and time on the x-axis on the bottom plot.

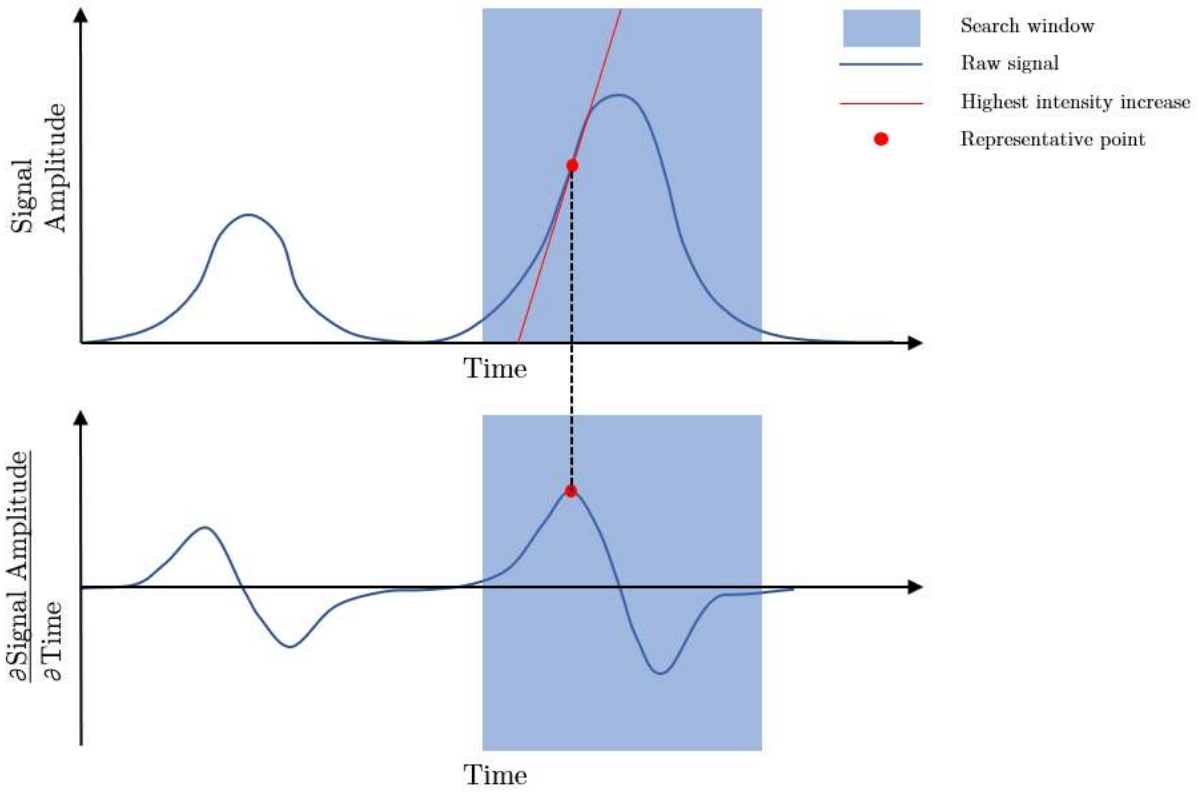

Figure 2.9: Echologger signal processing principle

2.3.3 Pressure gauges

General
As mentioned previously, two different types of RBR instruments are used; RBR-Solos and RBR-Virtuosos.

Pressure correction
The devices measure the total pressure. This means the air pressure and, if the devices are submerged, the water pressure. The devices use a single pre-defined value for the air pressure. However, the air pressure varies over time. With a Solinst levelogger the air pressure was measured. Then the water pressure can be calculated by extracting the measured air pressure from the total pressure, measured by the RBR-devices. Next, with a conversion: 1 meter water column equals 0.1 dbar, the water depth above the instrument can be derived.

Additionally, the water depth above the bed, retrieved from the devices, needs to be corrected. The top of the devices, which is where the pressure sensor is located, is not flat with the ground. The device is elevated above the bed by a few centimetres. This elevation needs to be added to the depth data. Then the water depth above the bottom level is known.

Inundation periods
The water depth gives also information about the inundation period. To actually calculate the inundation period, the under-water periods were identified. As water depths are calculated every 5 minutes, there can be some inaccuracies calculating the exact inundation period. The measurement accuracy is thus 10 minutes.

Waves
Due the fact that the RBR-Solos only output water depths, pressure and temperature, another method to derive wave heights has to be used. This was done by conducting a spectral analysis. The spectral analysis is executed via a Python script, created by Rik Gijsman. The spectral analysis is executed according to Hegge and Masselink (1996), Horstman et al. (2014) This requires a Fourier analysis. In Appendix G the spectral analysis is explained. Wave properties have been derived from this analysis.

Wave attenuating Wave attenuation is calculated per tide. The maximum significant wave height per tide and average significant wave height per tide are used to calculate wave attenuation. The attenuation is calculated as:

$$H_{att} = \frac{H_1 - H_0}{H_1} \cdot 100 \tag{2.1}$$

with H_{att} as the wave attenuation in %, H_1 the average or maximum significant wave height per tide at the inland location (m) and H_0 the average or maximum significant wave height per tide at the forest fringe location (m).

2.3.4 Vegetation

Per vegetation plot, the height, diameter and the number of leaves of 20 seedling has been averaged. This allows to see the development of the height, diameter, the number of

leaves per seedling and the number of seedlings itself. The average 20 seedlings were not the same for every measurement moment. At each corner of the 1 m^2 square, 5 seedlings, that were average for the whole plot, were measured.

To compare the vegetation data with the measured hydro- and morphodynamics, the data has to be averaged. The data has to be averaged, as the measuring frequency is not the same. For vegetation the frequency is 2 to 3 weeks, while the water levels for example have a measuring frequency of 10 minutes. The front two seedling plots of both the A and B transect have been merged together as they are replicates. This allows to account for the spatial variability. The same has been done for the other three plots on both transects. This has been done based on the position of the plots. The front 2 plots for each transect, so A0 and A1 for the A-transect, are the closest to the forest fringe measuring devices. The back three plots are closer to the inland measuring devices. Finally, the growth-rate of the number of seedling per week is determined for each set of plots. However, the change in the number of seedlings is not the same for every period as the periods do not have a similar length of days. To be able to use the seedling data in the Delft-FM model, the change in the number of seedlings has been recalculated to a growth factor.

$$G_N = \left(\frac{N_x}{N_{x-1}} \right)^{7/(T_x - (T_{x-1}))} \tag{2.2}$$

In Equation 2.2 G_N is the growth factor of the number of seedlings per m^2 per week, N_x the number of seedlings at x, where x is the date of the measurement, so $x - 1$ is date of the previous measurement.

Chapter 3

Field data results

This chapter presents the observed dynamics of the Sungei Buloh Wetland Reserve mangroves at transect A and B. Distinction has been made between observed bed level changes, water depths, waves, seedlings and established trees and pneumatophores. Furthermore, an analysis of important parameters affecting seedling growth and establishment has been executed.

3.1 Hydrodynamics

This section presents the hydrodynamics with respect to waves, tides, water depths and current velocities, measured at transect A. The water levels give us information on the inundation period, which is a key parameter to link vegetation growth and mortality, (Balke et al., 2011). Furthermore, wave characteristics are needed to see the effect on, and explain, bed level changes. Current speeds are used for the calibration of the Delft-FM model.

3.1.1 Water depths

In Figure 3.1 the observed water depths are plotted. The water depths have been measured at two locations, close to the forest fringe and further inland. Firstly, it can be noticed that the water depth is decreasing inland due to the elevation change, as the inland location has a higher elevation than the forest fringe location. Secondly, there is a diurnal inequality. So within a period of 24 hours, a difference can be observed of approximately 1 meter between the consecutive maximum water levels. Lastly, the tides, at for example the 14th of December, are way higher compared to 6th of December. This is approximately a 7 days difference which also refers to spring and neap tides.

Negative water depths have been filtered out. These occur due to the standard air pressure setting in the instrument. The air pressure changes constantly and is not measured by this instrument. So, when correcting the water pressure with the air-pressure, the real air-pressure might be higher. This then means that the instrument outputs a negative water depth. Negative water depths are filtered and put to 0, so there is no water. Negative water depth only exist at the start and end of an inundation period. An overview of the maximum water depth for all periods, on both locations, can be seen in Table 3.1.

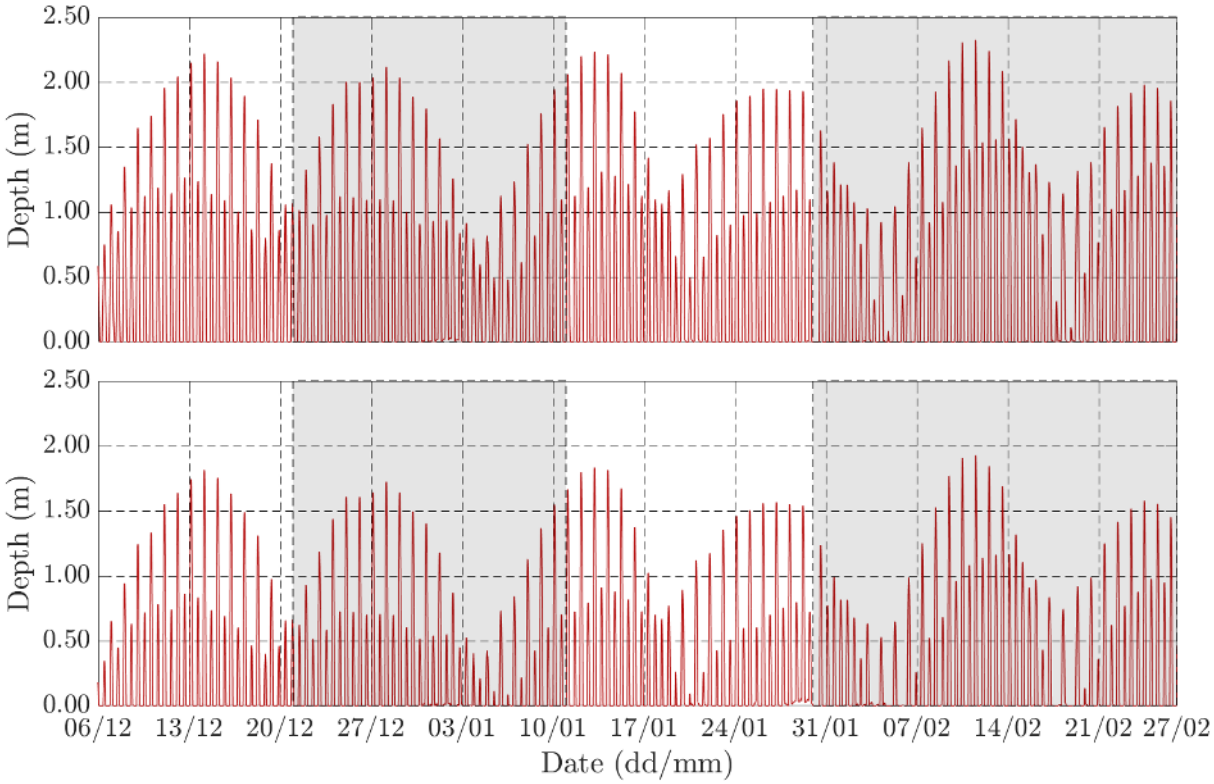

Figure 3.1: Water depth at Transect A. Top plot shows the water depth at the forest fringe location and the bottom plot shows the water pressure at the inland location. Grey and white boxes separate each fieldwork period.

Table 3.1: Maximum water depth (m) per location per period.

Location	Period 1	Period 2	Period 3	Period 4
Forest fringe	2.22	2.12	2.23	2.32
Inland	1.81	1.72	1.83	1.92
Difference	0.41	0.40	0.40	0.40

As can be seen on Table 3.1 the water depths slightly differ between each period. Period 1 and 3 are comparable to each. Period 2 is slightly lower compared to periods 1 and 3 and period 4 has a slightly higher maximum water depth compared to period 1 and 3. Furthermore, the differences between the forest fringe and inland locations is for all periods approximately 0.40 m. These differences can also be seen in Figure 3.1, as the water depths for the land-side location are lower compared to the seaside location. The differences between the maximum water depths give us the relative elevation difference between both measuring locations.

3.1.2 Inundation periods

The water depth also give us information about the inundation period. In Table 3.2 the average and maximum inundation periods per location and per fieldwork period can be seen. The table shows that the inundation periods are larger for the forest fringe location, compared to the inland location. This is due the fact that the forest fringe location lays at a lower elevation, so it gets flooded 'first'. Also, due to this, the forest fringe location emerges later than the inland location. Furthermore, the differences are not as steady as the difference between the maximum water depths. This can be a result of the 10-minute

time interval that is used to calculate the inundation periods. The data in Table 3.2 is also visualised in a Figure, see Figure 3.2. In Appendix B the inundation periods for each fieldwork period for both the forest fringe as the inland measuring locations can be seen.

Table 3.2: Average and maximum inundation periods (min) per location per period.

Location	Period 1	Period 2	Period 3	Period 4
Inland average	290	270	290	290
Forest fringe average	390	370	360	370
Difference average	100	100	70.00	80
Inland maximum	350	360	350	360
Forest fringe maximum	550	450	430	490
Difference maximum	200	90	120	130

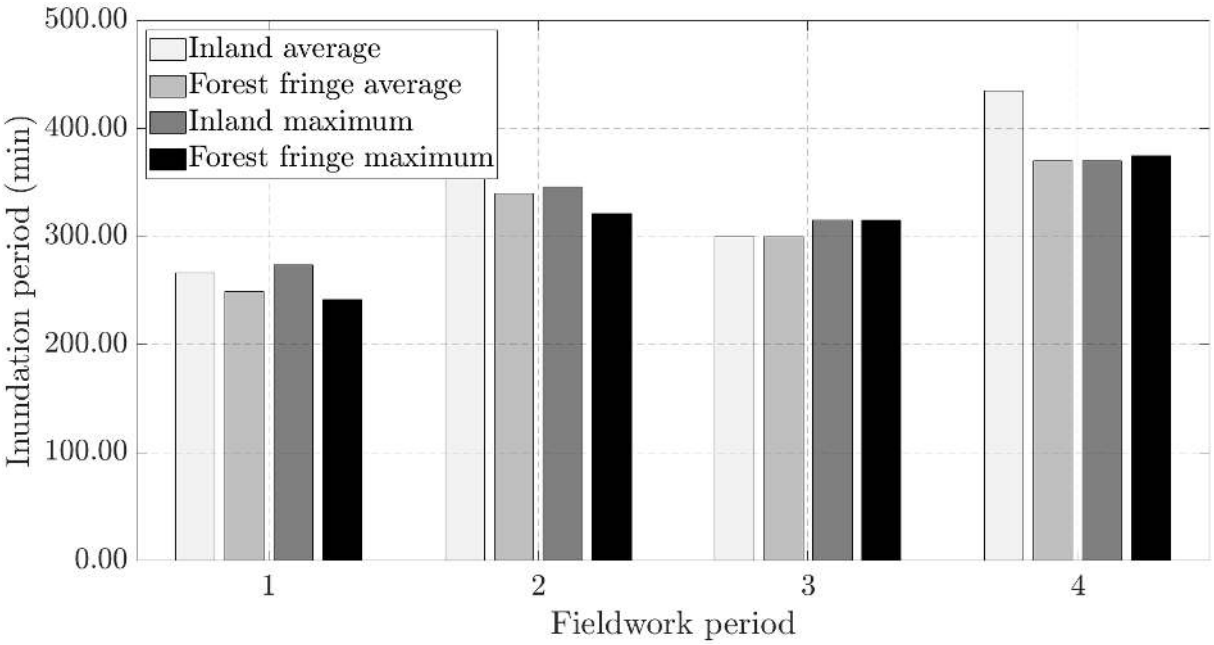

Figure 3.2: Average and maximum inundation periods per fieldwork period.

3.1.3 Wave climate

In Figure 3.3 the significant wave height at transect A is shown for the forest fringe and the inland location. The first thing to notice is that the wave heights are relatively small. The largest waves reach a significant wave height of approximately 0.13 m. The mean significant wave height at the inland location is 0.018 m. The mean significant wave height at the forest fringe location is 0.016 m.

The average and maximum wave heights for both the forest fringe and the inland location can be seen in Table 3.3. As can be seen in Table 3.3, the significant wave height, both maximum and mean, are larger at the inland location. Only in fieldwork period 3 a higher maximum significant wave height was measured at the forest fringe location. So, rather than that waves get attenuated, waves seem to increase land-inward. However, the frames are only 7.6 m apart from each other. In Figure 3.4 the wave attenuation in % is shown. The maximum and mean wave attenuation show approximately the same trend.

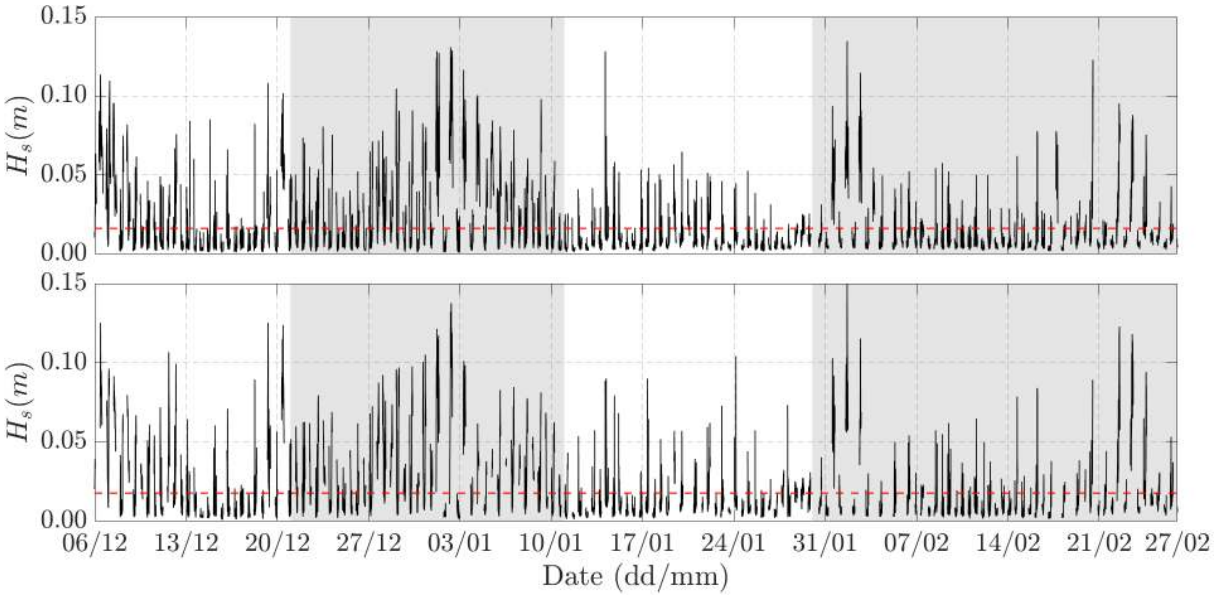

Figure 3.3: Significant wave height (H_s). Top plot shows H_s for the forest fringe location. Bottom plot shows H_s for the inland location. Horizontal red lines show the average significant wave heights; forest fringe: 0.016 m, inland: 0.018 m. Alternating back ground shows the four fieldwork periods.

However, at approximately the 17th of December and from approximately the 10th till the 17th of February, the wave attenuation of the maximum significant wave heights show a quite large negative attenuation. This is because only the wave attenuation between 100 and -100 % are shown in this figure. For some tides the waves get 'attenuated' with -300 %.

Table 3.3: Significant wave heights per fieldwork period.

Fieldwork period	**Period 1**	**Period 2**	**Period 3**	**Period 4**
H_s inland max.	0.1252	0.1377	0.1041	0.1519
H_s forest fringe max.	0.1136	0.1309	0.1283	0.1347
H_s inland mean	0.0250	0.0246	0.0117	0.0135
H_s forest fringe mean	0.0220	0.0224	0.0093	0.0134

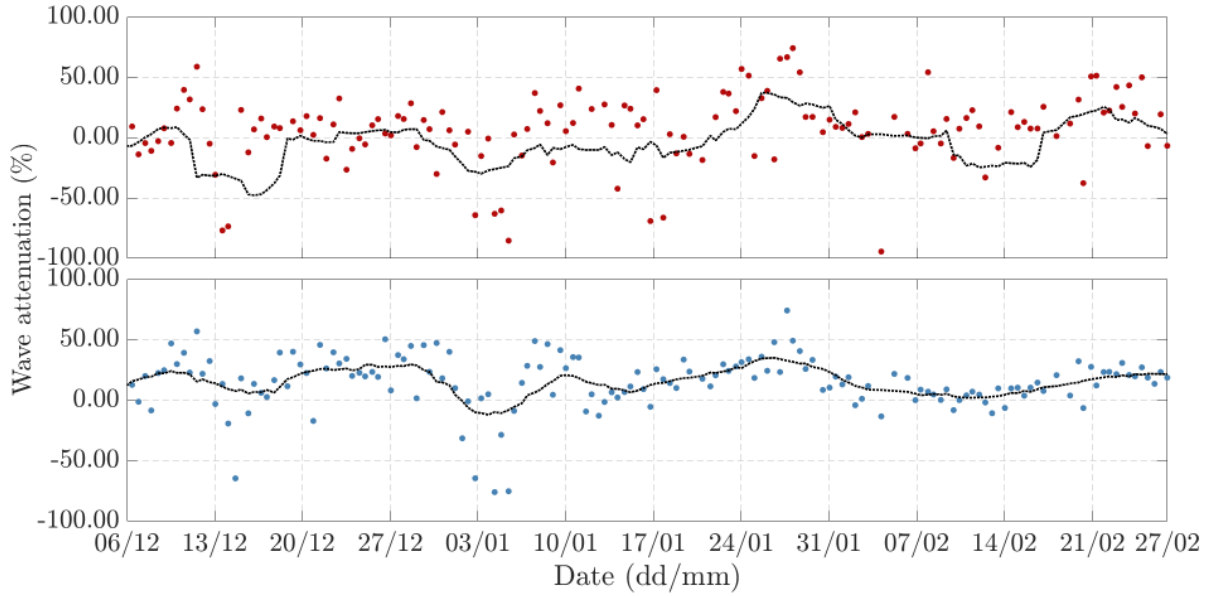

Figure 3.4: Wave attenuation between the forest fringe location and the inland location. Black dotted line shows the moving mean (Window size: 2 weeks). Top plot shows the wave attenuation of the maximum significant wave heights. Bottom plot shows the wave attenuation of the average significant wave heights.

3.1.4 Current velocities

In Figure 3.5 the current speeds of the forest fringe location, top-plot, and inland location, bottom-plot, are shown. The current speeds at the forest fringe location are lower compared to the inland location. The flow velocities are sluggish (0.00 - 2.00 cm/s). This might be due to the fact that the current flow is generally sluggish in this part of the mangroves and due to the row of poles, which are placed at the edge between the mangrove forest fringe and the mudflat. Furthermore, on average the flow at the beginning of the inundation period is higher, compared to the end of the inundation period. Also, the water depth at the inland location is lower compared to the forest fringe location. As the TCMs only measure the bottom 25 centimetre of the water column, the flow velocities will be higher at the inland location.

Additionally, the direction of the currents is also measured by the TCMs. In Figure 3.6 and Figure 3.7 the current directions of both the forest fringe as the inland locations are shown. The figures show the speeds in cm/s, coloured. Then, the direction of the bar indicate the direction of the flow. So, for the inland location the flow is mostly coming from the south-east side, while for the forest fringe location the flow is coming mostly from the north-west. The black line represents the shoreline. Then, the percentages can be used to see how many percent of the incoming flow comes from which side.

Figure 3.6 shows that the direction of the currents is mainly north-west orientated, while for Figure 3.7 this is almost rotated 180 degrees. This is strange as the devices are on the same cross-shore transect. There might be a circulation taking place between the poles and the stop bank at the back of the mangrove area because of the effect of the poles in front and the currents behind the poles.

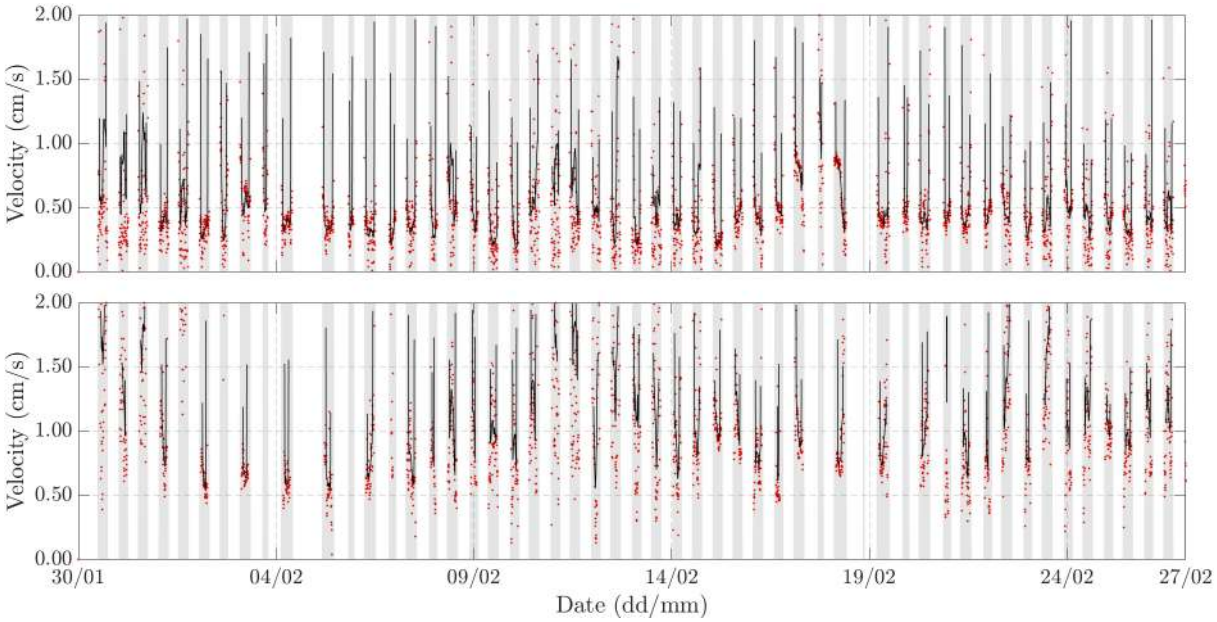

Figure 3.5: Current speeds transect A. Top plot represents the forest fringe location, bottom plot represents the inland location. Black lines indicate the moving average of red dotted data points.

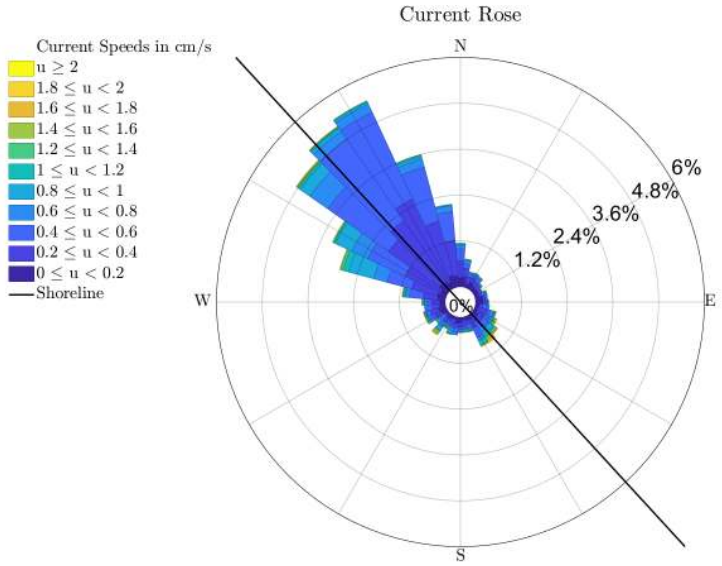

Figure 3.6: Current direction transect A forest fringe location. Colours show the velocity. Black line shows the shoreline.

A close up of the current speeds from the 9th of February till the 14th of February can be seen in Figure 3.8. This shows how the current speeds change within an inundation period, which is harder noticeable at Figures 3.7 and 3.6. The flow velocities are relatively high at the start, end and middle of the the last fieldwork period. This can especially be seen at the forest fringe location. During the start, middle and end of the fourth fieldwork period, waves are also relatively high, see Figure 3.3. So, increasing current velocities coincide with increasing wave heights.

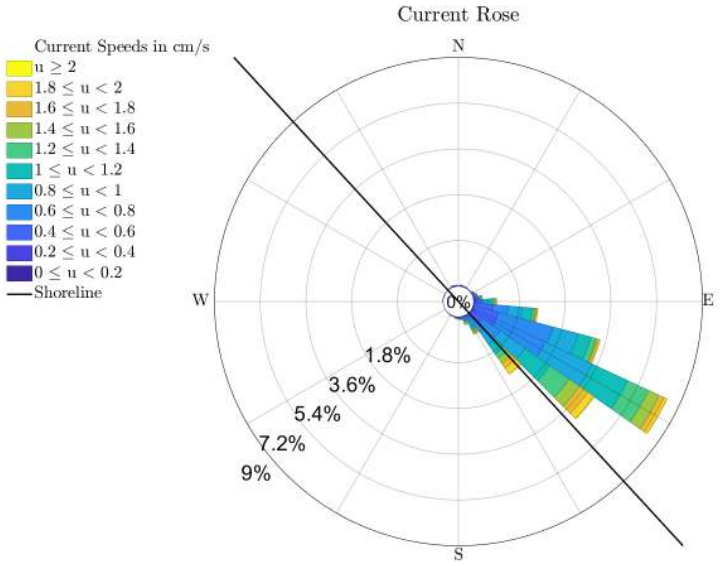

Figure 3.7: Current direction transect A inland location. Colours show the velocity. Black line shows the shoreline.

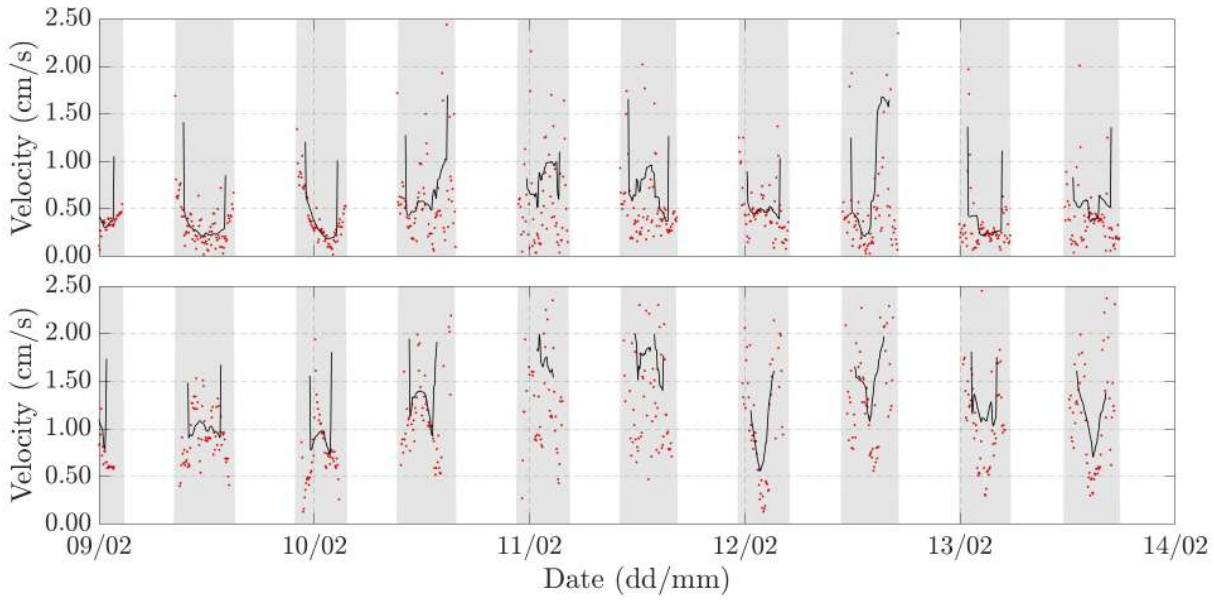

Figure 3.8: Close up of current speeds transect A. Top plot represents the forest fringe location, bottom plot represents the inland location. Black lines indicate the moving average of red dotted data points.

3.2 Morphodynamics

Morphodynamics, as in accretion and erosion have been measured. This section shows the results of measurements at the forest fringe and inland location.

3.2.1 Surface accretion and erosion

In Figure 3.9 the bed level changes of both the forest fringe and the inland Echologgers at transect A are shown. The red dots represent the raw data, which have been received via the method mentioned previously. Furthermore, a moving mean (μ) is plotted as well

as the moving mean plus or minus the moving standard deviation (σ). A window length of 3.5 days has been chosen, which represent a quarter of a spring-neap tide. A window length of 3.5 days has been chosen, because a smaller window size does not represent average values. Smaller windows show too much change in the height variation of the bed, which is not realistic. A larger window does not give a useful representation of the data, which results in no temporal variation. In grey, the different measurement periods are marked out. At the end and start of each period the Echologgers were retrieved and deployed.

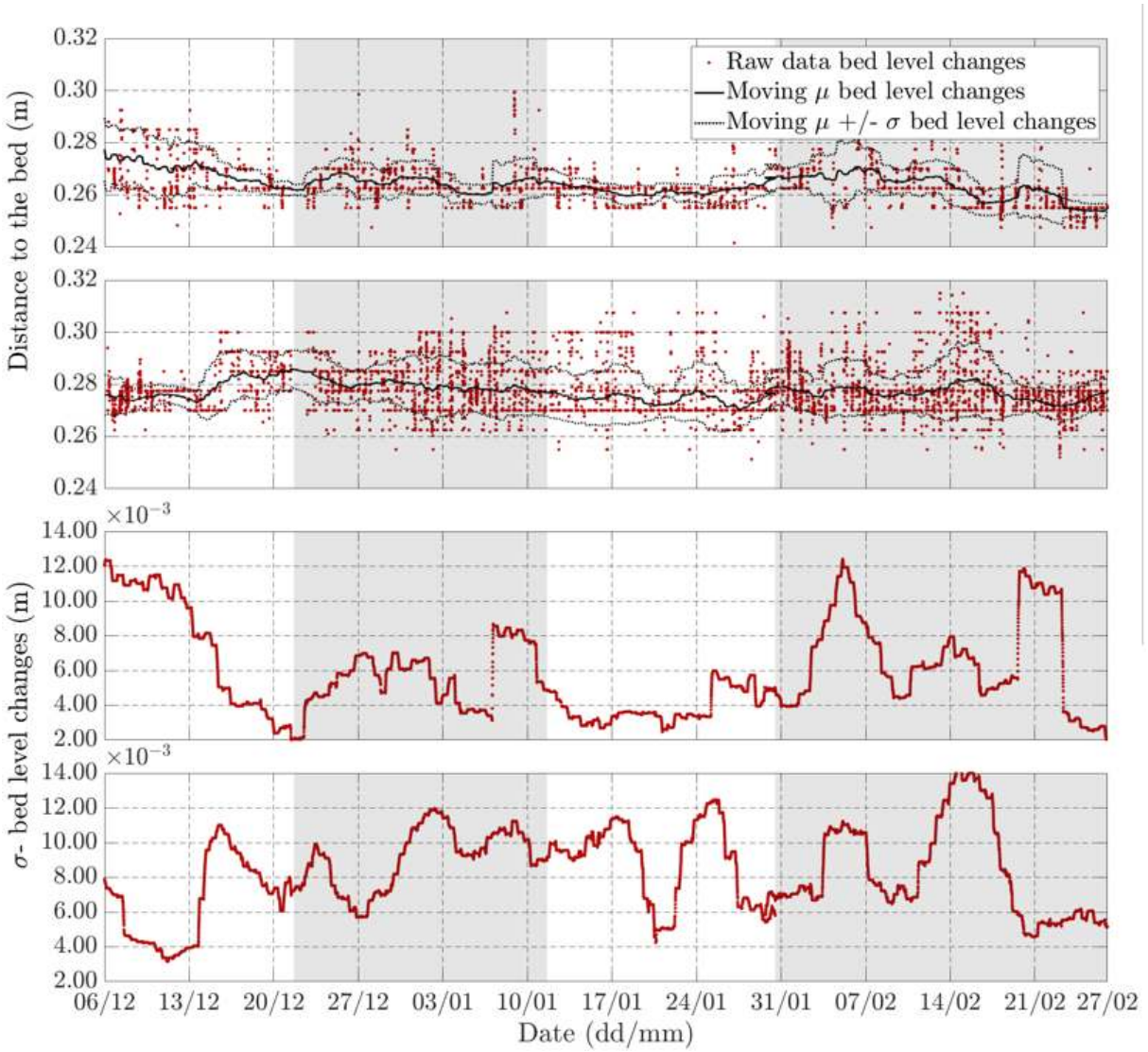

Figure 3.9: Bed level changes transect A. First plot distance to the bed at the inland location. Second plot distance to the bed at the forest fringe location. Third plot the standard deviation of the bed level changes at the inland location. Fourth plot shows the standard deviation of the bed level changes at the forest fringe location. Grey and white background colours indicate the measuring periods.

Figure 3.9 shows that the forest fringe Echologger shows way more variations compared to the inland Echologger. The inland Echologger shows some large fluctuations at the beginning of the graph. This is due trampling the soil caused by installing the frames. Furthermore, the inland Echologger shows that distance to the bed has changed from approximately 27.5 cm to 25.5 cm, which would mean that the bed level has risen due

to accretion with 2 cm. The forest fringe Echologger does not show many differences between the start and the end of the fieldwork period. The forest fringe Echologger does however show more fluctuations. This is as expected as, the water depth at the forest fringe location is larger, compared to the inland location. Due to this, waves occur more often at this location than the inland location. At the end of the fieldwork period, at the forest fringe location, quite some fluctuations can be observed. This could possibly be an effect of a large branch which was located right underneath the Echologger. The branch was found during the retrieval of the instrument on the 27th of February. Also, an important thing to keep in mind is the presence of barnacles. It was observed that a lot of barnacles were found when the instruments were retrieved. The barnacles might influence the acoustic signal of the Echologgers. This could possible mean that there is some delay or some deflection of the signals, which might lead to some inaccuracies. It is however unclear what the exact effect of the barnacles is. The bottom plot of Figure 3.9 does however not show a significant change of the height above the bed at the end of the fourth fieldwork period. This might mean that barnacles do not really affect the signals.

Next to a moving mean, also a moving standard deviation has been plotted, see Figure 3.9. The moving standard deviation is similar to the moving standard mean. It is calculated over a sliding window size, similar to the moving mean. The resulting figures give an indication of the dynamic depth of the bed level. A high standard deviation means that bed levels show more variability. A low standard deviation means that the bed levels are more or less stable. In Figure 3.9 the third plot shows the inland Echologger. In this plot the moving standard deviation is high at the start of the first fieldwork period. During the second and third fieldwork period it stabilises more or less between 0.03 and 0.08 cm. For the forest fringe Echologger, these values are not similar. The values in the second and third fieldwork period are more less stable between 0.07 and 0.11 cm, and thus are higher compared to the inland Echologger. This means that the bed level changes at the inland Echologger do fluctuate less compared to the forest fringe Echologger. In the last fieldwork period the standard deviation changes for both Echologgers. Where in period two and three the values are more or less stable, the values rise for the fourth fieldwork period.

3.3 Vegetation results

This section shows the results of the measured seedlings and established trees. To compare vegetation data with the observed hydro- and morphodynamic data, an average plot has made for the forest fringe and the inland measuring location. For the forest fringe location, plots A0, A1, B0 and B1 are used. For the inland location, plots A2, A3, A4, B2, B3 and B4 are used. This is based on their location with respect to the frame position.

3.3.1 Seedling dynamics

Number of Seedlings
In Figure 3.10 the average number of seedlings per averaged plot can be seen on the top left plot. The number of seedlings is shown at different dates for the average inland and average forest fringe plot. The dates represent the date of which the measurement has been taken (also marked with a red dot). The number of seedlings for both the forest fringe as the inland location is generally decreasing in time. Only for the first and

last fieldwork period, at the forest fringe location, the average number of seedlings per plot is increasing. The second and third period show a general decrease of the number of seedlings. A decrease of the number of seedlings is not rare to observe, as only the strongest seedlings survive and extend their growth. The plots of the number of seedlings can also be seen more clearly in Appendix F.

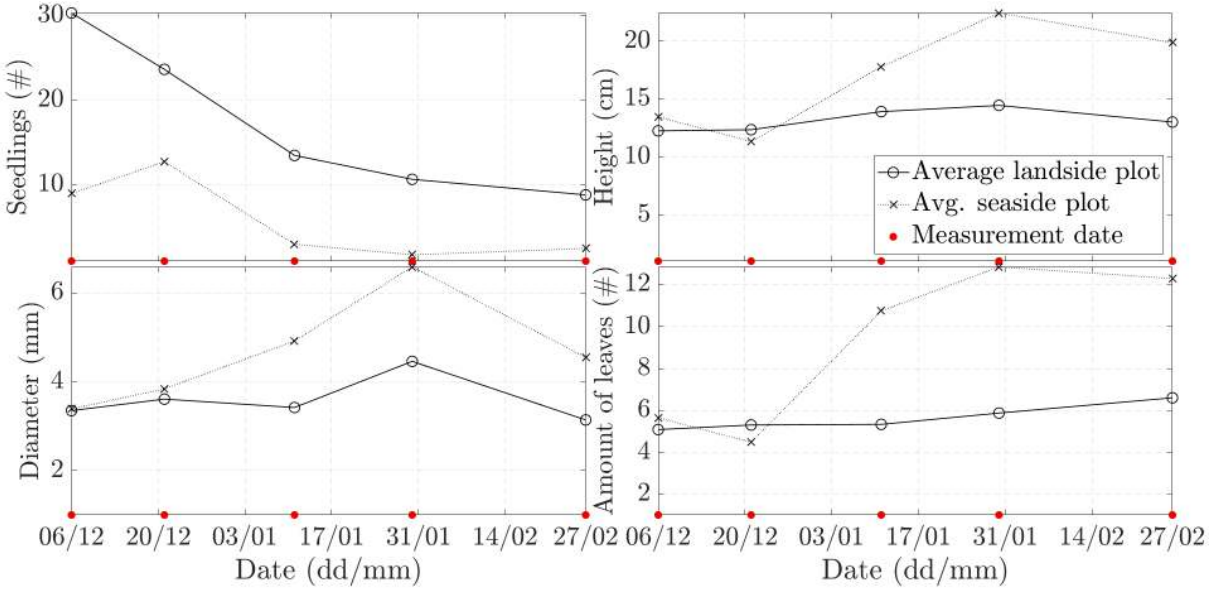

Figure 3.10: Average inland and forest fringe plot properties.

Average seedling height

In Figure 3.10 the average seedling height can be seen for the average inland and forest fringe plot at the top right figure plot. Generally, the average seedling height per plot is increasing. For the forest fringe location, only during the first and last period, the average seedling height is decreasing. During these periods the number of seedlings increased. In Figure 3.11 the correlation between the number of seedlings and the average seedling height per plot, for the combined forest fringe and inland plots is shown. It can be seen that there is a correlation between both seedling properties. The average seedling height increases as the number of seedlings decreases. This means that the largest seedlings survive, while smaller seedlings do not, and the seedlings keep growing.

Average seedling diameter

In Figure 3.10 the average seedling diameter can be seen for the average inland and forest fringe plot at the bottom left plot. The graph is similar to the graph that show the average vegetation height. Overall, the average seedling diameter seems to increase in time. In Figure 3.12 the correlation between the number of seedlings per plot and the average seedling diameter is shown. This figure is also very similar to Figure 3.11. However, the correlation coefficient for the inland location is lower compared to the correlation coefficient of the seedling height and the number of seedlings. The correlation coefficient of the forest fringe location is exactly the same. This means that there is also a correlation between the average seedling diameter and the average seedling height. In the previous section it was mentioned that only the tallest seedlings survive. These tall seedlings also have the largest diameter. Only the strongest seedlings survive and become stronger as they keep growing. The strongest seedling can withstand larger forces due to waves and or bed-level changes. This is similar to what Balke et al. (2011) found.

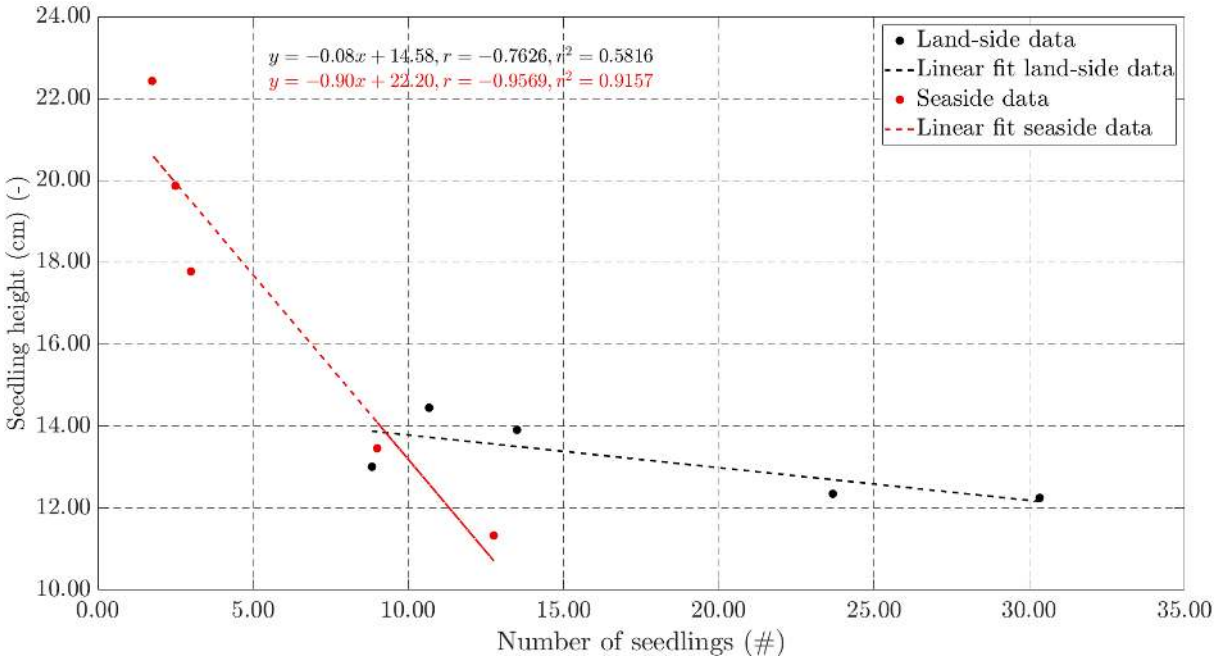

Figure 3.11: Correlation between the number of seedlings per plot and the average seedling height per plot for the average land-side plot and the average seaside plot.

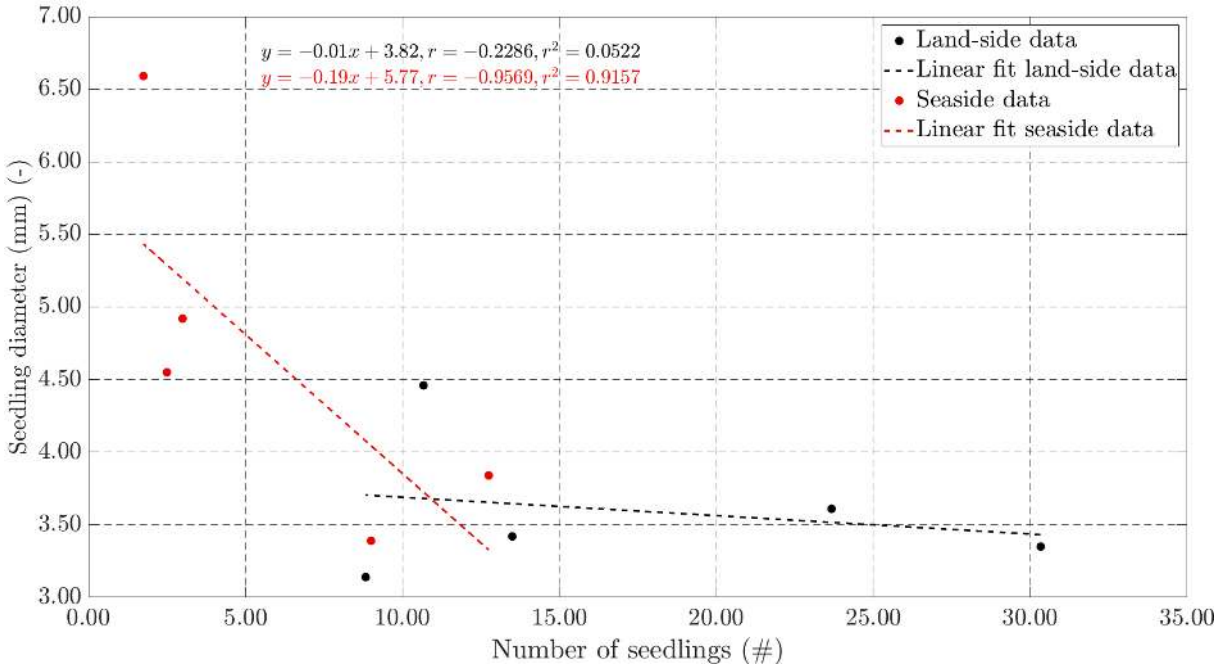

Figure 3.12: Correlation between the number of seedlings per plot and the average seedling diameter per plot for the average land-side plot and the average seaside plot.

Average number of leaves per seedling
The average number of leaves per seedling can also be found in Figure 3.10 on the bottom right plot. There is no visible trend in the increase or decrease of the number of seedlings. The average number of leaves per seedling seems to increase for the first 3 periods. The last period, the number of leaves is decreasing. Larger seedlings have relatively more leaves compared to young seedlings. When only the strongest, and thus the largest seedlings survive, the average number of leaves thus increases. During the fourth fieldwork period, the number of seedlings per plot is slightly increasing. This might be the reason for the decrease of the average number of leaves per seedling as young seedling tend to have a relatively low number of leaves.

3.3.2 Avicennia & Sonneratia trees

The existing trees were measured once at each transect. Trees in the first category (0 - 10 mm diameter) are measured at height of 0.1 m and 0.5 m. Trees in the other categories have been measured at 0.10, 0.50, 1.00, 1.50 and 2.00 m. Next, per tree category, per transect, the mean diameter is determined. Next, the average of both representative tree per category for both the transects is calculated. The plot size of transect A and B is approximately 25 x 10 m. In Table 3.4 the properties of each representative tree in each category is shown for the averaged transect A and B.

Table 3.4: Average representative trees properties for transect A and B.

Representative trees

Diameter category	**Average number per location** [#]	**Average height** $[m]$	**Average diameter** $[m]$	**Density** $[\text{Trees}/m^2]$
0 - 10 mm	36.50	0.5	0.01	0.183
10 - 25 mm	37.50	1.5	0.02	0.188
25 - 100 mm	10.00	> 2	0.07	0.050
100 - 200 mm	3.00	> 2	0.16	0.015
200 - 300 mm	0.50	> 2	0.24	0.003
$>$ 300 mm	2.50	> 2	0.40	0.013

Noticeable is the fact that the density, so the number of trees per square meter, is decreasing. This means that there are way more smaller trees than bigger trees. However, the number of trees per m^2 is bigger for trees in the category larger than 300 mm than 200 - 300 mm. At transect A no trees were found with a diameter between 200 and 300 mm, and only one tree of that category was found at transect B. In addition, more larger trees (>25 mm) were found at at transect A than transect B. At transect A 11 larger trees were found, while only 6 were found at transect B. However, more smaller trees (< 25 mm) were found at transect B compared to transect A. In total 101 smaller trees were found at transect B and 'only' 62 were found at transect A. Furthermore, Table 3.4 show in the 'Average number per location' column that there are half trees. This is due to averaging over two transects (A and B).

3.3.3 Pneumatophores

Pneumatophores are measured at transect A. These have been measured in the same plots as the seedlings at transect A are measured. So, in total five plots have been used to measure the pneumatophores. Their height, diameter and the number of pneumatophores

have been measured. Measurements show that the pneumatophores can be divided into two classes: dense and sparse. Plot 4 has been put in the sparse class, as it 'only' has 67 pneumatophores per m^2. This plot is the most inland one. Fieldwork has shown that *Avicenna* and *Sonneratia* trees are found more towards the seaside of the measurement area. Due to this, less pneumatophores are found at the most inland plot. Other plots showed a quite similar number of pneumatophores. The number of pneumatophores is somewhat constant, however the height of these pneumatophores increases seawards. For the most inland plot, the average height of 20 of random pneumatophores in the plot is 3.87 cm. For the other plots, going from plot 3 to 0 (landward to seaward), the average heights are: 3.96, 5.94, 7.64 and 8.13 cm. The diameter however is not increasing. The diameters of the plots, from 4 to 0, are: 5.60, 4.78, 5.15, 8.45 and 5.35 mm. This shows that the are approximately ranging between 4.78 till 5.60 mm. Only plot 1 shows an average diameter size of 8.45 mm. This is because this plot is close to either a *Avicennia* or *Sonneratia* tree. Pneumatophores decrease in height as they are located away from the tree. The average properties of both the dense and the sparse pneumatophore classes can be seen in Table 3.5.

Table 3.5: Average pneumatophore properties for sparse and dense areas

Average Pneumatophore	**Number per m^2 [#]**	**Height [cm]**	**Diameter [mm]**
Sparse area	67	3.87	5.60
Dense area	226	6.42	5.93

3.4 Explaining bed level changes

Either waves, currents and or a combination of both causes bed level changes. In Figure 3.13 and 3.14 the observed hydrodynamics and σ- bed level changes for the last fieldwork period for the inland and forest fringe location can be seen.

In Figure 3.13 the last fieldwork period is shown. This is the only fieldwork period where flow velocities have been measured. During this period there were two periods showing a higher σ of the bed level changes. The first peak starts at approximately 02-02-2020. At that date the water depths are low, which means that this was during neap-tide. Flow velocities were not that high during that period. Waves however seem to be quite high at the start of the peak (0.12 m), compared to an average H_{rms} of 0.0065 m. A combination of low water levels and quite high wave heights might be the cause of the increase of the σ bed level changes. Then gradually the water depths increase. At approximately 19-02-2020, the water depths are again quite low. Then, the σ bed level changes immediately goes past 0.10. Wave heights and flow velocities were not that high during that period. Low water depths mainly seem to cause an increase of the σ bed level changes, nevertheless how 'high' the waves and or flow velocities are. The bed shear stress increases with lower water depths, which thus means that the σ bed level changes increase.

In Figure 3.14 the measured dynamics for the last fieldwork period at the forest fringe location can be seen. Similarly to the inland location, at 02-02-2020 an increase of the σ bed level changes can be seen. Again, water depths are relatively low during this period, causing an increase of the σ bed level changes. However, the peak seen at the inland

location, starting approximately at 19-02-2020, can not be detected at the forest fringe location. However, a peak can be seen starting at approximately 12-02-2020. At that time flow velocities seem to be a bit higher. Furthermore, waves seem to be a little higher during that period as well. A combination of both higher waves as well as an increase in the flow velocities might indicate in an increase of the σ bed level changes. At 12-02-2020 however, the water depths are high due to the spring-tide. The increase of the σ bed level change at this point is however opposite of what happened at the inland location.

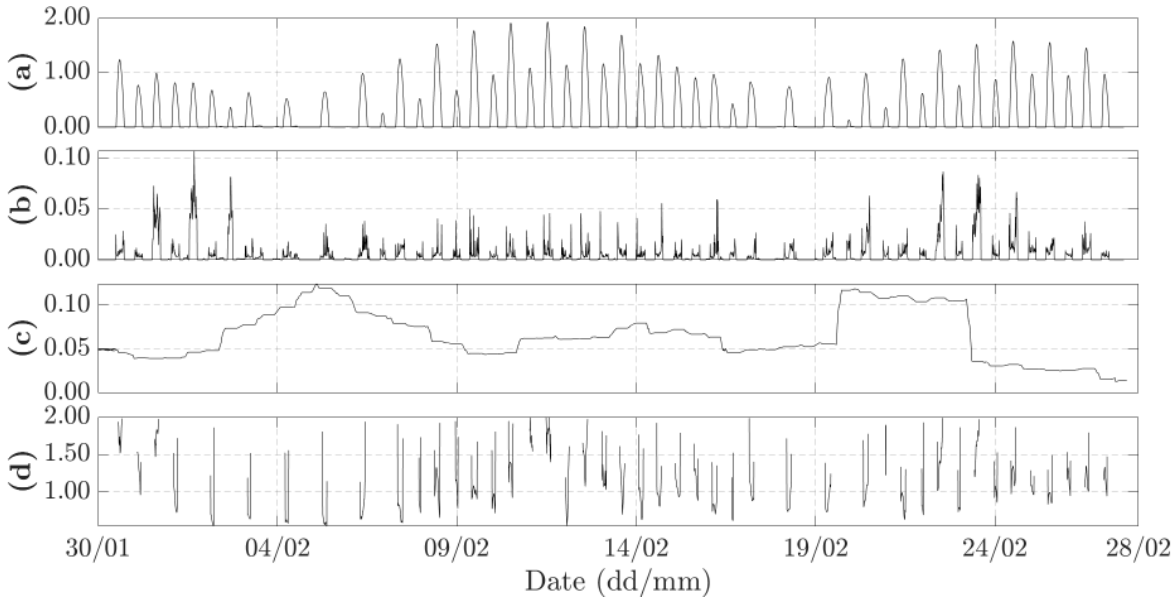

Figure 3.13: Observed hydrodynamics and bed level changes for the last fieldwork period at the inland location.(**a**): water depths (m). (**b**): root-mean-square wave height (m). (**c**): σ-bed level changes (m). (**d**): Current velocities (cm/s).

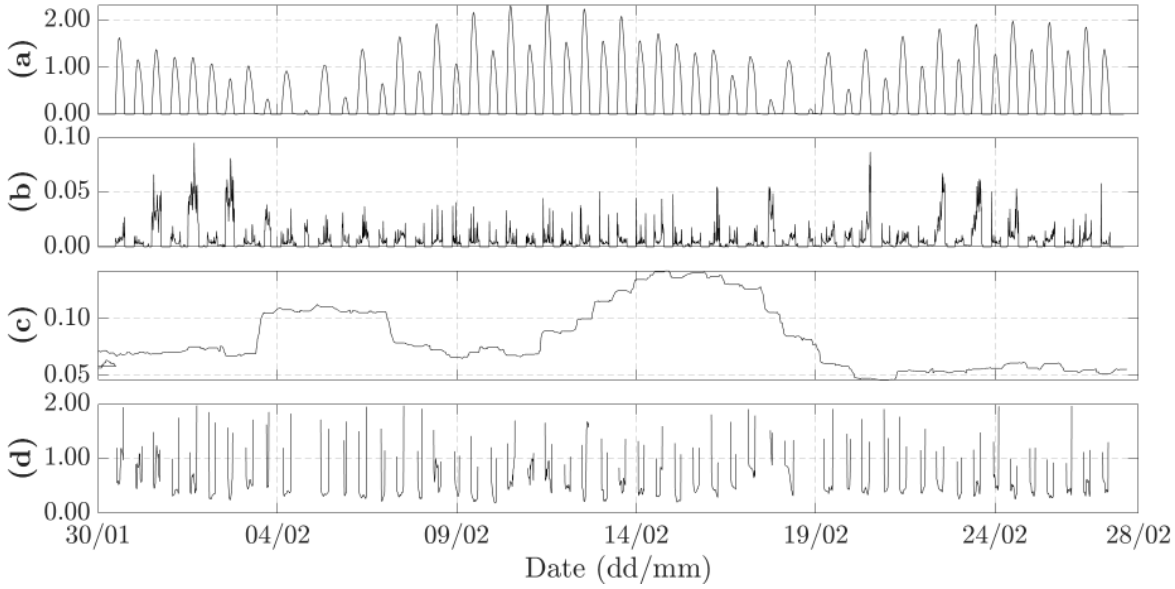

Figure 3.14: Observed hydrodynamics and bed level changes for the last fieldwork period at the forest fringe location.(**a**): water depths (m). (**b**): root-mean-square wave height (m). (**c**): σ-bed level changes (m). (**d**): Current velocities (cm/s).

3.5 Explaining seedling dynamics

To understand what the effects of waves, tides and bed level changes are on the establishment of seedlings, correlations between the observed physical parameters and seedlings have been determined. This is useful to see the effect of all parameters on the seedlings and which of those parameters has the most crucial role in the growth and or mortality of seedlings. Furthermore, by finding the correlations a trend between each parameter and the number of seedlings is determined, as input for the Delft-FM model. In Figure 3.15 and 3.16 plots with all the measured variables can be seen for the inland and forest fringe location. At approximately 01-01-2020 there is a period of larger waves. During that period also an increase in the bed level changes (c) can be seen. Between 21-12-2019 and 11-01-2020 the average number of seedlings also strongly decreases. This could possibly be due to the increased waves and or bed level changes. Furthermore, at approximately 20-01-2020 the bed level changes are small. Also, the water levels and the waves during that period are quite small. Furthermore, the peak in the bed level changes also look like they occur during the maximum water depths.

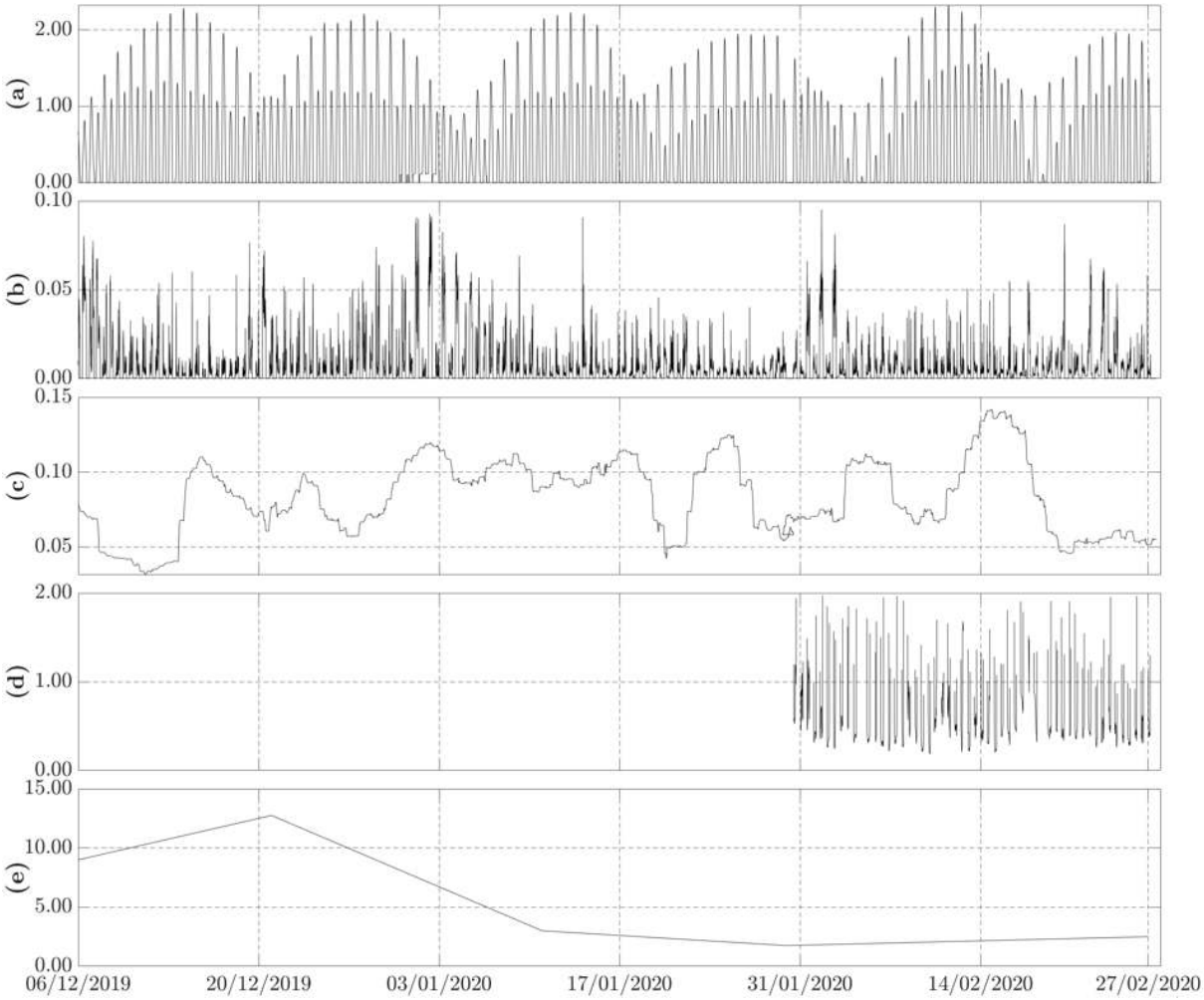

Figure 3.15: Total observed dynamics for the whole measuring period at the forest fringe location. (**a**): water depths (m). (**b**): root-mean-square wave height (m). (**c**): σ-bed level changes (m). (**d**): Current velocities (cm/s). (**e**): Average number of seedlings (#).

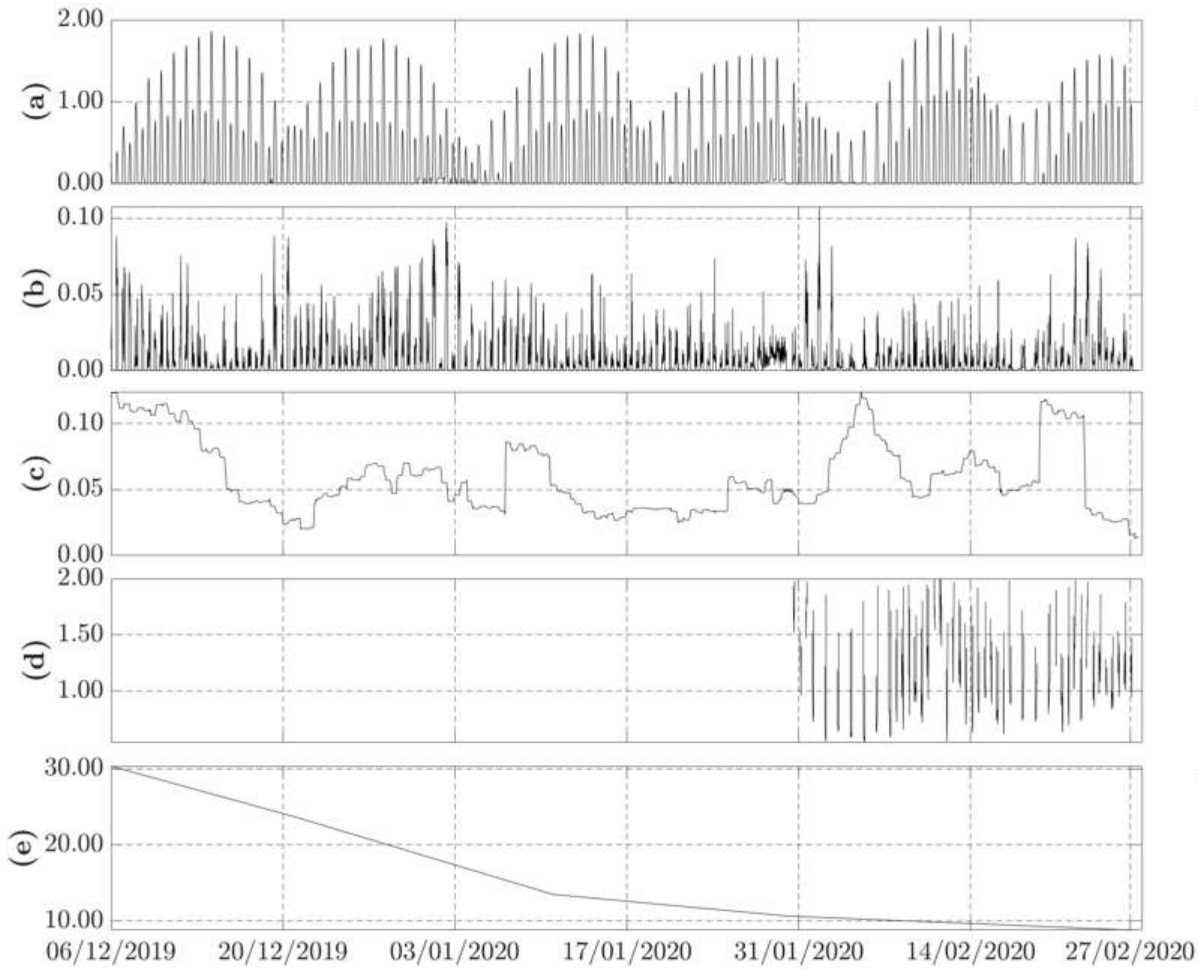

Figure 3.16: Total observed dynamics for the whole measuring period at the inland location. (**a**): water depths (m). (**b**): root-mean-square wave height (m). (**c**): σ-bed level changes (m). (**d**): Current velocities (cm/s). (**e**): Average number of seedlings (#).

3.5.1 Inundation and the number of seedlings

Balke et al. (2011) established in his Windows of Opportunity theory that stranded propagules need a certain inundation-free period to develop roots rapidly. Per fieldwork period the maximum inundation period is calculated. Not the mean but the maximum inundation period is chosen to be correlated to the number of seedlings. This because the average inundation period per day would not be a sufficient parameter to correlate the differences in the number of seedlings, as it always the same. The average inundation period determines if seedlings can grow and establish on certain areas, while the maximum inundation period gives data about the change of the number of seedlings. The average inundation period can be defined as the normal circumstances for seedlings. It is the 'unusual' circumstances that change the behaviour of the seedlings. Alongside with the maximum inundation period goes the inundation-free period. So, a large inundation period additionally means that the inundation-free period is low.

In Figure 3.17 the correlation between the maximum daily inundation period and the weekly growth rate of the number of seedlings per m^2 is shown. The correlation coefficient (r) of the forest fringe data is 0.55. For the inland data, this coefficient is -0.53.

The correlation coefficient defines the strength of the relation between two variables. So a large correlation coefficient shows that there is a strong relation between the variables. While a low correlation coefficient, close to 0, shows that there is no relation between the variables. Furthermore, the (r^2), the coefficient of determination, is determined for the forest fringe, the inland and the combined locations. This coefficient describes the strength of the relation between the independent and depended variable, where the growth rate is the dependent variable. As can be seen in Figure 3.17 both the r as the r^2 values

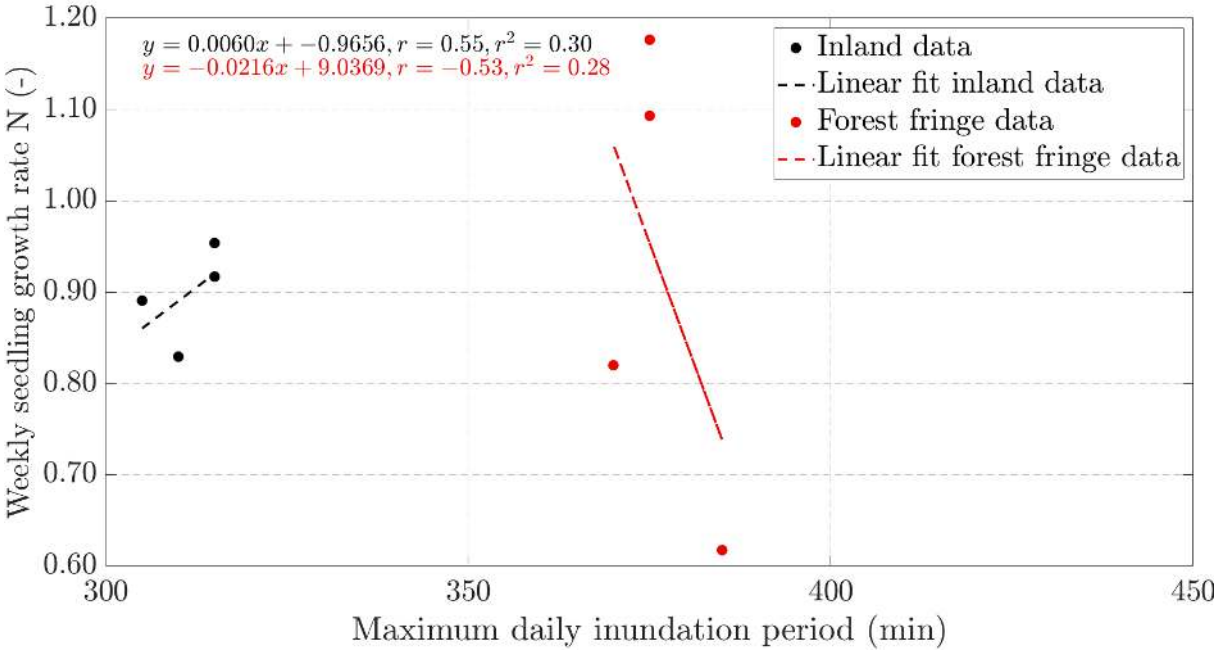

Figure 3.17: Correlation between the inundation period and the weekly growth rate of seedlings per m2. Black coloured data represents the inland data, red coloured data represents the forest fringe data.

are not great for all locations (< 0.60). Especially the combined location does not show a good correlation coefficient nor a good coefficient of determination. So, the inundation period can not be used to determine the growth rate.

3.5.2 Root mean square wave height and the number of seedlings

Additionally to the inundation period, the root mean square wave height (H_{rms}) is correlated to the change in the number of seedlings. The maximum H_{rms} per fieldwork period is calculated. Where the inundation period was calculated per week, the H_{rms} is calculated per fieldwork period. As only one value can be used to correlate to the growth rate per fieldwork period. Furthermore, it does not make any difference in what week the maximum H_{rms} is found. In Figure 3.18 the correlation between the maximum H_{rms} and the seedling growth factor can be seen.

As can be seen in Figure 3.18 the correlation coefficients are not that high, similar to the inundation period. Additionally, the coefficient of determination is not as high either. For the forest fringe location, the R^2 value is 0.23. For the inland location the R^2 is even smaller (0.01). Also graphically can be seen that the correlation between the H_{rms} and the growth rate is not ideal. So, the H_{rms} has a poor correlation with the growth rate.

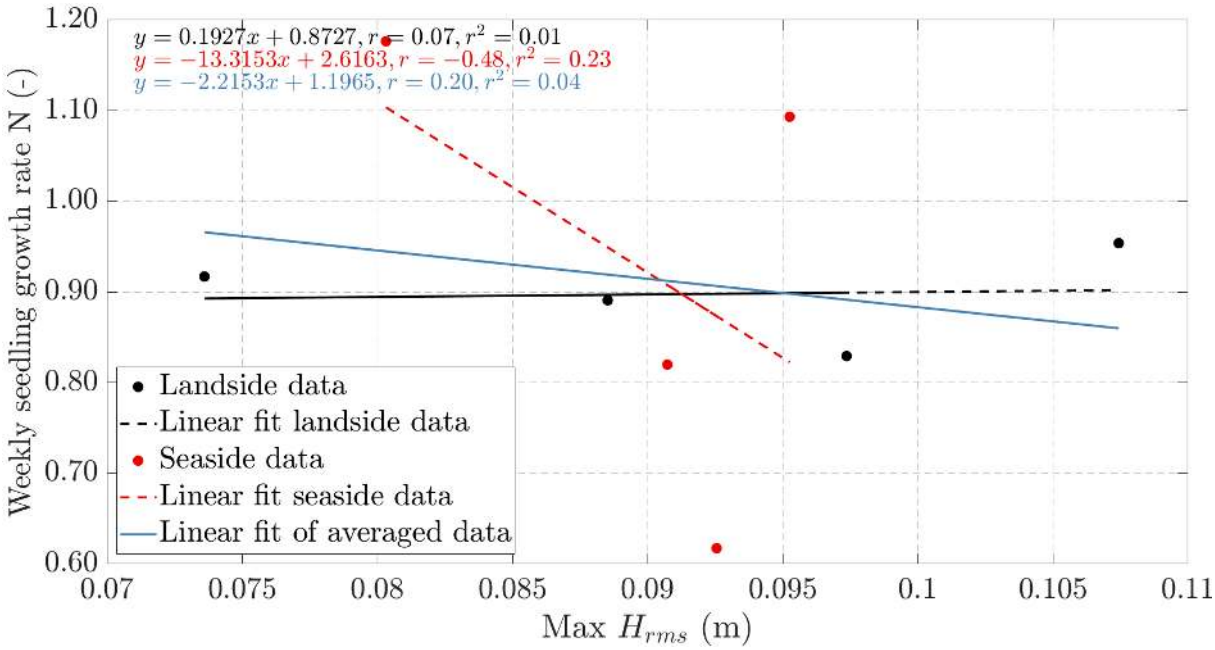

Figure 3.18: Correlation maximum H_{rms} per fieldwork period and the weekly growth rate of seedlings per m2. Black coloured data represents the inland data, red coloured data represents the forest fringe data. Blue is the average of both.

3.5.3 Bed level changes and the number of seedlings

Finally, the bed level changes are also correlated to the growth rate of the number of seedlings. Firstly, the maximum weekly change between the maximum and minimum bed level per fieldwork period has been determined. So, this means that the maximum and minimum bed levels per week have been found. Then the difference between both has been calculated. Per fieldwork period a maximum weekly bed level change is used. This means that the bed level changes during one week, within a fieldwork period, are used to correlate to the growth rate of the number of seedlings. The difference between the maximum and the minimum has been chosen in stead of the difference between the start and the end of the bed level of each week. This because, if only the start and the end of the bed level was taking into account, dynamics within that week were filtered out. By applying the maximum and minimum method, changes within the week are also taken into account. Figure 3.19 shows the correlation between the maximum bed level changes and the growth rate of seedlings.

The coefficient of determination at the forest fringe location is relatively high (0.77). The R^2 value for the inland location is low (0.31). However, the average of both location does show a decent R^2 value (0.68). The averaged line, blue colour, in Figure 3.19 shows a positive gradient. This is not as expected. This means that if the bed level changes increase, more new seedlings will grow, if the bed level changes are higher than approximately 0.095 m per week. A higher maximum bed level change correlates with bigger waves. So, this shows the opposite effect as is expected. A reason can be the fact that seedling grow and can withstand higher bed level changes. If then at least one new seedling establishes, the growth rate already increases. The correlation and the coefficient of determination are higher compared to those of the inundation period and the H_{rms}. Especially, the forest fringe location and the combined location show good coefficients. Out of the three variables, the bed level changes per week seems to be the most reliable

parameter to explain the seedling growth rate.

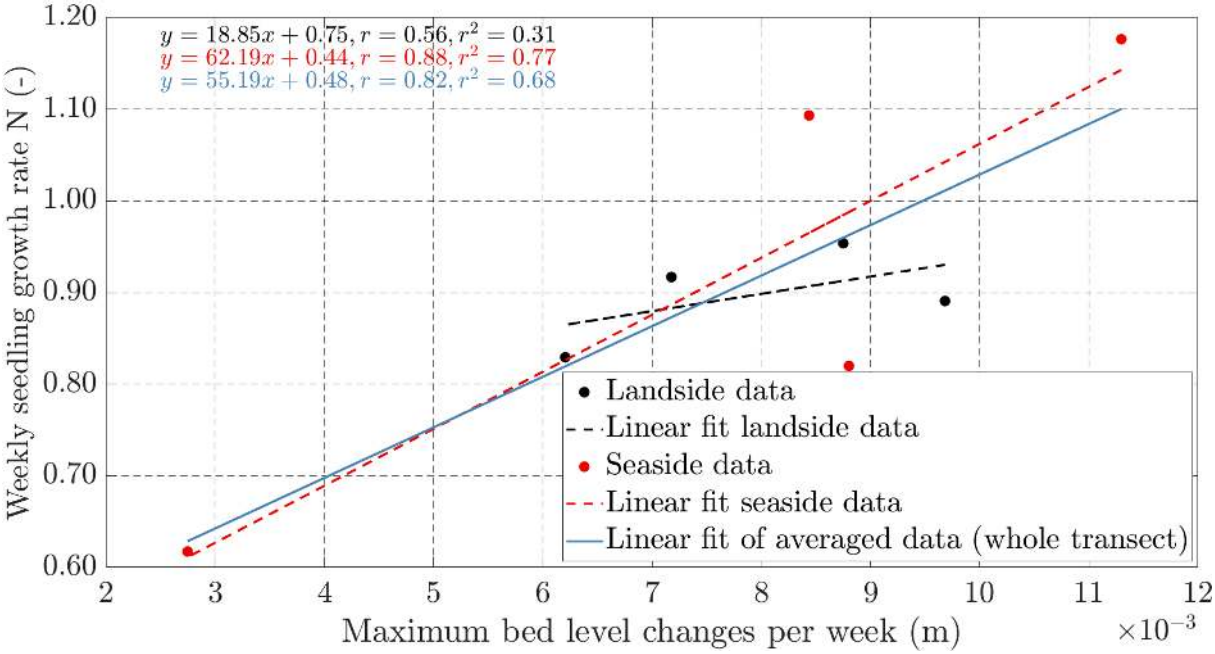

Figure 3.19: Correlation between the maximum bed level changes per measuring period and the weekly growth rate of seedlings per m2. Black coloured data represents the inland data, red coloured data represents the forest fringe data. Blue is the average of both.

3.5.4 Multiple linear regression

The parameters previously mentioned relate to the growth rate of seedlings. However, it is unclear if the growth rate of seedlings can be best parameterised using one or multiple variables. By executing a multiple linear regression, the effect of each parameter, and combinations of these parameters, on the growth rate of seedlings can be determined. For the multiple linear regression, the fitlm function in Matlab is used. This function, or model as it is defined, returns a linear regression model for the variables. In this case the data in the model is the maximum inundation period, the maximum bed level change and the H_{rms}. The response variable is the growth rate N of seedlings. Eventually the model has an output formula which will be used in the Delft-FM model. The formula can be written as:

$$y = \beta_0 + \beta_1 x_1 + \beta_2 x_2 + \epsilon \tag{3.1}$$

In Equation 3.1 y is the depended variable, β_0 the intercept, β_n the coefficient corresponding to observations of x_n and ϵ a random error term. Using the model in Matlab gives us information about the variables. The first variable that was taken into account is the coefficient of determination R^2. Next, the probability value, or p-value, which is used for testing the statistical significance. All variables, mentioned in the previous section, were used in the model, separately, or combined. In Table 3.6 the variables, including there R^2-values and p-values can be seen. Additionally, there coefficients, β_n are also stored in the table.

In Table 3.6 the first top half part of the model table consists of models with just one variable, which have been showed in Section 3.5. The second half of the table consist of multiple variables. The variables can be seen in the first column of the table. Next to the

Table 3.6: Fit linear regression model. R^2-o as the ordinary coefficient of determination, R^2-a as the adjusted coefficient of determination.

Fit linear regression model

	Sea-side location				**Land-side-location**				**Combined**			
Variables: 1	R^2-o	R^2-a	p	β_n	R^2-o	R^2-a	p	β_n	R^2-o	R^2-a	p	β_n
Intercept	0.28	-0.08	0.43	9.04	0.30	-0.05	0.68	-0.97	0.00	-0.16	0.27	0.85
Inundation			0.47	-0.02			0.45	0.01			0.93	0.0002
Intercept	0.77	0.65	0.16	0.44	0.31	-0.02	0.04	0.75	0.68	0.63	0.01	0.48
Δz_b			0.12	62.19			0.44	18.85			0.01	55.19
Intercept	0.23	-0.15	0.35	2.62	0.01	-0.49	0.07	0.87	0.04	-0.13	0.10	1.19
H_{rms}			0.52	-18.52			0.93	0.27			0.65	-3.13
Variables: 2	R^2-o	R^2-a	p	β_n	R^2-o	R^2-a	p	β_n	R^2-o	R^2-a	p	β_n
Intercept	0.87	0.62	0.55	-8.35	0.99	0.97	0.10	-2.38	0.70	0.59	0.65	0.22
Inundation			0.53	0.02			0.07	0.00			0.57	0.0007
Δz_b			0.28	94.43			0.07	30.29			0.02	54.45
Intercept	0.43	-0.71	0.57	9.28	0.30	-1.09	0.79	-0.98	0.04	-0.35	0.32	1.16
Inundation			0.66	-0.02			0.63	0.01			0.96	0.001
H_{rms}			0.70	-15.46			0.79	-0.98			0.69	-3.10
Intercept	0.77	0.31	0.96	0.15	0.31	-1.06	0.26	0.75	0.69	0.56	0.25	0.56
Δz_b			0.37	65.40			0.62	18.96			0.02	54.59
H_{rms}			0.92	2.95			0.98	-0.07			0.84	-0.89

variables, also the intercept can be seen for each set of variable(s). The single variables represent the correlation between the specific variable and the growth rate of seedlings. The ordinary R^2 values can also be seen in the figures representing the correlation between the variable and the growth rate of seedlings. The $R^2 - a$ is the adjusted R^2, which is used to determine the reliability of the correlation. Table 3.6 also shows the differences between the forest fringe, inland and the combined locations.

For the single variables, the bed level changes shows the strongest relation with the seedling growth. The individual locations do not show a good p-value. However, the combined location does show good p-values. For the multiple variables, the bed level changes and the inundation period have the best R^2 values. Especially, the inland location shows a good R^2 value. However, if we take into account the p-values, there are no combined variables that show a good p-value. In fact, there is only one option that shows a statistical significant p-value, which is for the combined location of the bed level changes. Additionally, the β_n values for the forest fringe and the inland location of the bed level changes are somewhat similar. At least they do not change between positive and negative. So, all in all the bed level changes shows the best fit for the growth rate. This means the growth factor can be formulated as:

$$y = 0.48 + 55.19 \cdot x_{\Delta z_b}, \tag{3.2}$$

where $x_{\Delta z_b}$ is the observed weekly bed level change.

Chapter 4

Model methodology

The model will be used to simulate future scenarios in the Sungei Buloh Wetland Reserve mangroves in Singapore. Mainly possible future wave scenarios will be simulated. Field research will be used to validate and update the Delft-FM model.

4.1 Model preparation

The model will be used to simulate vegetation dynamics. In order to accomplish this, a Delft-FM model has been applied on the Sungei Buloh mangroves: **Mangrove Dynamics Model**. Delft-FM allows to have a online coupling between vegetation, which is modelled in Python, and thy hydro- and morphodynamics modelled in Delft-FM.

There are already quite some models used to simulate hydro- and morphodynamics around Singapore. For example the Singapore Regional Model (SRM). This model is used to provide accurate tidal information for the Singapore Strait region (Kernkamp et al., 2005). Part of this model is the Sungei Buloh Local Model (SBLM), which is just one of the parts of the SRM. It is however more detailed than the SRM and thus focuses only on the Sungei Buloh area. The model is refined with new depth contours and validated for hydrodynamics and residence times of pollutants (Hasan et al., 2012, Kurniawan et al., 2011). The SBLM is also used by Willemsen et al. (2016) for their Mandai model. The Mandai model is used to analyse the initial response of the sediment trapping capacity of the mangrove system (Willemsen et al., 2016). The main characteristics of the Mandai model will be used to set-up the new Delft-FM model. The bathymetry, roughness heights and sediment characteristics are thus based on the Mandai model.

The previously mentioned models do not include temporal vegetation dynamics. These models predict long-term scenarios, while the new model will simulate on a smaller timescale. In order to simulate vegetation dynamics, the Delft-FM model will be extended by a Python module, see Section 4.2.3. Previously, this type of model was already used for salt-marshes (Odink, 2019, Van den Broek, 2020). The Python module allows to simulate temporal vegetation dynamics via a online coupling with Delft-FM (Herman and Dijkstra, 2020). The model used by Odink (2019) and Van den Broek (2020) combines the Windows of Opportunity Balke et al. (2011), with the Population Dynamics principle of Temmerman et al. (2007). A similar set-up to the models of Odink (2019) and Van den Broek (2020) is used to make a new Delft-FM vegetation module for the Sungei Buloh mangroves.

4.2 Model description

This subsection contains the model description. It describes the way a Delft-FM works, what parts of the model are used and how the extended vegetation dynamic module will be set-up.

The model consists of three parts: hydrodynamics, morphodynamics and vegetation dynamics. The hydro- and morphodynamics are part of the Delft-FM model itself. The vegetation dynamics is added via a vegetation module, set-up in Python. In Figure 4.1 the typical Delft-FM setup with a wave and morphology module is shown. The 2DH (2-dimensional horizontal), or depth averaged, model of Delft-FM is used. The 2DH model is used, in stead of the 3D model, because of calculation time. Furthermore, the differences between the 2DH and the 3D model are minimal (Horstman et al., 2015).

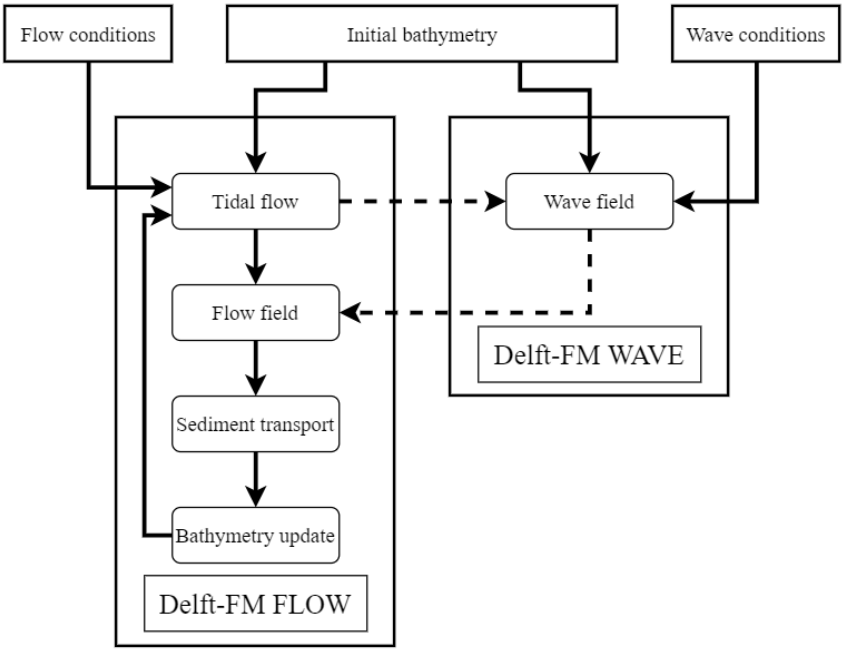

Figure 4.1: Typical Delft-FM setup based on a Delft3D setup description from (Tran, 2011).

4.2.1 Hydrodynamics

The flow part of Delft-FM is referred as D-Flow. D-Flow solves the depth-averaged continuity equations for incompressible flows (Deltares, 2019a):

$$\frac{\partial h}{\partial t} + \frac{\partial Uh}{\partial x} + \frac{\partial Vh}{\partial y} = Q \tag{4.1}$$

In this equation, h is the depth, t represents time, U and V as depth averaged velocities in x- and y-direction and Q as the source or sink term. The momentum equations in horizontal, so x- and y-direction are as follows:

$$\frac{\partial u}{\partial t} + u\frac{\partial u}{\partial x} + v\frac{\partial u}{\partial y} - fv = -\frac{1}{\rho_0}P_x - \frac{gu\sqrt{u^2+v^2}}{C_{2D}^2 h} + F_x + F_{sx} + M_x \tag{4.2}$$

$$\frac{\partial v}{\partial t} + u\frac{\partial v}{\partial x} + v\frac{\partial v}{\partial y} + fv = -\frac{1}{\rho_0}P_y - \frac{gv\sqrt{u^2+v^2}}{C_{2D}^2 h} + F_y + F_{sy} + M_y \tag{4.3}$$

In these equations, u and v are the flow velocities in x- and y-direction, f as the Coriolis force, ρ_0 as the density of water,g the gravitational constant, P as baroclinic pressure in x- and y-direction, F_x and F_y as Reynolds stresses, F_{sx} and F_{sy} as stress due to secondary flow, M_x and M_y as forces due to external sources and C_{2D} as the roughness coefficient. The Coriolis force is a function of the geographical latitude ϕ and the angular speed of the rotation of the earth Ω. The equation to calculate the force is: $f = 2\Omega \sin \phi$ (Deltares, 2019a). For this model the 2DH version of D-Flow FM is used. So, the ∂z term can be neglected in both Equations 4.2 and 4.3.

Waves are implemented via D-Waves. The D-Waves module is based on the SWAN (Simulating WAves Nearshore) calculation core (Deltares, 2020). The spectral action balance equation is used for the wave spectrum Hasselmann et al. (1973):

$$\frac{\partial}{\partial t}N + \frac{\partial}{\partial x}c_x N + \frac{\partial}{\partial y}c_y N + \frac{\partial}{\partial \sigma}c_\sigma N + \frac{\partial}{\partial \theta}c_\theta N = \frac{S}{\sigma} \tag{4.4}$$

wit: N as the action density spectrum, σ as the relative frequency, θ as the wave direction,c_x and c_y as the propagation velocities in x- and y-direction, c_σ as propagation velocity in σ-space, c_θ the propagation velocity in σ direction and S as the source term for effect of generation, dissipation and non-linear wave-wave interactions (Deltares, 2020).

4.2.2 Morphodynamics

In order to simulate bed level changes, the morphodynamic module of the Delft-FM model is used (D-Morphology). This module allows to simulate sediment transport as bedload transport and suspended load transport due to waves and currents.

Suspend sediment transport is calculated using the advection-diffusion equations for three dimensions (Deltares, 2019b):

$$\begin{aligned}\frac{\partial c^{(l)}}{\partial t} + \frac{\partial u c^{(l)}}{\partial x} + \frac{\partial v c^{(l)}}{\partial y} + \frac{\partial (w - w_s^{(l)}) c^{(l)}}{\partial z} \\ - \frac{\partial}{\partial x}\left(\varepsilon_{s,x}^{(l)} \frac{\partial c^{(l)}}{\partial x}\right) - \frac{\partial}{\partial y}\left(\varepsilon_{s,y}^{(l)} \frac{\partial c^{(l)}}{\partial y}\right) - \frac{\partial}{\partial z}\left(\varepsilon_{s,z}^{(l)} \frac{\partial c^{(l)}}{\partial z}\right) = 0\end{aligned} \tag{4.5}$$

In Equation 4.5 $c^{(l)}$ is the mass concentration of sediment, $\varepsilon_{s,x}(l)$, $\varepsilon_{s,y}(l)$ and $\varepsilon_{s,z}(l)$ the eddy diffusivities of sediment fraction and $w_s(l)$ the sediment settling velocity. The last term on the left side of Equation 4.5 can be neglected, as the model is depth averaged.

The settling velocity is calculated as:

$$w_s^{(l)} = \left(1 - \frac{c_s^{tot}}{C_{soil}}\right)^5 w_{s,0}^{(l)} \tag{4.6}$$

where C_{soil} is the reference density, $w_{s,0}$ the sediment fraction of the settling velocity and c_s^{tot} the sediment mass fraction (Deltares, 2019b).

4.2.3 Vegetation modelling

Vegetation modelling is split into two parts: static and dynamic. The dynamic vegetation will be simulated using Python, while the static vegetation will be implemented into Delft-FM. The dynamic vegetation allows the increase and decrease of the density of seedlings in time. The static vegetation is used to simulate existing trees, which of the width and height do not increase or decrease significantly in time for the model run.

Static vegetation
To model static vegetation, Delft-FM has the options to use resistance classes, called trachytopes, to simulate vegetation. Parametrisations of the bed roughness are used to model vegetation. This however gives a drawback as due to this approach the bed roughness increases. This means that the bed shear stress increases, which means that sediment transport rates increase (Deltares, 2019a). In order to fix this, a $-\frac{\lambda}{2}u^2$ term has been implemented in the momentum equations, with λ as the flow resistance of vegetation, the fourth option. When non-submerged the net bed roughness C and λ can be formulated as:

$$C = C_b \qquad \text{and } \lambda = C_D n \tag{4.7}$$

with, C_b as the real bed roughness, C_D as the drag coefficient and n as the density of the vegetation ($n = mD$ where m as the number of stems per square and D the stem diameter).
In case of submerged flow, the calculation for the beg roughness can be executed into two parts, with one part as the average flow u and net bed roughness C, and the other part with the velocity in the vegetation layer (u_v and the real bed roughness C_b:

$$\frac{u^2}{C^2} = \frac{u_v^2}{C_b^2} \tag{4.8}$$

Then the formula for the net bed roughness C can be written as:

$$C = C_b + \frac{\sqrt{g}}{\kappa} \ln\left(\frac{h}{h_v}\right)\sqrt{1 + \frac{C_D n h_v C_b^2}{2g}} \tag{4.9}$$

and the flow resistance λ as:

$$\lambda = C_D n \frac{h_v}{h}\frac{C_b^2}{C^2} \tag{4.10}$$

In Equations 4.9 and 4.10, h_v is the vegetation height, h the water depth and κ the Von Kármán constant (0.4). Also, the flow is submerged when $h_v < h$ and non submerged when $h_v > h$. In case $h_v = h$, Equation 4.7 is used (Deltares, 2019a).

Dynamic vegetation
Dynamic vegetation is not yet standard implemented in Delft-FM. To implement dynamic vegetation into Delft-FM, a dynamic vegetation module will be used via Python. Dynamic vegetation can be interpreted in multiple ways. The vegetation can be dynamic as in vegetation can grow (z-direction) and spread out in x- and y-direction (space). It can develop over time (time). Or the vegetation can be dynamic as it can bend, etc. With dynamic vegetation in this research, the dynamic vegetation in space is meant. Bending vegetation and vegetation dynamics in z-direction can also be modelled in Python. Python is the main script for the model. It calls on the DFM model to calculate the hydro- and morphodynamics (Van den Broek, 2020). The script is combined with the 'Basic Model Interface'

(BMI) to exchange variables between both. Within the Python code, variables can be extracted from the BMI and can be adapted. For example the vegetation density can be extracted and updated based on rules about growth and mortality of vegetation. Via the vegetation module, mortality, growth and diffusion of vegetation can be modelled. Via the principle of the Population Dynamics model of Temmerman et al. (2007), the growth and mortality of seedlings will be simulated.

Population dynamics
The Population Dynamics principle of Temmerman et al. (2007) is used. This principle allow for vegetation growth and mortality, vegetation establishment and diffusion. The principle is based on the next equation:

$$\frac{\partial n_b}{\partial t} = \left(\frac{\partial n_b}{\partial t}\right)_{est} + \left(\frac{\partial n_b}{\partial t}\right)_{diff} + \left(\frac{\partial n_b}{\partial t}\right)_{growth} - \left(\frac{\partial n_b}{\partial t}\right)_{flow} - \left(\frac{\partial n_b}{\partial t}\right)_{inund} \tag{4.11}$$

With:

$$\left(\frac{\partial n_b}{\partial t}\right)_{est} = P_{est} n_{b,est}, \tag{4.12}$$

$$\left(\frac{\partial n_b}{\partial t}\right)_{diff} = D\left(\frac{\partial^2 n_b}{\partial x^2} + \frac{\partial^2 n_b}{\partial y^2}\right), \tag{4.13}$$

$$\left(\frac{\partial n_b}{\partial t}\right)_{growth} = r\left(1 - \frac{n_b}{K}\right) n_b, \tag{4.14}$$

$$\left(\frac{\partial n_b}{\partial t}\right)_{flow} = PE_\tau\left(\tau - \tau_{cr,p}\right), \qquad \text{when } \tau\ \tau_{cr,p} \tag{4.15}$$

$$\left(\frac{\partial n_b}{\partial t}\right)_{inund} = PE_H\left(H - H_{cr,p}\right), \qquad \text{when } H\ H_{cr,p} \tag{4.16}$$

Table 4.1: Population dynamics variables

Symbol	Variable	Unit
n_b	Stem density at the bottom	m^{-2}
t	Time	s
P_{est}	Change of plant establishment	yr^{-1}
$n_{b,est}$	Stem density of new established tussock	m^{-2}
D	Plant diffusion coefficient	$m^2 yr^{-1}$
x, y	Coordinates of grid cells	m
r	Intrinsic growth rate of stem density	yr^{-1}
K	Maximum carrying capacity of stem density	m^{-2}
PE_τ	Plant mortality coefficient related to flow stress	$m^{-2}s^{-1}$
τ	Bottom shear stress	$N\ m^{-2}$
$\tau_{cr,p}$	Critical shear stress for plant mortality	$N\ m^{-2}$
PE_H	Plant mortality coefficient related to inundation stress	$m^{-3}yr^{-1}$
H	Inundation height at high tide	m
$H_{cr,p}$	Critical inundation height for plant mortality	m

The establishment term (est) allows seedling to establish as a random process in a grid-cell with certain characteristics, as density and height. The diffusion term (diff) allow

seedlings to spread to neighbour cells. This makes it possible for seedlings to grow in other cells. When this term is neglected, only via the random establishment process, new seedlings can form in cells. The growth term is the growth of the amount of seedling per cell. This can thus change the plant density. The flow term describes the mortality of seedling due to tidal flow stress Temmerman et al. (2007). The inundation term (inund) described the mortality of seedlings due to tidal inundation stress Temmerman et al. (2007).

4.3 Model set-up

The model will be set-up in Delft-FM online coupled with a vegetation growth module. In Figure 4.2 the set-up can be seen.

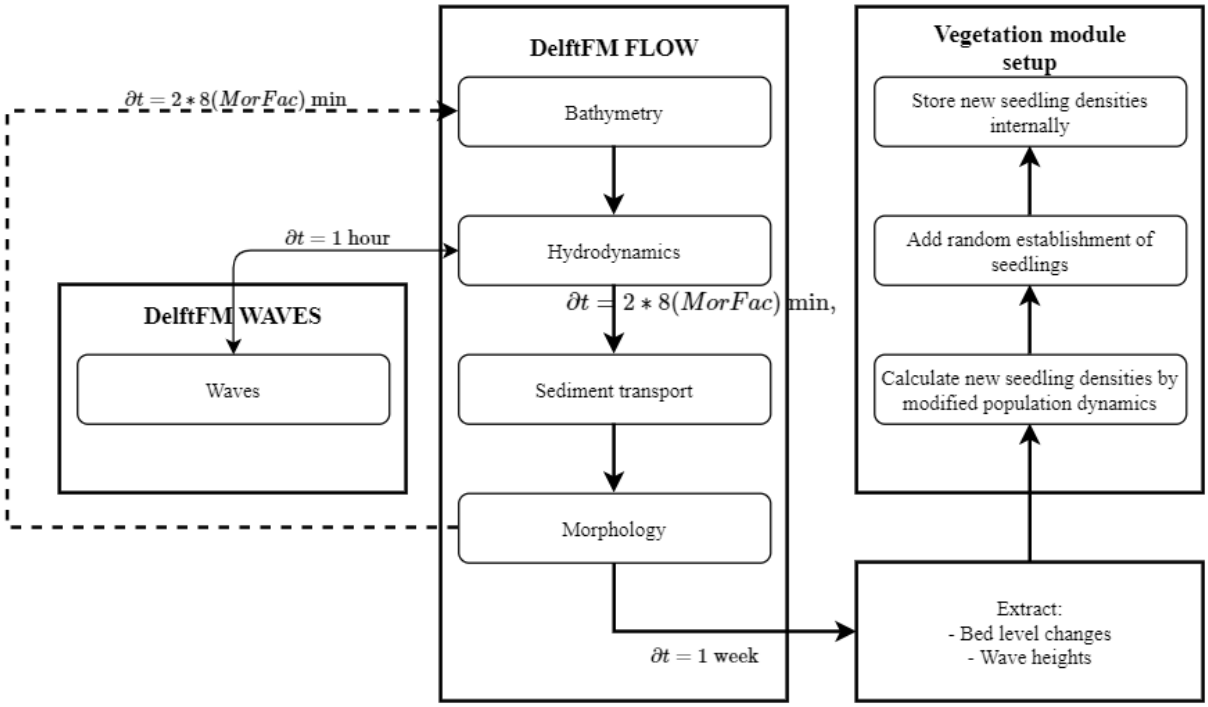

Figure 4.2: Model set-up

4.3.1 Model domain and grid

The grid of the model is rectangular. The grid contains one transect and thus no variation in y-direction (longshore). The bathymetry of the transect is based on the the Mandai model (Willemsen et al., 2016). In Figure 4.3 the profile of the transect is shown. With the red dot, the location of the sea-ward measuring station is marked. The grid is has a width of 500 m and a length, which can be seen in Figure 4.3 of 716 m. So, the grid has one cross-shore profile. The grid cell sizes are 5 x 1.43 m ($x \cdot y$). This is because of the relatively short transect.
The wave grid is slightly bigger compared to the flow grid. The wave grid consists of two parts; the inner and outer. The inner grid consists of cell sizes of 5 x 5 m, while the outer grid has cell sizes of 15 x 15 m. The elevation and wave grid (5 x 5 m) can be seen in Figure 4.4.

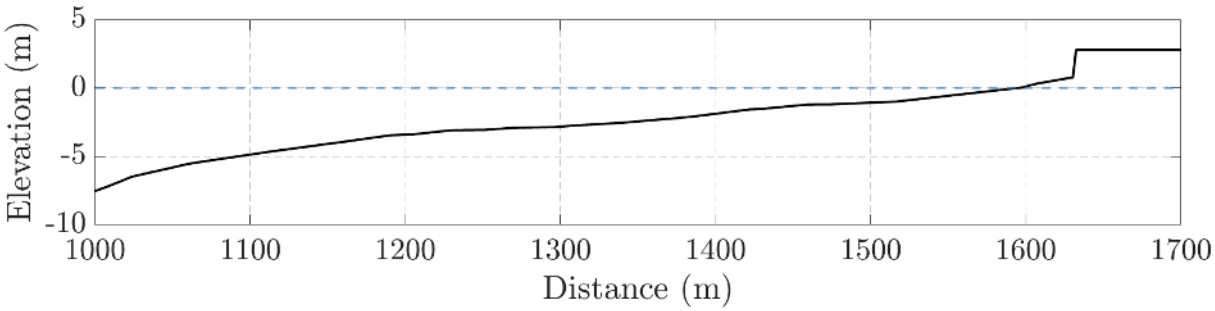

Figure 4.3: Profile of the transect A at the Sungei Buloh Mangroves.

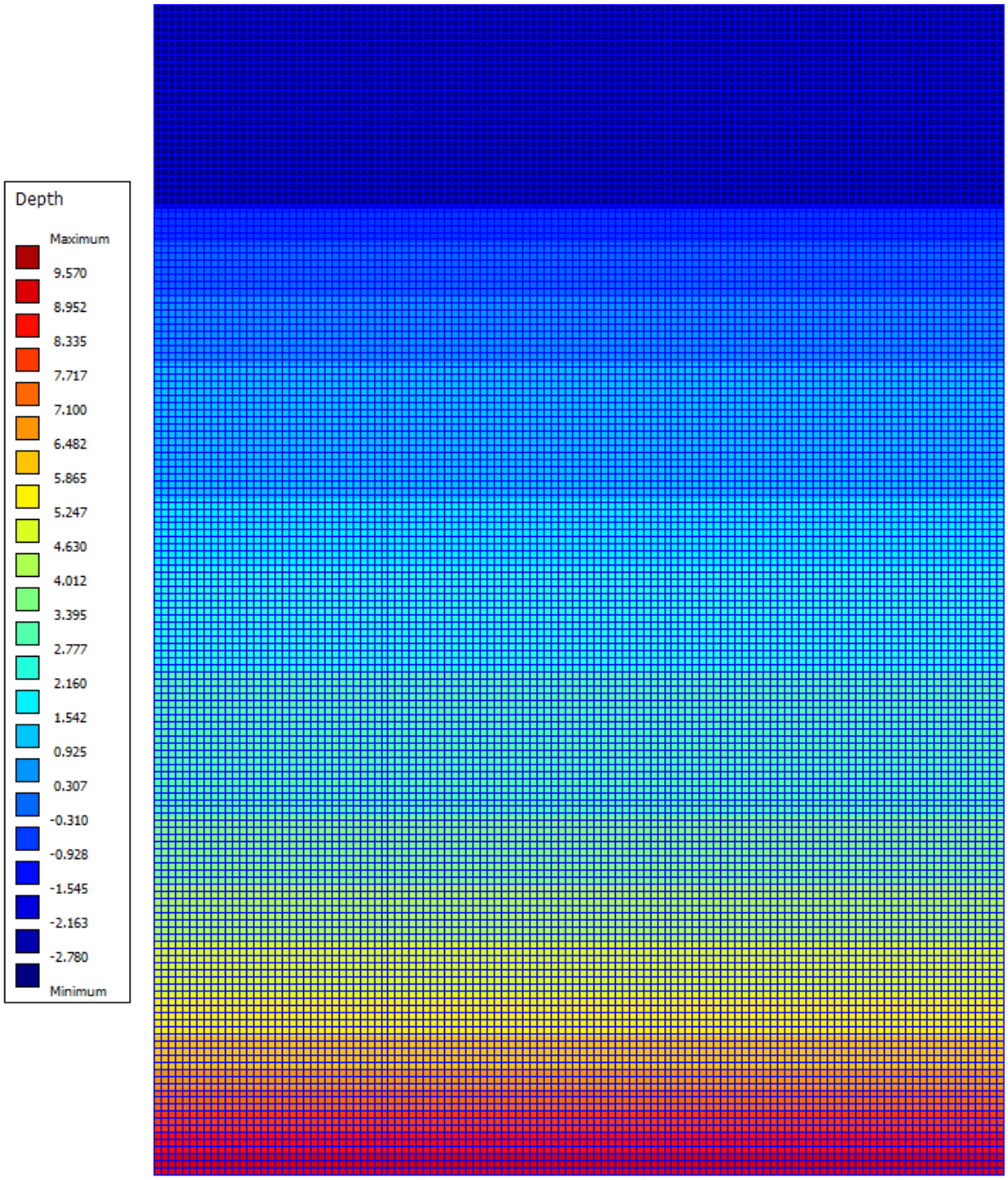

Figure 4.4: 5 x 5 m wave grid and elevation of model domain

4.3.2 Hydrodynamic set-up

The flow part of the model is calculated every 2 min. Waves are calculated every hour. Both flow and waves need a definition at the boundary. For flow, a time series of water levels is used at the boundary. To get the time series, the observed water levels have been used as input in U-Tide to determine the used tidal constituents Codiga (2011). Then, via the reconstruction part of U-Tide the received tidal constituents were used to see if the water levels were correct. In Figure 4.5 the observed and U-Tide calculated water levels can be seen.

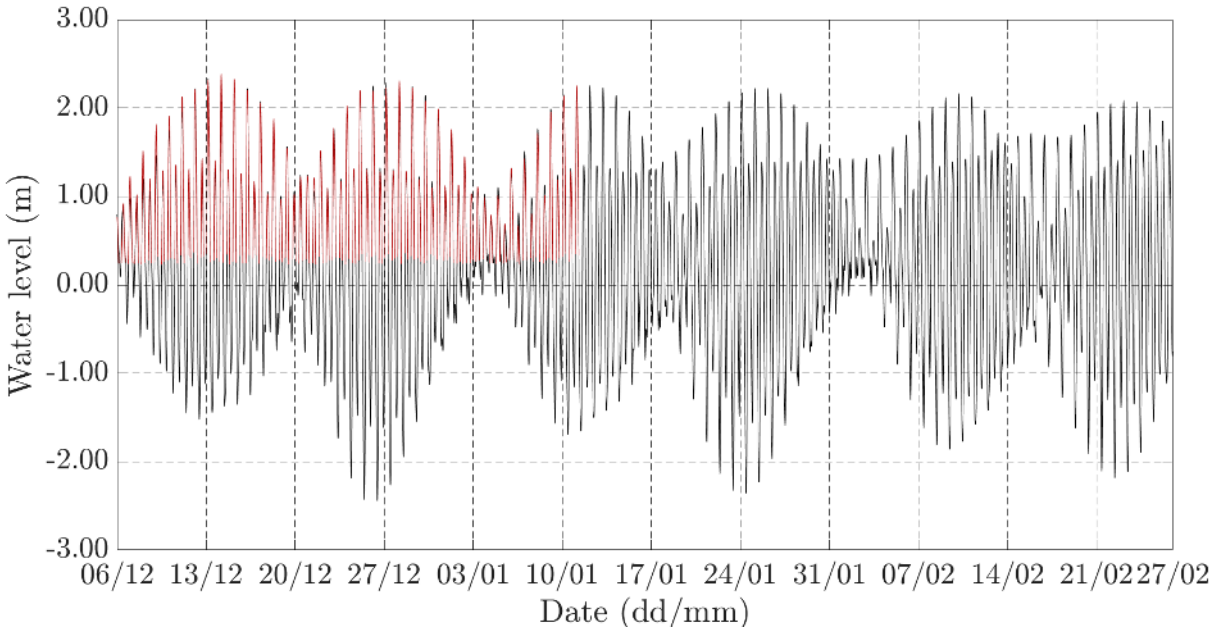

Figure 4.5: Observed water levels at the sea-side measurement location (red) and U-Tide calculated water levels (black).

Then, for every 10 minutes, the water levels have been extracted from the U-Tide program from 05-12-2019, the start of the fieldwork period. These water levels were then used as the hydrodynamic boundary. An overview of the used tidal constituents of the water level time series can be found in Appendix A.

An important parameter for the flow part of the model is the bottom friction. The bottom friction is defined based on the Manning's coefficient. An initial value of 0.023 $m^{1/3}/s$ has been used. This value will be calibrated to get similar flow velocities as has been measured.

For waves, via Linear Wave Theory, the wave height at the boundary is calculated based on the fieldwork observations. A constant wave height and wave period is used on the boundary. Furthermore, the wave height will be calibrated. This will be further explained in Section 5.1. Waves are calculated every 6 minutes. With a MorFac of 8, this means that every 48 minutes waves are calculated.

To conclude, the MorFac has some drawbacks for the hydrodynamic boundary conditions. A measured tide is used as boundary condition. However, without changes to this boundary condition, a single tide would have a period of $\approx 12.5 \cdot 8(\text{MorFac}) = 100$ hours. So, the MorFac stretches the boundary condition. To account for this, the period of the hydrodynamic boundary is scaled by 8. The flow part of the model is calculated for every

2 model minutes, which is, due to the MorFac of 8, 16 minutes. Waves are calculated every 6 minutes, which is, due to the MorFac of 8, 48 minutes, see Table 4.4.

4.3.3 Morphodynamic set-up

The morphodynamics can also be simulated in Delft FM. To simulate the morphodynamics, sediment and morphology input files have to defined. The sediment input files has characteristics of all sediment fractions. These characteristics will be based on the found characteristics of the sediment in the field. A morphological acceleration factor (MorFac) is used to reduce computation time (Lesser et al., 2004, Roelvink, 2006). The value for the MorFac is set to 8, which thus means that the hydrodynamic processes get speed up with a factor 8 (e.g. a spring-neap cycle has a period of approximately 12 hours in normal circumstances. With a MorFac of 8, a spring-neap cycle has a period of 1.5 hours). A consequence of this is that the water level boundary has to be tweaked in order to account for the MorFac. The Mangrove Dynamics Model is made to simulate the evolution of the mangrove for half a year. With a MorFac of 8, only $\approx$ 23 model days are needed ($23 \cdot 8 = 166$). One hydrodynamical day now is multiplied by 8.

To be able to run the morphodynamic part of the model, sediment properties have to be defined at the boundary. In Table 4.2 sediment characteristics can be seen. These values are based on the Mandai model (Willemsen et al., 2016). The critical bed shear stress for erosion $\tau_{critERO}$ is initially set to 0.50. This parameter will be tweaked in order to calibrate the model. Sediment starts flowing into the system at t=0 and ends at t=∞. The amount of sediment flowing into the system is 0.15 kg/m^3 (Willemsen et al., 2016).

Table 4.2: Sediment characteristics

Property	Value	Unit	Description
C_{ref}	1600	kg/m^3	Reference density for hindered settling calculations
ρ_{sol}	2650	kg/m^3	Specific density
w_{s0}	$1.00 \cdot 10^{-4}$	m/s	Settling velocity
$\tau_{critSED}$	$1.00 \cdot 10^{3}$	N/m^2	Critical bed shear stress for sedimentation
$\tau_{critERO}$	0.50	N/m^2	Critical bed shear stress for erosion
ero_{par}	$1.00 \cdot 10^{-4}$	$kg/m^2/s$	Erosion parameter
C_{dry}	$1.20 \cdot 10^{3}$	kg/m^3	Dry bed density

4.3.4 Vegetation set-up

The set-up for modelling vegetation is divided into two parts: static and dynamic vegetation. The static vegetation represents trees with a diameter $>$ 10 mm. These trees grow, but on a large timescale. The dynamic vegetation represents seedlings and trees with a diameter $<$ 10 mm.

Static vegetation
Static vegetation will be based on the executed fieldwork. As mentioned in Section 3.3.2 the existing trees have been measured. The trees then will be analysed and put in the model. Per tree category (diameters) the density, diameter and height will be used in the model. Additionally, the averaged pneumatophores are also implemented in the model via the same method. The values for each category can be seen in Table 4.3. Delft-FM

allows only one vegetation type. The used values for each category will thus be averaged over each grid cell.

Table 4.3: Static vegetation parameters

Tree category (diameters)	**Density ($\#/m^2$)**	**Diameter (m)**	**Height (m)**
Between 0 and 10 mm	0.183	0.01	0.50
Between 10 and 25 mm	0.188	0.02	1.50
Between 25 and 100 mm	0.050	0.07	2.00
Between 100 and 200 mm	0.015	0.16	2.00
Between 200 and 300 mm	0.003	0.24	2.00
Bigger than 300 mm	0.013	0.40	2.00

In front of the seaward frame at the Sungei Buloh mangroves a row of poles was located. The row of poles might affect the flow velocities. Currently, implementing a row of poles in Delft-FM directly is not possible. To solve this problem, the row of poles was implemented as static vegetation. A small polygon was made in front of the most seaward frame. Then, per m^2 a total of 100 'trees' has been defined, with a diameter of 0.10 m and a height of 1.5 m.

Dynamic vegetation
As mentioned in Section 4.3.4 the Population Dynamics principle of Temmerman et al. (2007) will be used to simulate seedling growth and mortality. However, the population dynamics model is set-up for salt marshes and simulates the growth and mortality of *Salicornia*. In this case, *Avicennia* seedlings will be simulated. Also, some of the mortality factors in Equations 4.11 and 4.12 are changed. Firstly, the diffusion part will be neglected. *Avicennia* seedlings do not show clonal growth. Propagules of the *Avicennia* trees are transported across the mangrove and, when the conditions are sufficient, be able to establish and grow. The *Salicornia* species are able to spread and thus the diffusion term can not be neglected for these species. Furthermore, the flow and inundation mortality factors in these equations will be replaced by other factors. This because the field measurements will be used to simulate the growth of the *Avicennia* seedlings. The growth rate formula of the Mangrove Dynamics Model can be seen in Equation 4.17. The formula is not similar any more to the Population Dynamics equation, see Equation 4.11.

$$n_b(n) = n_b(n-1) \cdot (55.19 \cdot \Delta z_b + 0.48) + n_{b,est} \tag{4.17}$$

Unfortunately, Delft-FM only accepts one type of vegetation. In this case 'static' and 'dynamic' vegetation is used. 'Normally', the newly calculated vegetation characteristics are pushed back in the Delft-FM model. Every weekly time-step the vegetation dynamics are calculated. If the newly calculated seedling density is pushed back into Delft-FM, the static vegetation is replaced by the dynamic vegetation. This is not preferable, as the 'static' vegetation causes more friction compared to the small seedling, defined as 'dynamic vegetation'. To deal with this problem, the 'dynamic' vegetation is not pushed back into Delft-FM. The 'dynamic' vegetation still uses the needed parameters, see Equation 4.17. The newly calculated vegetation will then be stored in the vegetation module. This effectively means that the vegetation module could be decoupled from the Delft-FM model. It would be possible to add the seedlings to the 'static' vegetation every time-step. The seedlings give a very small contribution to the hydrodynamics. This is assumed to

be very small, so this method is not used.

The vegetation module stores the bed level for each cell, every 4 model hours. After one week, so 42 stored bed levels, the maximum and minimum bed level values are calculated for each cell. Then the difference between both is determined and stored again. Then Equation 4.17 can be calculated and the growth rate of the seedlings for each cell is determined. Now, the new seedlings for each cell are determined. Then, one 'vegetation step' (7 model days) is completed and the run is continued.

4.3.5 Set-up summary

A summary of the model set-up can be seen in Table 4.4.

Table 4.4: Model Set-up summary

Property	Explanation
Grid	
Size	Rectangular grid; width x length (500 x 716 m)
Flowgrid	Width x length (500 x 716 m)
Flowgrid cellsize	Width x length (5 x 1.43 m)
Wavegrid	Inner; width x length (550 x 750 m)
Cellsize	Width x length (5 x 5 m)
Wavegrid	Outer; width x length (xx)
Cellsize	Width x length (15 x 15 m)
Hydrodynamics	
Flow boundary	Time dependent, retrieved via U-Tide and measured water levels
Bottom friction	To be calibrated
Flow calculation	Every 2 minutes (w.o. MorFac)
Wave boundary	To be calibrated
Wave calculation	Every 6 minutes (w.o. MorFac)
Morphodynamics	
MorFac	8
Sediment characteristics	See Table 4.2
Critical erosion parameter	To be calibrated
Vegetation	
Static	Based on field measurement diameter classes
Dynamic	Population Dynamic principle for growth rate; $n_b(n) = n_b(n-1) \cdot (55.19 \cdot \Delta z_b + 0.48) + n_{b,est}$
Other	
Row of poles	Modelled as static vegetation

4.4 Calibration

In order to use the model to predict seedling growth on a longer term, the model needs to calibrated first. The model will be calibrated for the following parameters: current velocities, waves and bed level changes.

4.4.1 Current velocities

To calibrate the current velocities, the modelled and the measured current velocities will be compared. The current velocities can be calibrated by tweaking the bed roughness. The shear stress at the bed caused by flow is calculated with:

$$\tau_b = \frac{\rho_0 g U|U|}{C_{2D}^2} \tag{4.18}$$

With τ_b as the bed shear-stress, U as the depth-averaged horizontal velocity and C_{2D} as the Chézy coefficient (Deltares, 2019a). As can be seen, the bed shear-stress is a function of the Chézy coefficient. The Chézy coefficient is calculated with Manning's formulation:

$$C_{2D} = \frac{\sqrt[6]{R}}{n} \tag{4.19}$$

With R as the hydraulic radius and n as Manning's coefficient. Increasing n results in a lower Chézy coefficient, which means that the bed roughness gets larger. A decreasing n results in a higher Chézy coefficient, which thus means the bed is smoother. By tweaking this parameter, the current speed get adjusted. The goal of tweaking the friction coefficient is to get the same model results as the measured results, regarding the current velocities.

The Manning coefficient, as thus is used in the UnifFrictCoef, is based on Broekema (2013), Willemsen et al. (2016), Zhang et al. (2012). The initial value of this coefficient is set to 0.023. Based on Willemsen et al. (2016), Zhang et al. (2012) a range between 0.02 and 0.05 is used to calibrate the model. Four runs will be used to calibrate the model with Manning Coefficients equal to: 0.02, 0.03, 0.04 and 0.05 $s/m^{1/3}$. Both the seaward as the land-ward frame will be used to compare the observed modelled flow velocities and the measured flow velocities. The model period will start at 31-01-2020 and will simulate for a total of 1 month. This start time is the same as the start time of the measured flow velocities with the TCMs.

4.4.2 Waves

Waves will be calibrated based on the field measurements. The observed waves at the seaside and the land-side location will be compare to the modelled waves. Waves are implemented in the model with constant values and time dependent values. The wave height will be tweaked. A range between 0.01 and 0.10 m will be applied to set as the boundary wave height. The modelled significant wave height at both the land- as the seaside location will then be compared to the modelled significant wave height. Waves will be simulated for a period of 4 weeks. In total five runs will be used with the next wave heights: 0.01, 0.015, 0.02, 0.03 and 0.10 m.

4.4.3 Bed level changes

The bed level can either increase or decrease due to sedimentation or erosion. In Delft-FM erosion and deposition fluxes are calculated with the Partheniades-Krone formulations

(Deltares, 2019b):

$$E^{(l)} = M^{(l)} S(\tau_{cw}, \tau_{cr,e}^{(l)}), \tag{4.20}$$

$$D^{(l)} = w_s^{(l)} c_b^{(l)} S(\tau_{cw}, \tau_{cr,d}^{(l)}), \tag{4.21}$$

$$c_b^{(l)} = c^{(l)} \left(z \frac{\Delta z_b}{2}, t \right), \tag{4.22}$$

Where: $E^{(l)}$ is erosion flux, $M^{(l)}$ is the erosion parameter, $S(\tau_{cw}, \tau_{cr,e}^{(l)})$ the erosion step function, $D^{(l)}$ the deposition flux, $w_s^{(l)}$ the fall velocity, $c_b^{(l)}$ the average sediment concentration, $S(\tau_{cw}, \tau_{cr,d}^{(l)})$ the deposition step function, τ_{cw} the maximum bed shear stress due to currents and waves, $\tau_{cr,e}^{(l)}$ the critical erosion shear stress and $\tau_{cr,d}^{(l)}$ the critical deposition shear stress (Deltares, 2019b). The critical erosion parameter is the parameter that will be modified. The fall velocity, the erosion parameter M and the critical bed shear stress for deposition will not be calibrated. The critical erosion parameter determined the minimum value for which erosion occurs. So, if this value is exceeded, erosion occurs, while if the calculated value is less, no erosion occurs. Willemsen et al. (2016) used a value of $5.0 \cdot 10^{-1}$ for the critical erosion in their Mandai model. Furthermore, a range of $2.5 - 7.5 \cdot 10^{-1}$ was used for their sensitivity analysis. Horstman et al. (2015) used values between 0.05 and $0.30 N/m^2$. Based on test runs, the range is set to $0.05 - 0.25 N/m^2$. Four runs are used to calibrate the critical erosion parameter: $0.05, 0.10, 0.15$ and $0.25 N/m^2$.

The model runs for this calibration will start at 05-12-2019. This is also the start time of the field measurements. In total, the model run time will be 12 weeks. This is similar to the length of the total fieldwork period. Per week the maximum and minimum bed level changes will be determined. Then the differences per week can be calculated and compared to the observed weekly bed level changes per week. The first 3 weeks will be neglected, as the morphology part of the model requires a spin-up time, where no significant bed level changes will be observed.

4.5 Increased and variable wave heights

The wave boundary will be increase to simulate model runs with increased wave heights. The wave height can be increased by adjusting the wave boundary. Furthermore, a time dependent wave boundary will be implemented to see the differences between a constant and a dynamic boundary condition. The time dependent wave boundary is based on the field measurements. For this, every 10 minutes the wave height will be calculated. The increased wave height for the constant wave boundary will be 5 and 10 times as high as the original' wave height. Time dependent waves will be 1.5 and 2 times as high as the 'original' wave height. So, for example if the the Significant wave height of 1 inundation period is 0.10 m, for the 1.5x increased scenario this wave height will be 0.15 m and for the 2x increased scenario, this wave height will be 0.20 m. The first two scenario runs will have wave heights of 0.10 and 0.20 m respectively.

4.6 Model runs overview

In Table 4.5 an overview of the model runs can be seen.

Table 4.5: Model runs overview

Calibration	**Parameter**	**Range**	**Unit**	**Number of runs**
Flow velocities	n (Manning Coeff.)	0.02 - 0.05	$(s/m^{1/3})$	4
Waves	H (wave height)	0.01 - 0.10	(m)	5
Bed level changes	$\tau_{cr,e}$ (crit. erosion parameter)	0.05 - 0.25	(N/m^2)	4
Validation				
Number of seedlings	N_{veg}	-	(#)	1
Scenarios				
Increased wave height				
Scenario run one	H	0.1	(m)	1
Scenario run two	H	0.2	(m)	1
Variable waves				
Scenario run three	H	variable	(m)	1
Scenario run four	H	variable $\cdot$ 1.5	(m)	1
Scenario run five	H	variable $\cdot$ 2.0	(m)	1

Chapter 5

Model results

This chapter shows the calibration runs of the model and the whole model runs itself. Furthermore, the complete run with different wave settings has been presented as well.

5.1 Calibration

The model needs to be calibrated to see if the model represents the reality fair enough as we do not know the input value yet. The model is calibrated for flow velocities and bed level changes.

5.1.1 Water levels calibration

The water levels were calibrated first. As mentioned before, T-Tide was used to derive the tidal constituents of the observed water levels. Then a time-series of the tidal constituents was made and implemented as boundary condition. In Figure 5.1 the modelled and observed water levels are plotted. As can be seen, the water depths are almost exactly overlapping. This means that the water levels are correctly implemented as a boundary condition.

5.1.2 Flow velocities calibration

First of all, the bed roughness was calibrated. In Figure 5.2 and 5.3 the modelled flow velocities with different Manning coefficients, which quantifies the bed roughness, and the observed flow velocities can be seen. The modelled flow velocities in Figure 5.2 are a bit lower than the measured flow velocities. Only the peaks at each inundation period are somewhat comparable, but the average flow velocities for the field measurements are lower. Changing the bed roughness by tweaking the Manning coefficient between 0.023 and 0.05 does not cause substantial changes of the simulated flow velocities.

In Figure 5.3 the flow velocities for the land-side frame are plotted. The measured flow velocities are higher than the measured flow velocities at the seaside location, also see Figure 3.8. The average velocities at the inland location have a better match than for the seaside location. Furthermore, the differences for the Manning coefficient are really small.

In Figure 5.4 a scatter plot of the modelled and measured average and maximum flow

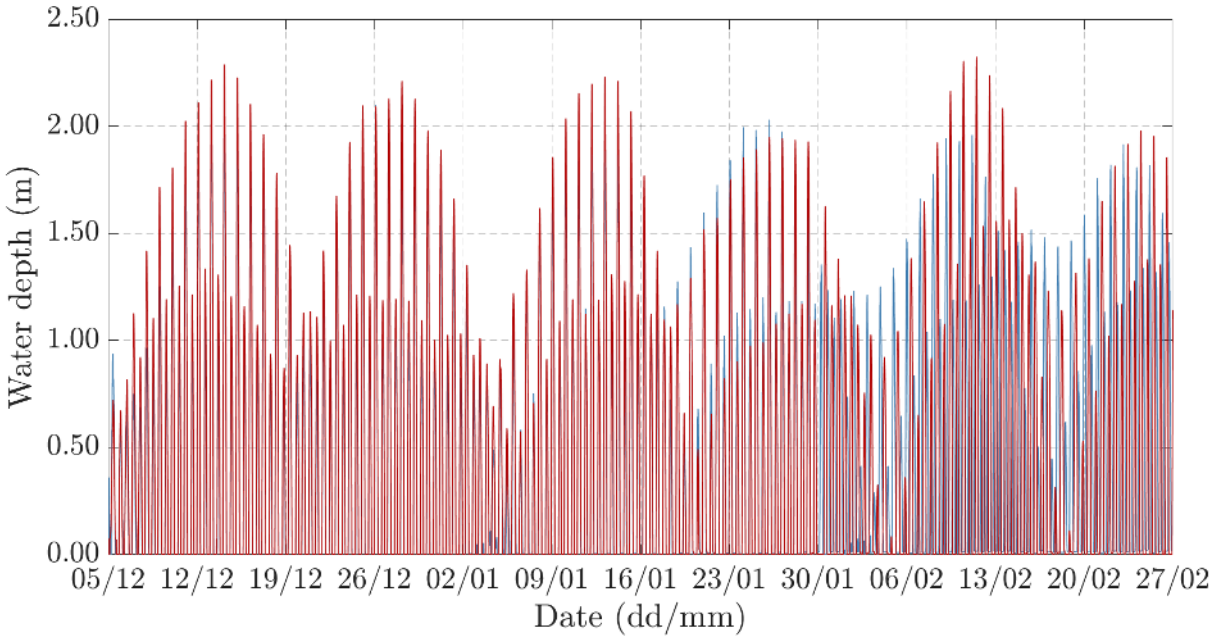

Figure 5.1: Modelled (blue) and measured (red) water depth at forest fringe location.

velocities can be seen. For the forest fringe the average flow velocity does not show a significant coefficient of determination (R^2). For the maximum flow velocities it does show a good R^2 value; 0.89, for a Manning coefficient of $0.05 s/m^{1/3}$. The inland location does not show a good R^2 for both the mean and maximum flow velocities. The modelled flow velocities and measured flow velocities are however more comparable to each other, sea Figure 5.3. Because the flow velocities with a Manning coefficient of $0.05 s/m^{1/3}$ are the smallest, this was chosen to be the calibrated Manning coefficient.

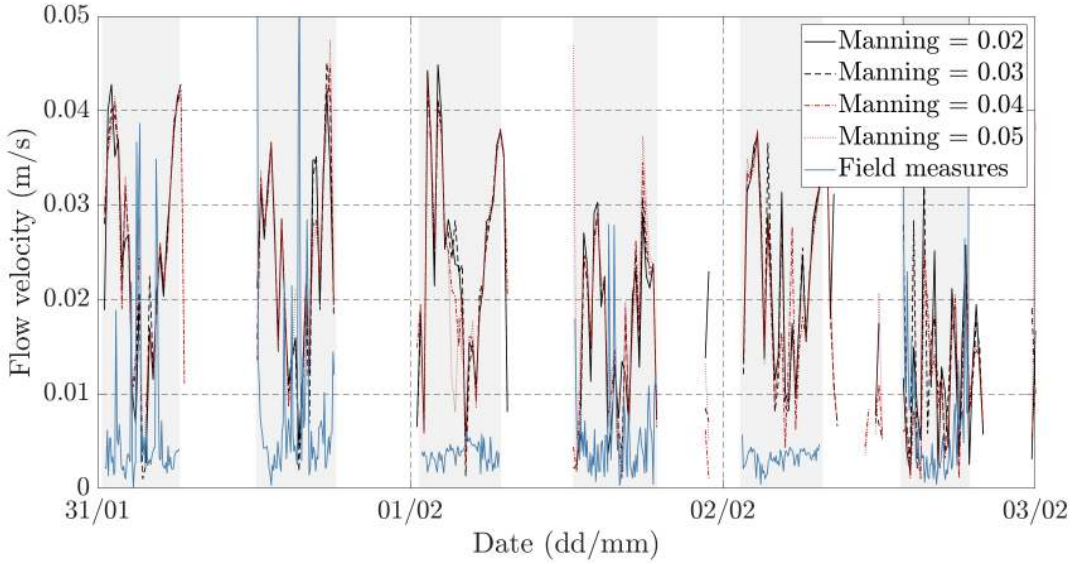

Figure 5.2: Modelled flow velocities with different Manning coefficients and observed flow velocities at the forest fringe location.

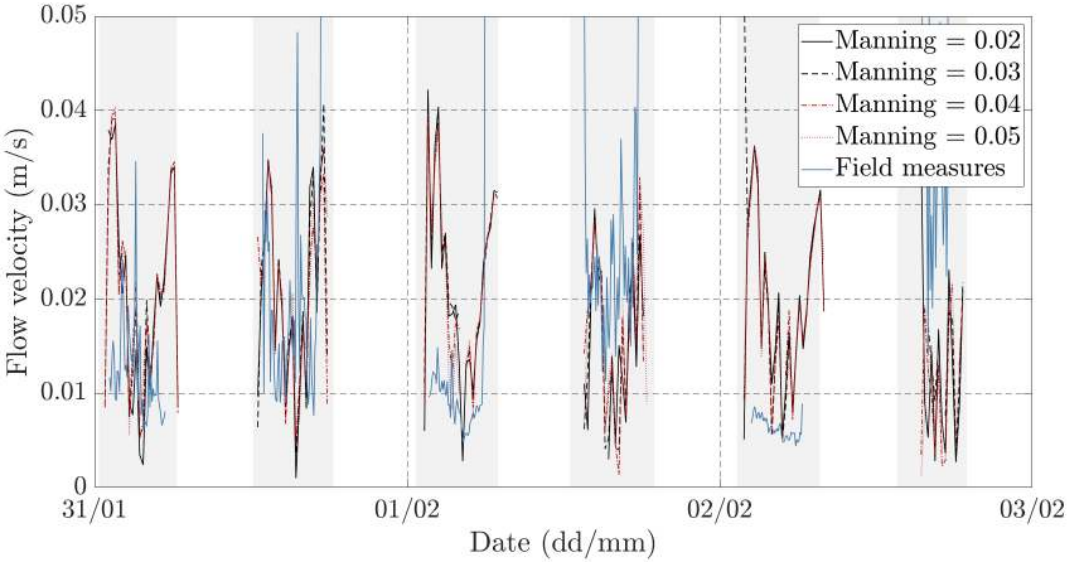

Figure 5.3: Modelled flow velocities with different Manning coefficients and observed flow velocities at the inland location.

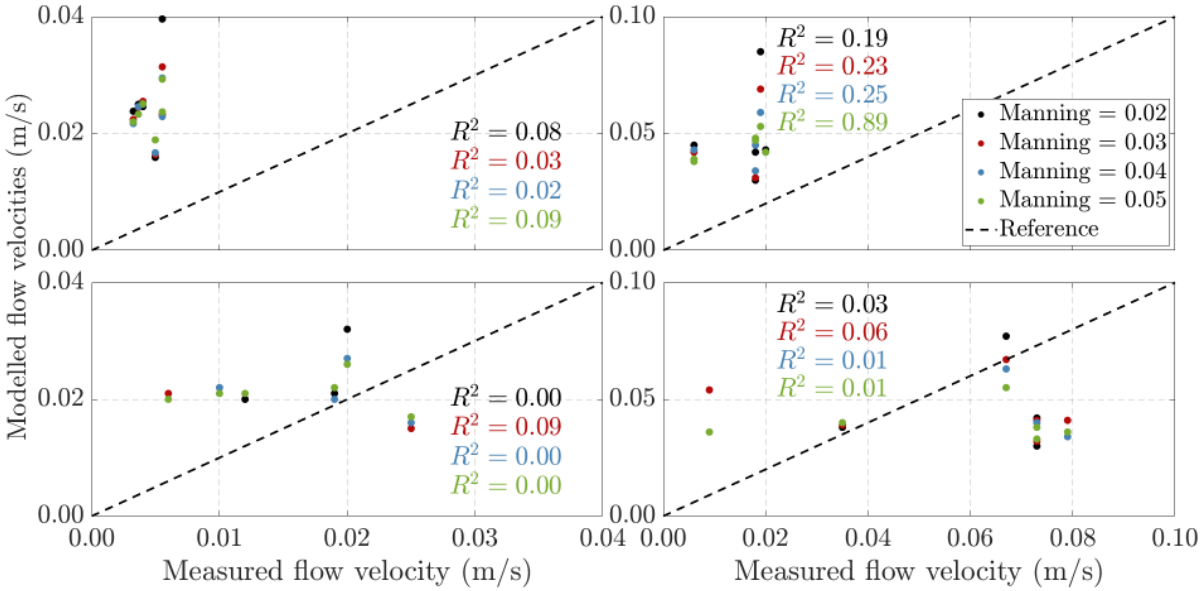

Figure 5.4: Modelled and measured average and maximum flow velocities for the first six inundation periods. Top left plot: average flow velocities forest fringe location. Top right plot: maximum flow velocities forest fringe location. Bottom left plot: average flow velocities inland location. Bottom right plot: maximum flow velocities inland location.

5.1.3 Wave calibration

On Table 5.1the modelled average significant wave height and the measured average significant wave height can be seen. As a constant wave boundary has been chosen, the average significant wave heights at both locations have been compared to the measured average significant wave heights. The applied boundary wave heights are ranging between 0.1 and 0.01. As can be seen on Table 5.1 the average significant wave heights are the closest to a boundary wave height of 0.02 m. This has been chosen to be the applied boundary wave height.

Table 5.1: Significant wave height calibration results

Wave height	H_s **forest fringe**	H_s **inland**
Measured	0.016	0.018
0.100	0.085	
0.030	0.028	
0.020	0.018	0.017
0.015	0.010	
0.010	0.009	0.008

5.1.4 Bed level change calibration

After the calibration of the current velocities and the waves, the bed level changes can calibrated. To do this, the critical erosion parameter $\tau_{cr,e}$ is calibrated. Model runs of 12 weeks have been used to calibrate this parameter. In Figure 5.5 the modelled weekly bed level changes are compared to the observed weekly bed level changes. The top plot represents the forest fringe location and the bottom plot represents the inland location. The R^2 values are not high for the inland location, and even lower for the forest fringe location. Lowering the critical erosion parameter only results in lower R^2 values. This would mean that a critical erosion parameter of $0.25 N/m^2$ would give the best result. The R^2 values however are not significantly strong for all erosion parameter. Although

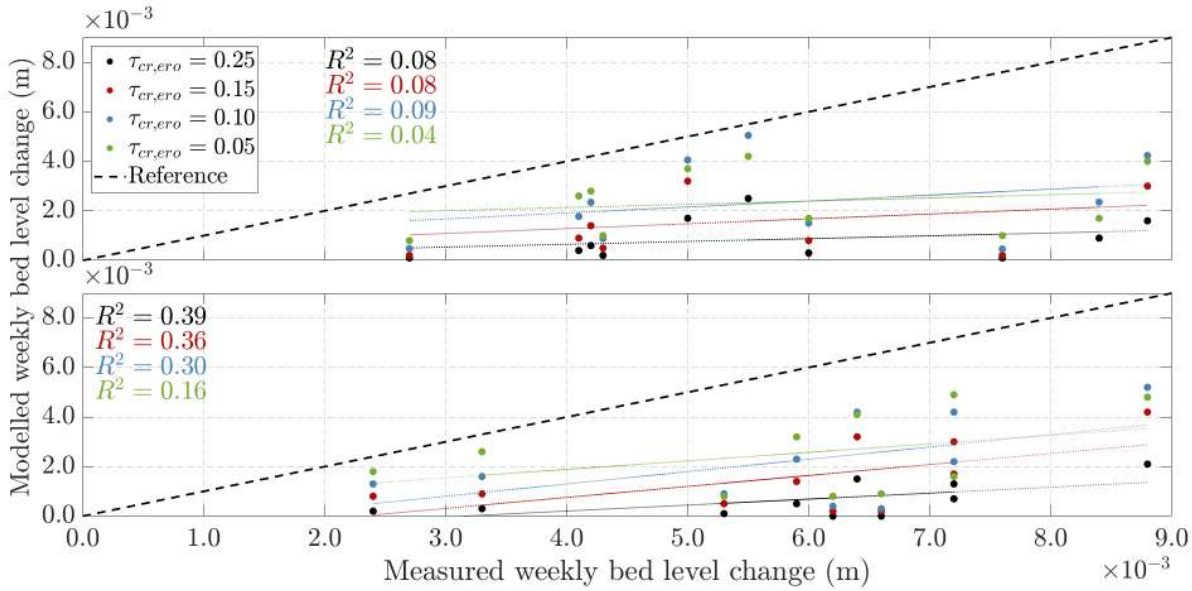

Figure 5.5: Calibrated weekly bed level changes for different critical erosion parameter settings, forest fringe (top) and inland (bottom) location.

a critical erosion parameter of $0.25 N/m^2$ gives the best R^2 values it is not significantly better than the other parameters. In Figure 5.6 the calibration results of the bed level changes for the forest fringe and inland location can be seen. As can be seen, the modelled weekly bed level changes with a critical erosion parameter of $0.25 N/m^2$ are really small (0 - 0.003 m). The observed bed level changes are way higher (0 - 0.009 m). So, if only the R^2 were taken into account, this value for the erosion parameter would be the best, however if also the values itself are taken into account, a critical erosion parameter of $0.05 N/m^2$ shows the best results.

The weekly bed level changes are approximately the biggest for a critical erosion pa-

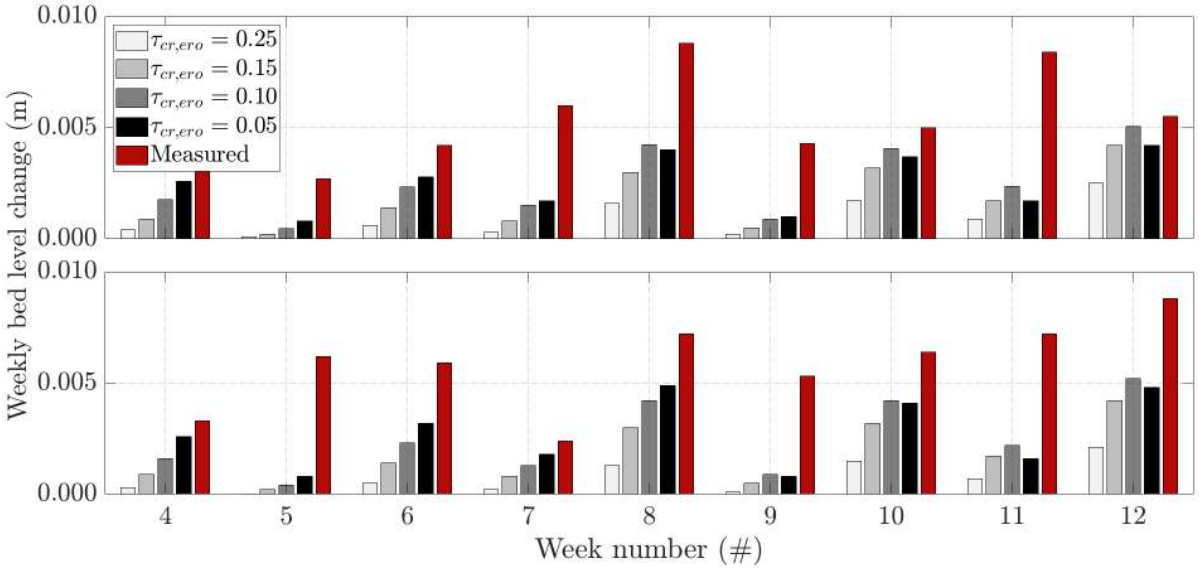

Figure 5.6: Modelled and measured weekly bed level changes for different critical erosion parameter values at the forest fringe (top) and inland (bottom) location.

rameter of $0.05 N/m^2$. However, at week 8,10, 11 and 12, the critical erosion parameter of $0.10 N/m^2$ shows the highest values. This is because no erosion occurs when using a value of $\tau_{cr,e} = 0.10\ N/m^2$ or higher. The difference between a value of 0.10 and 0.05 is not much. When using a $\tau_{cr,e} = 0.05\ N/m^2$ erosion does occur. Due to that, the best 'fit' for $\tau_{cr,e}$ is chosen to be $0.05\ N/m^2$. Still, the difference between the modelled and observed weekly bed level changes is quite significant, but they at least have the same order ($O^{-3}\ m/week$). Also, at the end of the period, week 10 - 12, the differences between the observed and modelled bed level changes gets lower. This might be due to the 'stabilisation' of the model.

5.2 Model validation

After the calibration, a full run was executed with the calibrated settings; the validation run. The length of the full run is 12 weeks, the same length as the fieldwork period and the bed level change calibration runs.

5.2.1 Modelled bed level changes

The modelled bed level changes at the forest fringe and the inland location can be seen in Figure 5.7. The bed levels have been subtracted by the original bed level elevation, so the change with the original bed level height is shown. As can be seen, the bed level changes mainly consist of accretion. Only small changes due to erosion can be observed. Furthermore, the accretion is higher for the forest fringe location compared to the inland location.

In Figure 5.8 the modelled water levels of the forest fringe location can be seen. If we compare Figures 5.7 and 5.8 we can see that the bed level changes increase as the water levels increase. So during spring-tide, the bed level changes are larger, compared to neap tide. During spring tide, the inundation period is longer. This means that sediment is longer transported land-inward and thus the bed level changes, as in accretion, are

larger. Also, the amount of sediment transport is more due to the increased water depth. Between 02-01 and 09-01, and 30-01 and 06-02, the water levels are really low. The water levels hardly reach the forest fringe location. But, during these low water levels, still waves of 0.02 can occur. During these low water levels, the orbital velocities near the bed are quite large. They are even that large that the soil erodes. These low water levels correspond to a decrease of the bed level changes, see Figure 5.7. A top view of the bed level changes for the whole model can be seen in Appendix H.

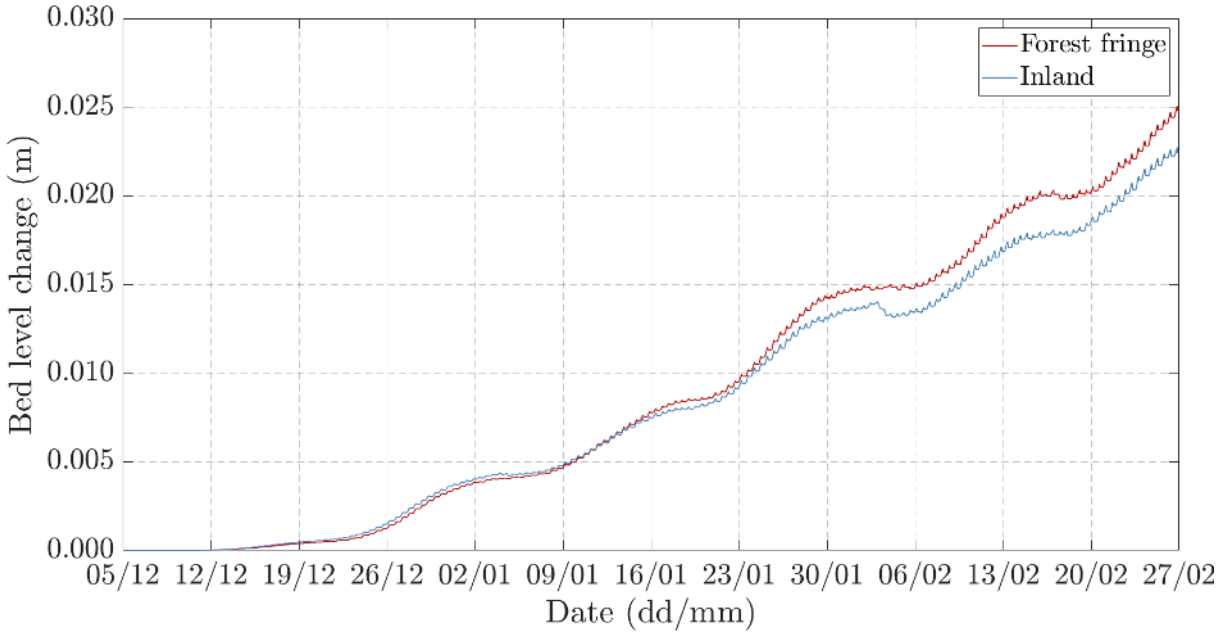

Figure 5.7: Modelled bed level changes since the start of the model run (05-12-2019).

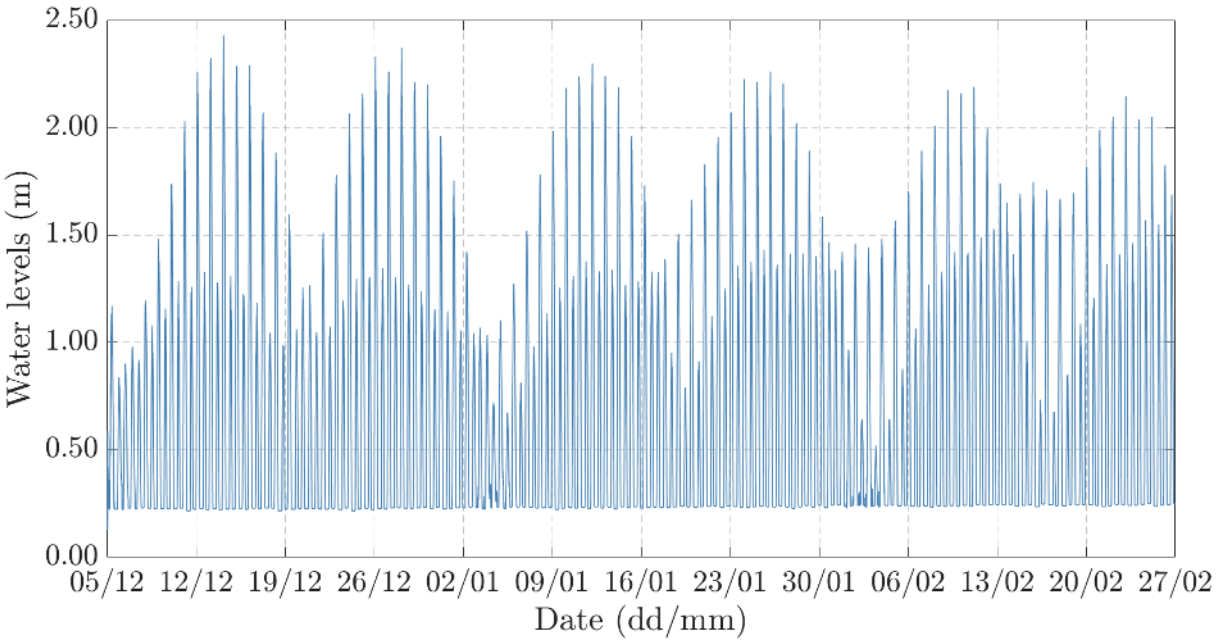

Figure 5.8: Modelled water levels for the forest fringe location.

Modelled seedling dynamics

As the transect is stretched out in x-direction, the number of seedlings get averaged in x-direction. So, for example: at y = 1600 m, a row of 100 cells of seedlings is modelled. The initial seedling fields are random, which means some cells contain seedlings, while other cells remain empty. To account for this, the average and the maximum number of seedlings at the representing forest fringe ($\approx y = 1600m$) and the inland ($\approx y = 1605m$) location have been determined. In Figure 5.9 on the top left plot left the average number of seedlings and the measured seedlings are shown. On the bottom left plot the average modelled seedling growth rate and the measured growth rate can be seen.

The modelled average (μ) number of seedlings is on average higher than the measured number of seedlings at the forest fringe location. At the inland location, the modelled average number of seedlings is lower compared to the measured number of seedlings. This can be seen at the values lying above and below the reference line. Both locations however do show good R^2 values (0.98 at the forest fringe and 0.97 at the inland location). At the forest fringe location, the highest modelled number of seedlings is the furthest away from the reference line. This is due to the initial plant density, which is randomised. A maximum initial plant density of 140 is chosen, based on field measurements. This value is thus at the beginning of the model run. Towards the end of the run, the modelled and measured number of seedlings gets close the reference line at the forest fringe location. The maximum number of seedlings, which can be seen on the top right plot Figure 5.9 again shows high correlation coefficient for both locations. Lower measured number of seedlings correspond better to the modelled number of seedlings than high measured number of seedlings. This is again due to the initial plant density. Both the maximum modelled number of seedlings at the inland and forest fringe location are at the beginning of the model run.

The growth rates for the average number of seedlings do not show a good correlation. The R^2 values are 0.12 for the forest fringe location and 0.05 for the inland location. This is somewhat strange as the modelled number of seedlings seems to be comparable to the measured number of seedlings. The growth rate is based on these number of seedlings, so should be similar to the measured growth rate. A possible reason would be the outlier at both the inland and forest fringe location (growth rates of 0.29 and 0.47). The maximum growth rate at the forest fringe and inland location can be seen on the bottom right plot of Figure 5.9. The R^2 value for the forest fringe location is quite good, while the R^2 value for the inland location does not represent a good correlation.

Additionally, plots for the whole transect have been made. The plots can be seen in Appendix H. The plots show the number of seedlings per week spatially. Throughout time, the number of seedlings decreases in generally. New seedlings can be observed at each time-step. This is again due to the random seedling establishment. Especially at y = 1600, the seedling survive longer compared to other locations. This is because the bed level changes are bigger around this y-value. The larger the bed level changes, the higher the growth rate. Only bed level changes greater than 9.4 mm, will lead to a positive growth rate. No bed level changes lead to a growth rate of 0.48, which means that more than half of the seedlings will die, see Figure 3.19.

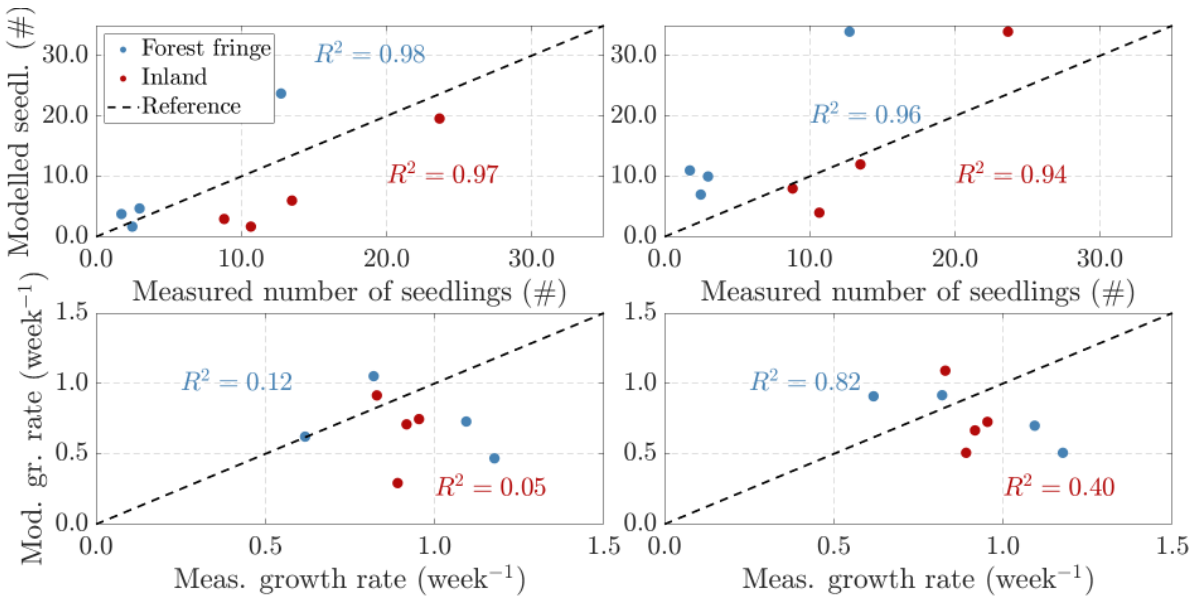

Figure 5.9: Scatter plot of measured and maximum and mean modelled number of seedlings. Top left: mean modelled number of seedlings. Top right: maximum modelled number of seedlings. Bottom left: mean modelled seedling growth rate. Bottom right: maximum modelled seedling growth rate.

5.3 Scenario results

Waves have been simulated using a constant wave boundary and a time dependent wave boundary. The constant wave boundary has 1 significant wave height for the whole model run, while the time dependent wave boundary is based on field results.

5.3.1 Constant wave boundary

Wave height have been increased to see the effect on vegetation and on bed level changes. Two runs with wave height of 0.10 m and 0.20 have been used to examine the effect.

Effect of increased wave heights on bed level changes

Waves do have effect on bed level changes. In Figure 5.10 the bed level changes for the increased wave scenarios for the forest fringe and inland location can be seen. Where the initial model run, with a constant wave height of 0.02 m, mainly showed bed level changes due to accretion, the model runs with constant wave heights of 0.10 and 0.20 m not only show accretion, but also erosion. For both the 0.10 and 0.20 m wave height runs the bed level slowly increases by 0.01 m for a wave height of 0.10 m and 0.05 m for a wave height of 0.20 m. Erosion is much more dominant in the increased wave height runs. Furthermore, there is a trend visible where erosion is larger than accretion due to the spring-neap tide. Also, during the first noticeable bed level changes, the erosion and accretion rates occurring at each tide are lower compared to the end of the simulation. It also seems that the erosion and sedimentation rates per tide are somewhat similar for the increased wave runs. The erosion and accretion rates per tide are also slightly bigger at the forest fringe location compared to the inland location.

The weekly bed level changes are slightly different for the increased wave height runs.

In Figure 5.11 the differences can be seen between the different wave height runs and the measured weekly bed level changes. The plot shows that the correlation is again bad for all runs at both locations. This is due to the weekly differences between consecutive weeks. Where a constant wave height of 0.02 m shows differences between consecutive weeks, constant wave heights of 0.10 m and 0.20 m do not show these weekly differences. This means that the correlation will not increase. The modelled bed level changes for a wave height of 0.10 m are generally more comparable to the observed bed level changes, see Figure 5.12. The net accretion is not that great for either the 0.10 as the 0.20 m wave height runs (0.005 and 0.01 m respectively). So, comparing with the measured bed level changes, a wave height of either 0.10 m or 0.20 m gives a better representation for the bed level changes compared to a constant wave height of 0.02 m.

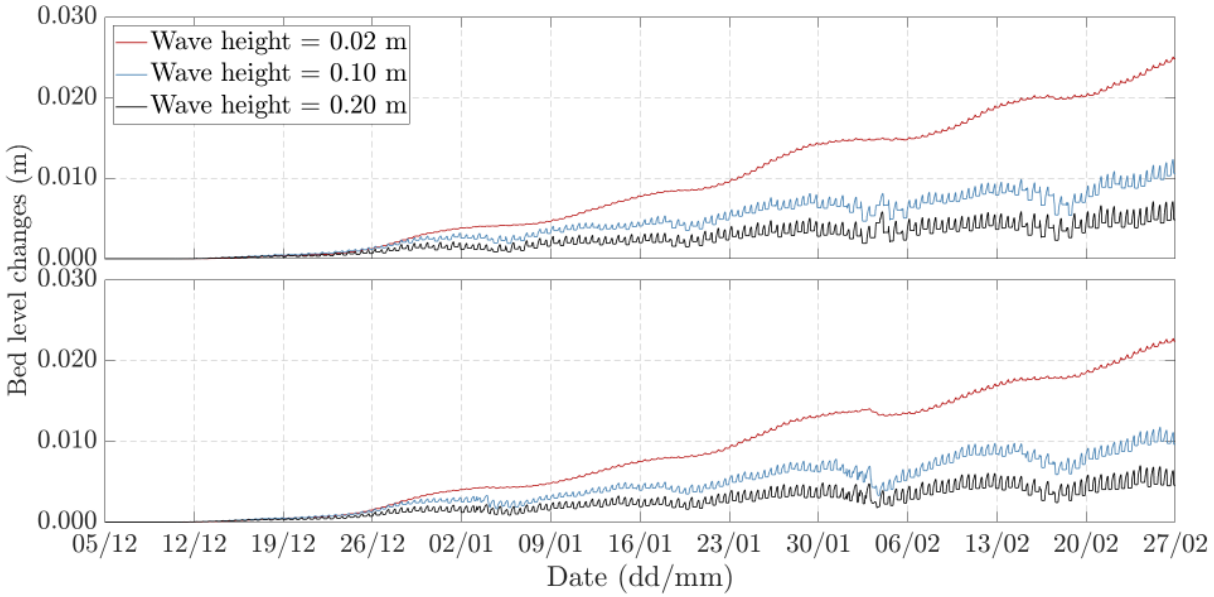

Figure 5.10: Bed level changes for the forest fringe (top) and inland location (bottom) for different wave scenarios.

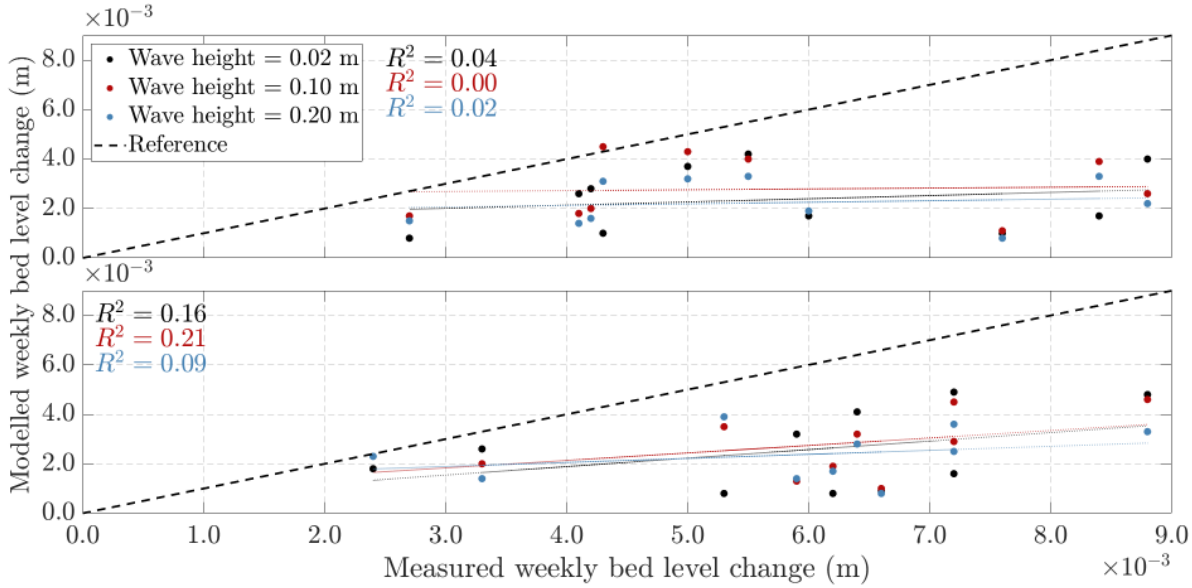

Figure 5.11: Weekly modelled and observed bed level changes for the forest fringe (top) and inland location (bottom) for different wave scenarios.

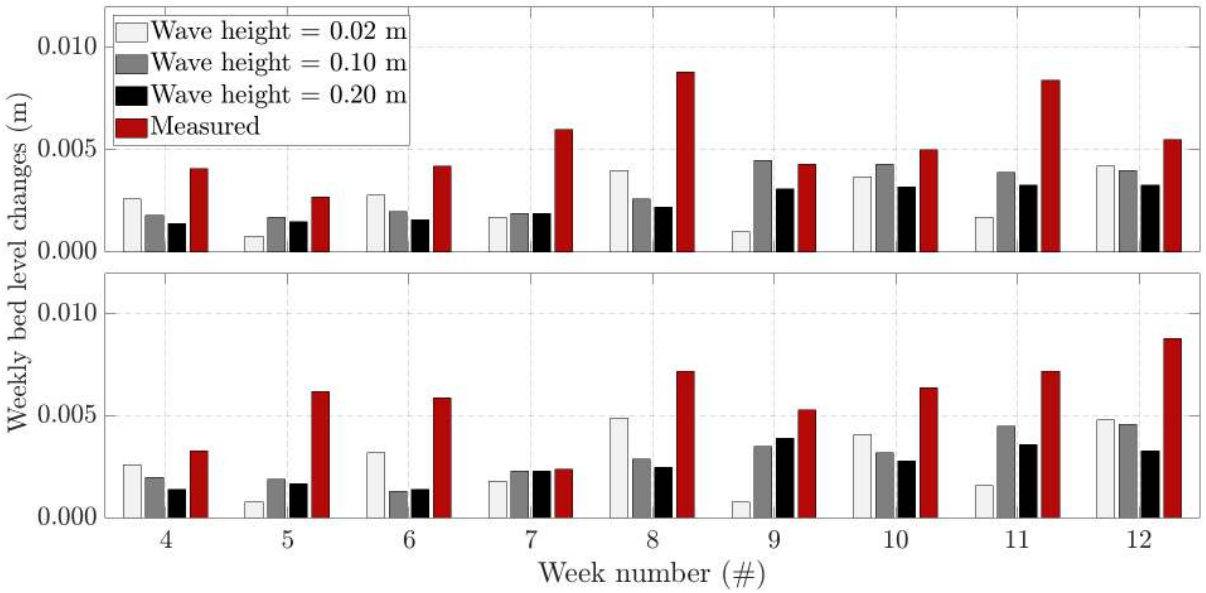

Figure 5.12: Weekly bed level changes for the forest fringe (top) and inland location (bottom) for different wave scenarios bar plot.

Effect of increased wave heights on seedlings

The average number of seedlings and the growth rate for the different wave height runs, the original model run and the measured seedlings and growth rates can be seen in Figure 5.13. On the left top plot the average number of seedlings at the forest fringe location (left) and the inland location (right) are shown. The increased wave height does not seem to have a large effect on the number of seedlings. Only one of the data points acts as an outlier at the forest fringe location. The value of this outlier increases for both wave heights. At the inland location again only one data point shows a significant difference for each wave height. The R^2 values for both the inland as the forest fringe location for both 0.10 m as 0.20 m waves are similar to the R^2 values of the original waves. The R^2 values can be seen in Table 5.2.

Table 5.2: Coefficient of determination for increased constant wave heights

R^2 values	Avg. nr. of seedlings (#)	Max. nr. of seedlings (#)	Avg. growth rate (week^{-1})	Max. growth rate (week^{-1})
H = 0.02 m				
Forest fringe	0.98	0.96	0.12	0.82
Inland	0.97	0.94	0.05	0.40
H = 0.10 m				
Forest fringe	0.99	0.95	0.00	0.03
Inland	0.96	0.82	0.59	0.37
H = 0.20 m				
Forest fringe	0.99	0.98	0.16	0.23
Inland	0.95	0.89	0.56	0.32

The growth rates of the average number of seedlings can be seen at the bottom plots, with left again the forest fringe location and on the right side the inland location. The maximum growth rate at the forest fringe location shows a high R^2 value. However, the average growth rates do not show high correlations for all wave scenarios. Only at the inland location for both the 0.10 m and 0.20 m wave height scenarios, the average growth rate R^2 values are decent (0.59 and 0.56). The R^2 for the maximum number of seedlings does not change significantly for all runs. This means that the number of seedlings does not change for increased constant wave heights. This is because, the number of seedlings are correlated with the measured number of seedlings. The spatial view of the number of seedlings per cell can be seen in Appendix H.

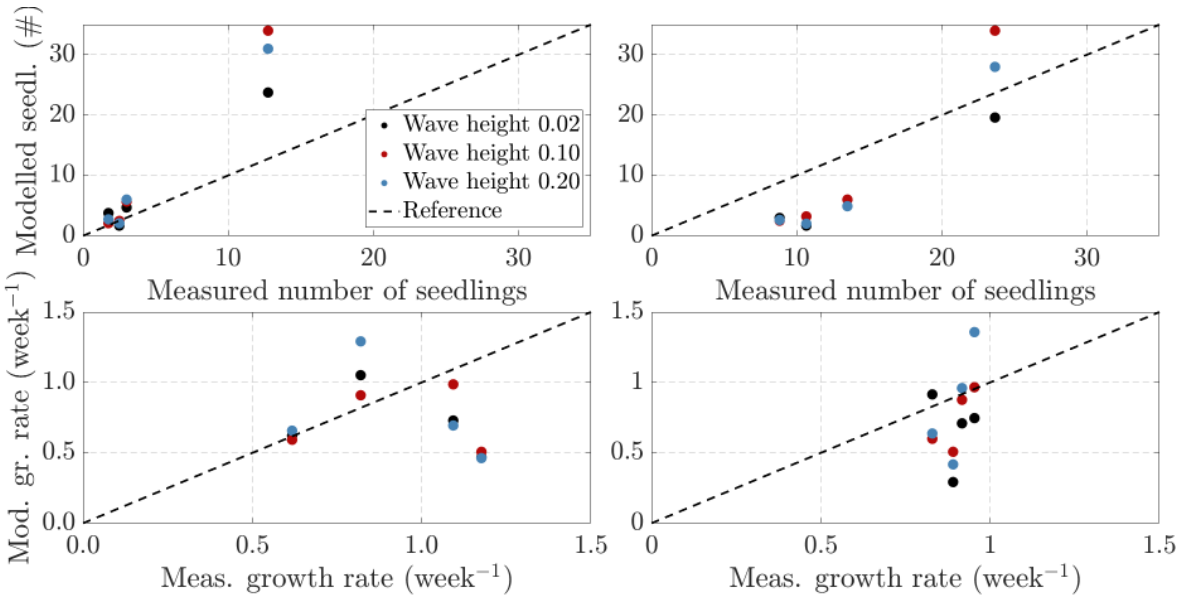

Figure 5.13: Modelled average number of seedlings for different constant wave height scenarios. Top left plot shows the average number of seedlings for the forest fringe location. Top right shows the average number of seedlings for the inland location. Bottom left shows the growth rate for the forest fringe location and bottom right for the inland location based on the average number of seedlings

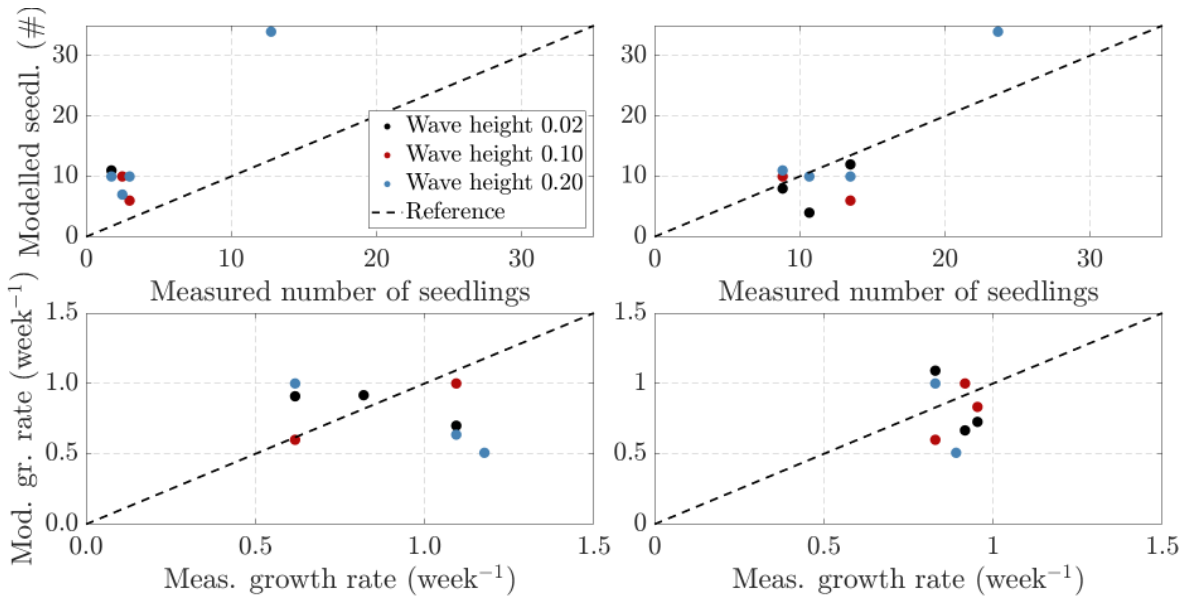

Figure 5.14: Modelled maximum number of seedlings for different constant wave height scenarios. Top left plot shows the maximum number of seedlings for the forest fringe location. Top right shows the maximum number of seedlings for the inland location. Bottom left shows the growth rate for the forest fringe location and bottom right for the inland location based on the maximum number of seedlings.

5.3.2 Variable wave boundary

Effect of the increased time dependent wave heights on bed level changes

The (increased) time dependent wave heights seem to have no impact on the number of seedlings. However, the (increased) time dependent wave heights do affect bed level changes. In Figure 5.15 the bed level changes due to the increased time dependent waves are shown. As can be seen in Figure 5.15, the bed level changes for the constant wave height of 0.02 m are only due to accretion. For the time dependent wave runs, bed levels change not only due to accretion but also erosion is visible. Especially between 30-01-2020 and 06-02-2020 quite some erosion can be observed. Until approximately week 8, all lines are somewhat similar. After that quite some changes can be noticed, with a time dependent wave height twice as high as the original time dependent wave height showing the maximum changes.

In Figure 5.16 the weekly bed level changes can be seen for the different variable wave scenarios and the measured weekly bed level changes. The R^2 values show that that there is almost no difference between the increase time dependent wave scenarios and show similar results. This is for the forest fringe location as well as the inland location. Furthermore, the data points on Figure 5.16 do not variate significantly for the different runs. All in all can be concluded that the increased variable wave heights do not show changes in the weekly bed level changes.

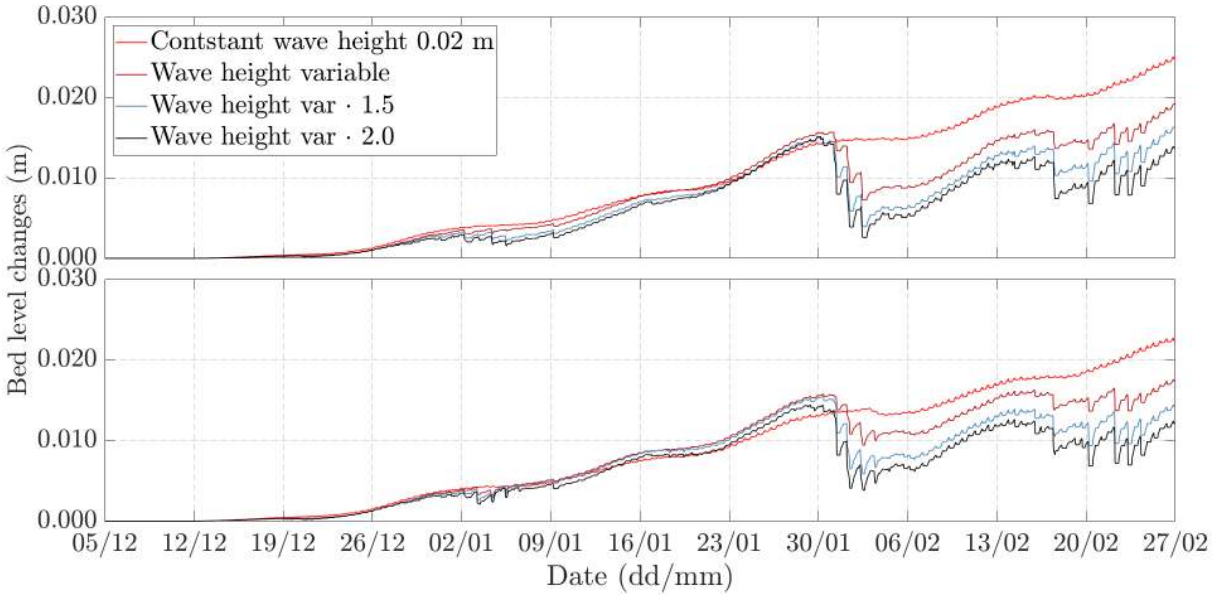

Figure 5.15: Bed level changes for the forest fringe (top) and inland location (bottom) for different time dependent wave scenarios.

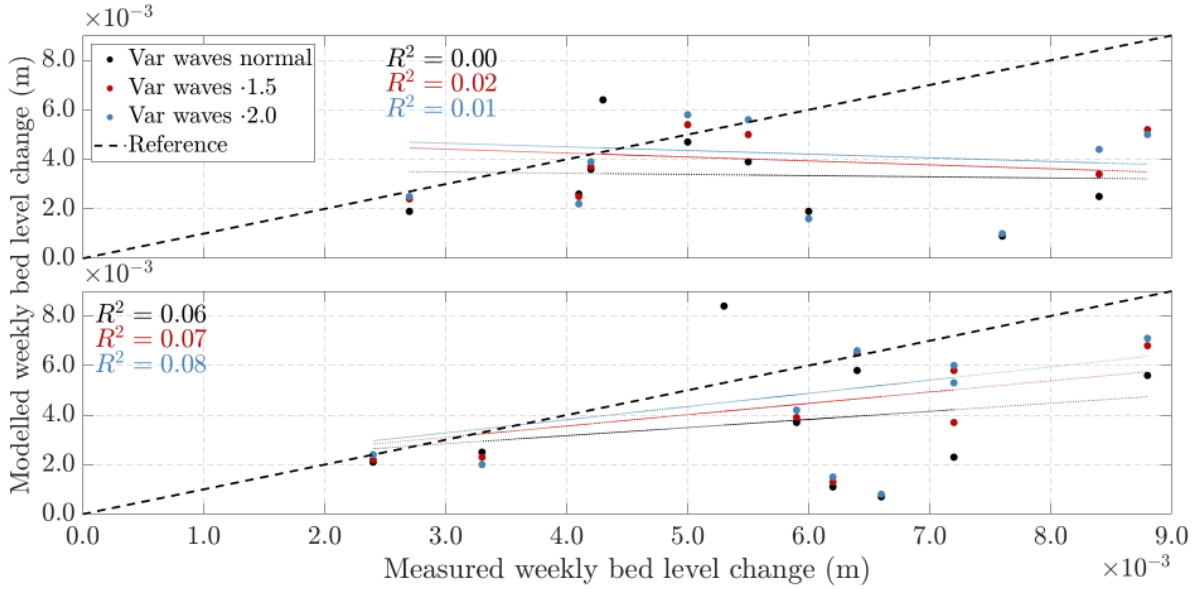

Figure 5.16: Weekly bed level changes for the forest fringe (top) and inland location (bottom) for different time dependent wave scenarios.

Effect of the (increased) time dependent wave heights on seedlings

In Figures 5.17 and 5.18 the average and maximum modelled number of seedlings for different time dependent wave variables for the forest fringe and inland locations can be seen. On first sight there seem to be no significant differences between an increase of the time-dependent waves. The data points on the top left and top right plot of Figure 5.17 are overlapping. The average growth rate does show some changes. On Table 5.3 the R^2 values for the mean and maximum number of seedlings and growth rates of the forest fringe and inland location can be seen. Again, the R^2 values for the average and maximum number of seedlings is similar for all runs. This thus shows that the number of seedlings is somewhat the same for all runs. The growth rate does not show high R^2 values.

Table 5.3: Coefficient of determination for (increased) time dependent wave heights

R^2 **values**	**Avg. nr. of seedlings (#)**	**Max. nr. of seedlings (#)**	**Avg. growth rate (week^{-1})**	**Max. growth rate (week^{-1})**
$H = var$				
Forest fringe	0.99	0.98	0.01	0.10
Inland	0.96	0.98	0.43	0.27
$H = var \cdot 1.5$				
Forest fringe	0.99	0.99	0.10	0.07
Inland	0.92	0.96	0.39	0.45
$H = var \cdot 2.0$				
Forest fringe	0.98	0.99	0.00	0.01
Inland	0.96	0.92	0.30	0.12

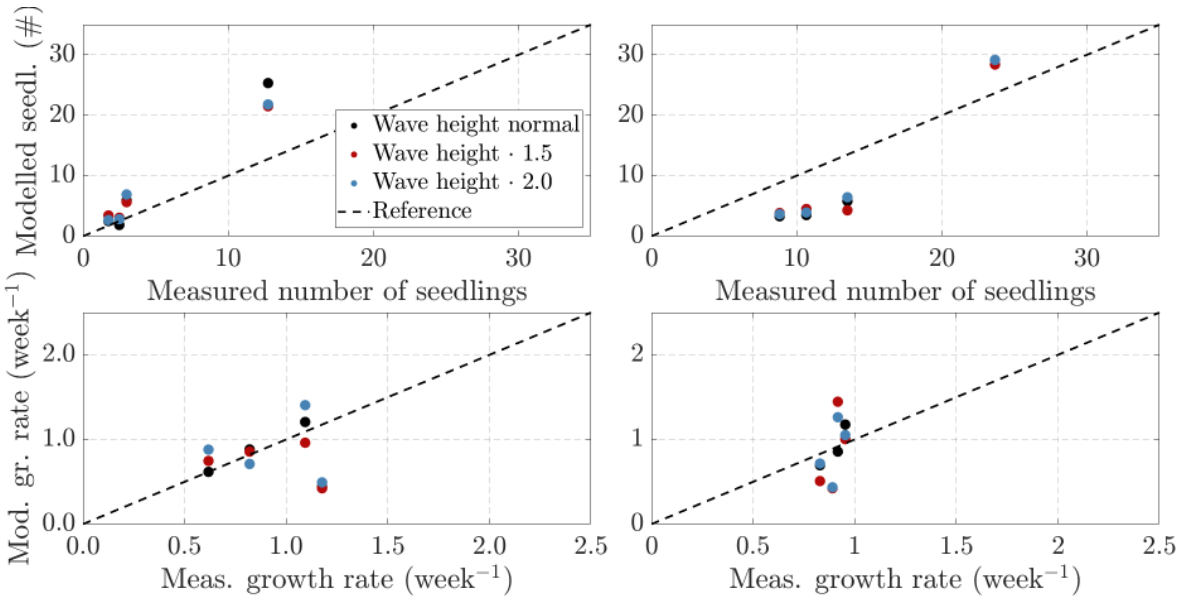

Figure 5.17: Modelled average number of seedlings for different time dependent wave height scenarios. Top left plot shows the average number of seedlings for the forest fringe location. Top right shows the average number of seedlings for the inland location. Bottom left shows the growth rate for the forest fringe location and bottom right for the inland location based on the average number of seedlings

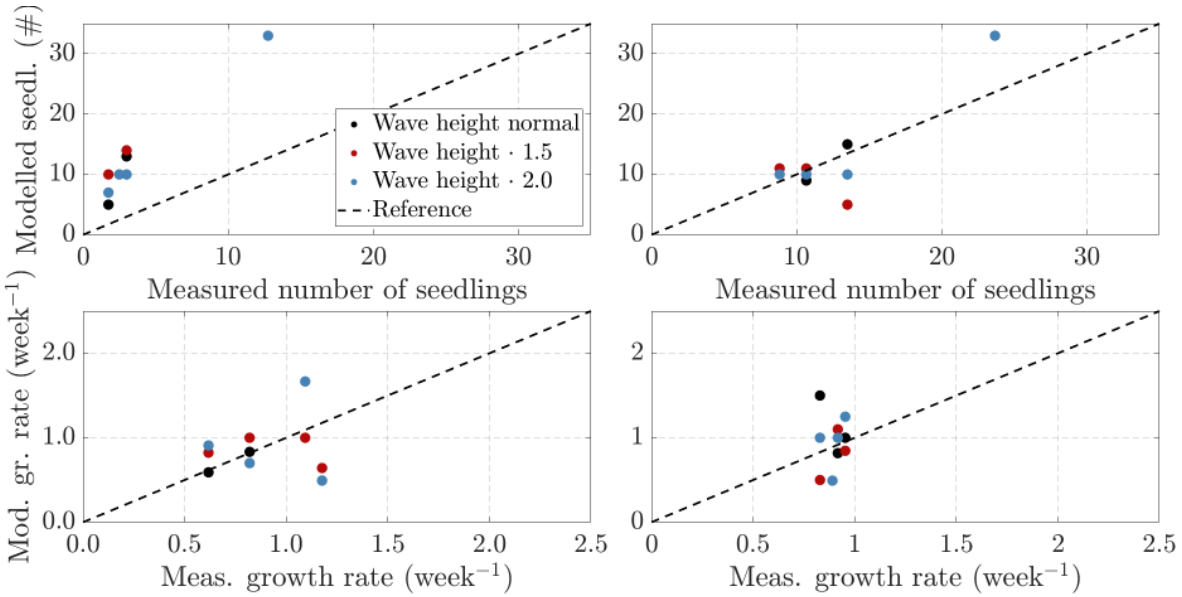

Figure 5.18: Modelled maximum number of seedlings for different time dependent wave height scenarios. Top left plot shows the maximum number of seedlings for the forest fringe location. Top right shows the maximum number of seedlings for the inland location. Bottom left shows the growth rate for the forest fringe location and bottom right for the inland location based on the maximum number of seedlings.

Chapter 6

Discussion

This research studied the effects of bed level changes and waves on vegetation establishment in the Sungei Buloh Wetland Reserve mangroves in Singapore. This chapter will present the limitations and implications of this study. Fieldwork, data processing and modelling will be the main focus of this chapter.

6.1 Bed level changes

A Delft-FM model was used with a new vegetation module to simulate the growth of mangrove seedlings for a transect of the Sungei Buloh Wetland Reserve mangroves in Singapore. The vegetation module is based on the Population Dynamics principle of Temmerman et al. (2007). A empirical formula was formulated in order to simulate seedling growth as a function of bed level changes. Additionally, different wave scenarios have been created to see the impact of an increase and variable waves on bed level changes and seedling growth.

Flow velocities, measured at the forest fringe and inland location, were calibrated for different Manning Coefficients. The model did not show good R^2 values for each of the different values of this coefficient. The measured flow velocities, on average between 0 - 0.02 m/s, which is similar to measurements at the Mandai mangroves at the back of the forest and the creek location (Willemsen et al., 2016). Nevertheless, the modelled flow velocities were still too high at the forest fringe location. At the inland location, flow velocities were more accurate to the measured flow velocities, although the R^2 did not show that.

Waves were calibrated with constant wave heights at the boundary. Applying a constant wave boundary of 0.02 m results in modelled significant wave heights (H_s) of 0.018 and 0.017, where 0.016 and 0.018 were measured, which shows that wave were calibrated fairly well. Bed level changes were calibrated for different critical erosion parameter values ($\tau_{cr,ero}$). An increase of ($\tau_{cr,ero}$) resulted in better comparable values to the measured weekly bed level changes. However, the model shows difference between sequentially weeks. This is however not shown in the field and is more 'random'. Furthermore, a value of $0.05 N/m^2$ has been chosen to be the best fit. This is a factor 10 lower compared to the critical erosion parameter used in the Mandai model Willemsen et al. (2016). Horstman et al. (2015) did however use a value of $0.10 N/m^2$ for their model.

An increase of wave heights did not lead to a significant difference of the weekly bed level changes. Increasing waves did show erosion, which, if the model continued to run, would let to even more erosion (Winterwerp et al., 2013). This then would concave-up the mudflat profile, which leads to a loss of mangrove habitat and an increase of waves Winterwerp et al. (2013).

The initial model run showed mainly bed level changes due to accretion. Only 1 - 2 mm of erosion can be observed at the inland location. Furthermore, the magnitude of the weekly bed level changes were in line with the observed bed level changes ($O^{-3}m/week$). Variable wave heights do show erosion. Erosion is measured at both locations, so variable waves seem more realistic to use in the model. However, the model shows mainly accretion the first 8 weeks. After those 8 weeks, the model shows accretion and erosion rates. A solution would be to run the model for a longer time and start $\approx$ 8 weeks earlier, so the erosion and accretion rates would be visible at the start of the model run. Additionally, if the modelled flow velocities would be more in line with the observed flow velocities, different accretion and erosion rates would be visible. In extent, a calibration of the settling velocity and implementing field based sediment characteristics, would be an improvement for the model.

6.2 Vegetation development

The modelled number of seedlings show a high coefficient of determination (R^2) with the measured number of seedlings. An increase of the wave heights, or variable wave heights, does not change the R^2 values. However, the growth rate for both the maximum and mean number of seedlings, has no high (R^2) values. This means that the number of seedlings is strongly influenced by the random establishment of the seedlings and not that much by the growth rate as a function of the bed level changes. So, the added random establishment of seedlings compensates the number of seedlings described by the empirical relation.

The found relationship between the observed bed level changes and seedling growth is somewhat unexpected. The growth rate and the observed bed level changes show a positive correlation. Thus, when the bed level changes increase, the growth-rate increases. This is the opposite of what Balke et al. (2013) found. They found out that if the bed level changes increase, as in erosion or accretion, the percentage of seedling survival decreases. Their research is however based on experiments. Also, they implemented erosion and accretion as a sudden change, while in reality, at the measured site and during the measured time, this is no sudden change as this happens more gradually. Furthermore, they applied erosion and accretion rates of 1 cm and 2 cm. Field measurements show that these values are a bit too high as a 1 cm bed level change only occurred once, at the beginning of the fieldwork period. Additionally, Balke et al. (2013) found that erosion causes a stronger decrease in the percentage of seedling survival compared to accretion. During this fieldwork period accretion was observed more frequent than erosion, which might indicate why there is still a positive relation between the seedlings and bed level changes.

Swales et al. (2007) measured mangrove seedlings and propagules at the First of Thames mangroves in New Zealand. Interesting to see is that they measured a strong decrease of the number of seedlings, which is comparable to the measured and modelled number of

seedlings. Furthermore, as seedlings grow they develop more leaves. Swales et al. (2007) found out that seedlings, with a higher number of leaves, have a higher change of surviving. This has been shown as well in the fieldwork part of this research. The diameter, height and the number of leaves increased in time.

Balke et al. (2015) modelled seedling establishment via the Windows of Opportunity principle. The first window, WoO1, describes what hydrodynamic forces are critical that prevent seedling from growing and establishment. WoO2 has the same principle as WoO1, but is not focuses on hydrodynamic forces but on erosion. A critical erosion parameter is used to model the survival of the seedlings. Additionally, wind speeds, water levels and suspended sediment concentration were also used in WoO2 (Balke et al., 2015).

Where in the past already quite some models were made to simulate physical processes in mangroves Broekema (2013), Horstman et al. (2015), Willemsen et al. (2016), this is (one of the) first models that simulates seedling establishment. Where the previously mentioned models were used to simulate mainly the physical processes, this is an extra addition to the dynamics that can be modelled.

6.3 Limitations of this research

6.3.1 Fieldwork

The first part of this study was mainly focused on getting field data out of the SBWR mangroves in Singapore. The main focus of the field work was transect A, which is located near the Kranji Nature trail, see Figure 2.2. Observed field results thus only show the dynamics measured at this transect. Furthermore, only one other transect has been used to measure hydro- and morphodynamics. This transect (C) is however not comparable to transect A, as it is much longer and does not show the same vegetation characteristics. Also, this transect only produced data for approximately 1 month, while the other transect presents data for a total of approximately 3 months.

Transect A was close to the location where NParks, the manager of the mangrove forest, planted seedlings. These seedlings were placed before the fieldwork period started. This might be the reason why the number of seedlings was that high during the first fieldwork day. It might also be just the moment where a lot of seedlings drop from the mangrove trees. Thus, observed vegetation dynamics might not be representative for the naturally behaviour of the mangrove area. Also, these newly planted seedlings might interfere with the naturally existing seedling. This might result in possible lower vegetation characteristics as height, diameter and the number of leaves, as these seedlings will be relatively young. Also, the seedlings were collected at two transects, close to each.

Soil samples were collected at transect A and C. Initially the plan was to analyse those soil samples to find the sediment characteristics of these locations. However, due to some unforeseen circumstances, the soil samples were not able to be analysed. This caused that the sediment characteristics of the Mandai model had to be used Willemsen et al. (2016). These characteristics are however from the Mandai mangrove area, which is east of the Sungei Buloh mangroves. The sediment characteristics might not be 100 % accurate for the measured area. Grain sizes and the density might be different for both locations. This

can change the settling velocity, as well as the critical bed shear stresses in the model. The elevation data of the field-site is not collected. The bathymetry is thus not validated and updated. The bathymetry used in the model is the bathymetry from the Mandai model (Willemsen et al., 2016). Especially this part of the mangroves was not that accurate as it is fairly new.

The Tilt Current Meter (TCM) data showed some weird rotation happening. There was almost a 180° rotation between both TCMs. There might me some weird rotation going on between the stop bank and the row of wooden poles, or the settings of the TCMs might not be correct. Additionally, the TCMs were only used for one fieldwork period. It would have helped if the TCMs were used one more period to see if the difference is the same for both periods. Additionally, the most seaward TCM produced very low flow velocities. The calibration of the flow velocities showed that for the land-side location the flow velocities were pretty similar for both the modelled and measured velocities. The modelled flow velocities at the seaside location did not match the measured ones. Unknown is what this caused. The TCM might produce to low current speeds.

6.3.2 Modelling

The model grid is a rectangle with a cross-section that does not change in long-shore direction. Initially the Mandai model would be used and adjusted. So, the Sungei Buloh mangroves would be the main focus point of the model. The adjusted Mandai model did however not work properly for this case and a more simple option had to used. The salt-marsh model was used as the base. The bathymetry of transect A was used to represent the area. However, this transect did not have the most accurate bathymetry of the original model. Due to this, the used transect was not very accurate. Via linear interpolation to transect height was determined. A representative height profile of the transect would definitely improve to model.

No real sensitivity analysis has been executed. The input values for the sediment properties for example might not be totally accurate for the Sungei Buloh mangroves as these were conform the Mandai model (Willemsen et al., 2016). It would be useful to investigate the sensitivity of such parameters as the settling velocity and other sediment characteristics. Additionally, the erosion parameter and the critical bed shear stress for sedimentation have not been modified. Only the critical bed shear stress for erosion has been tweaked as almost no erosion was occurring.

6.3.3 Vegetation modelling

Seedling are modelled via the Python module. The module allows interaction between the Python script and exchangeable parameters of Delft-FM. Currently, only one type of vegetation can be modelled. The seedlings, modelled in Python, are not put back in Delft-FM model. Although seedlings have low impact on flow velocities and waves, they contribute in a small way to flow separation, downward flow and create vortices, which also affect sediment transport Le Minor et al. (2019). Although their impact is minimal in comparison with for example *Rhizophora* trees, it would be interesting to see what their actual contribution is to the reduction of flow velocities and to sediment transport and bed level changes.

The vegetation module strongly depends on the random field of seedlings at the start of the model. Furthermore, random seedling establishment has also been put in the model. This influences the number of seedlings per cell. The measured number of seedlings at both the inland as the forest fringe location were compared with the average and maximum number of seedlings cross-shore. So, not only one cell was taken into account, but a total of 100 cells. The growth rate should initially be calibrated based on the fieldwork. However, the random establishment of seedlings seems to be determinant for the number of seedlings in each cell. So, in fact the growth rate is only used for the mortality of seedlings, while the random establishment account for the grow of the number of seedlings. For future research, the random establishment should be monitored. This research mainly focused on the growth rate, which was mainly negative (mortality). Interesting and a contribution to the model would be implementation of this random establishment, based on field measurements.

6.4 Applicability

This Thesis contributes to the general knowledge about biophysical interactions of mangrove forests. The model that is made can be used for other locations within the Sungei Buloh mangroves, or other mangroves. Nevertheless, it is based on field measurements which need to be gathered for other locations as well to calibrate the model. The Mangrove Dynamics Model is one of the first biogeomorpholgical model for mangroves. The model principle is strongly based on the earlier developed models for saltmarshes Odink (2019), Van den Broek (2020). These models however are thus used for saltmarshes.

The model gives information about the effect of both hydro- as morphological forces on seedling establishment. The model, and the found relations (based on fieldwork), can contribute to mangrove restoration projects. These project are important, not only for their ecological benefits, but also their use in nature based solutions for coastal protection Temmerman et al. (2013). Interesting would be the effect of artificial structures on seedling dynamics. Siemes et al. (2020) showed that these artificial structures minimise erosion and simulate salt marsh growth. As saltmarshes are somewhat the low-latitude variant of mangroves, these structures might also work for mangrove areas.

Observed bed level changes showed an increase of the bed level of approximately 0.02 m at the inland location. One of the key strategies for rehabilitating eroding mangrove-mud coasts is to trap sediment (Winterwerp et al., 2013). This can be done by placing permeable groins, which of the row of poles have a similar purpose. Additionally, Anthony and Gratiot (2012) described that a loss of the mangrove are, results in coastal erosion. Combining the research of Winterwerp et al. (2013) and Anthony and Gratiot (2012), the use of the row of poles might be crucial for further development of mangroves. This research also shows that seedlings establish and keep growing, even at the forest fringe location. So, potentially this research can contribute to see what mangroves can further develop based on bed level changes.

Chapter 7

Conclusion

The aim of this research was to understand the feedbacks between hydro- and morphodynamic stresses on mangrove seedling dynamics, on a short- to mid- (months) term timescale, and to predict how these feedbacks affect the development and resilience of a mangrove forest fringe over the coming half year. To reach this aim, one main research question, three research questions and multiple sub-research questions were drafted. The main research questions was:

What is the impacts of waves, over a period of months, on the bed-level changes and their combined impact on seedling establishment in the mangrove forest fringe of the Sungei Buloh Wetland Reserve in Singapore?

7.1 Driving factors of bed level changes

Research question: *What are the driving factors of the observed bed level changes in the Sungei Buloh Wetland Reserve mangroves from the 5th of December 2019 till the 27th of February 2020?*

The maximum inundation periods at the inland location was 360 minutes, while for the forest fringe location this was 550 minutes. Overall, the inundation periods were 70 to 100 minutes longer at the forest fringe location compared to the inland location. Wave observations show a maximum significant wave height H_s of 0.13 m for the forest fringe location and 0.15 m for the inland location. Waves get attenuated during some time periods, but in general the waves get amplified due to shoaling. Current velocities, measured only in the last fieldwork period, reach speeds of 2.00 cm/s. On average the flow velocities at the inland location lay between 0.25 and 1.00 cm/s, while for the seaside the flow velocities lay between 0.50 and 1.50 cm/s.

Surface accretion and erosion cause the bed level to rise at the inland location by approximately 2 cm, while for the forest fringe location the bed level does not change that much in general. All in all, weekly bed level changes range between a few millimetres to one centimetre as a maximum. The bed level changes are mainly caused by a combination of low water levels and waves at the inland location. At the forest fringe location also bed level changes occur due to an increase of wave heights and increased flow velocities.

7.2 Relation between hydro- and morphodynamics on seedling establishment

Research question: *What is the relation between spatial variation regarding the observed tidal currents,waves and bed level changes and seedling establishment?*

Seedlings have been measured at two locations; the forest fringe location and inland location. Both locations showed a decrease of the number of seedlings during the whole fieldwork period. At the inland location the number of seedlings ranged between 13 and 2 per average plot, while for the inland location the number of seedlings ranged between 30 and 9. The height and diameter of the seedlings increases as the number of seedlings decreases. This is because the strongest seedlings survive and the seedlings keep growing. The height at the inland location ranged between 13 and 14 cm, while the height at the forest fringe ranged between 12 and 24 cm. A height of 24 cm is due to the tall surviving seedlings. The tallest height and thickest diameter correspond to a low number of seedlings. Additionally, the number of leaves per seedling also increases as the number of seedlings decrease.

The inundation and bed level changes have been found out to be driving factors of seedlings establishment (Balke et al., 2015, 2013). Additionally, waves were found out to be driving factors of bed level changes and thus influence seedling establishment indirectly and directly. These three processes have been determined to be the main driver of seedling establishment.

7.3 Seedling dynamics parametrizations

Research question: *How can the relation between waves, tides and bed level changes and seedling establishment be translated to model parameterizations and be integrated with the Delft3D Flexible Mesh model?*

Seedling establishment is mainly correlated with bed level changes. The effect of the inundation period, waves and bed level changes has been researched. The inundation period has effect on waves and bed level changes, but is not directly related to seedling establishment. This has been confirmed with the Multiple Linear Regression (MLR) fit. Additionally, waves are not directly related to seedling establishment. The MLR showed that, if p-values are taken into account, that the best relation to parametrize seedling establishment is based on bed level changes only. Combining bed level changes with wave heights or inundation periods only increases the p-value and lowers the correlation coefficient.

The model parametrizations are thus based only on bed level changes. The Population Dynamics principle of Temmerman et al. (2007) is used to parametrise the driving factors. The negative terms in the used Equation, (4.11 and 4.12) and the growth term, were replaced by bed level change term, as this is the main driving factor of the 'growth' rate of seedlings, based on MLR fit. Via this MLR the coefficient of all factors has been determined. The diffusion term in Equation 4.11 has been neglected as mangrove seedlings do not show clonal growth. Then, the established term is still in the Equation. The es-

tablish term randomly 'places' a number of seedlings in a grid cell, which allows seedling to randomly establish in a certain cell. As the original formula of Temmerman et al. (2007) can not be used anymore, the new seedling growth rate formula of the Mangrove Dynamics model is:

$$n_b(n) = n_b(n-1) \cdot (55.19 \cdot \Delta z_b + 0.48) + n_{b,est} \tag{7.1}$$

The newly developed model does represent the observed seedling dynamics. The number of seedlings does change quite rapidly in the early weeks of the model run, due to the 'slow' start of the bed level changes. This causes some difference between the observed and modelled number of seedlings. However, after the first 2 weeks, the number of modelled seedlings follows the actual measured number of seedlings. For the forest fringe location, the average number of seedlings along shore is very accurate, while for the inland location, the maximum number of seedlings gives a better representation. However, both the maximum and average modelled and measured number of seedlings show a good coefficient of determination (R^2) (0.94 - 0.98). Growth rates do not show the same trend. The growth rates for both the inland and forest fringe location do not show high R^2 values for the average number of seedlings at the forest fringe location and the average and maximum number of seedlings at the the inland location.

7.4 The effects of increasing and variable waves on bed level changes and seedling establishment

Research question: *What are the effects on bed level changes and seedling establishment in the Sungei Buloh Wetland Reserve (SBWR) as a consequence of an increase and variable wave heights?*

The increase of wave heights results in an increase in the tidal erosion and accretion rates. Especially, the increase of the constant wave heights leads to an increase of tidal erosion and accretion rates. The initial wave heights show mainly accretion, while the increased wave heights show accretion and erosion rates per tide. These rate also vary between the neap- and spring tidal cycle. The weekly bed level changes for the constant wave heights are the highest for low waves. This because only accretion is happening. For the increased constant wave heights, each consecutive weekly bed level change, shows approximately the same rates, with some differences during spring- or neap-tide conditions. A low constant wave height does show large differences between each consecutive week. So high bed level changes occur during spring-tide, as a lot sediment gets transported into the mangrove, while low bed level changes happen during neap tide, where relatively less sediment gets transported into the mangrove.

The effect of the increased wave heights on seedling establishment is almost none. The number of seedlings is strongly affected by the bed level changes. The growth rate is low during the first few weeks, resulting in a low growth factor. A lot of seedlings thus die in these weeks. Later, the number of seedlings is that low, that a difference in the growth rate does not make a significant change. Additionally, the bed levels do not change much either due to waves. The erosion and accretion rates do changes, but all in all the bed level changes are similar to the bed level changes with low waves. There is almost no erosion with low waves, resulting in a certain accretion rate. With larger waves, the accretion

rate is less high due to erosion rates. As the growth rate is correlated with the relative bed level changes, it does not matter in which way this occurs, accretion or erosion. This shows that the number of seedlings is strongly compensated by the additional random establishment of seedlings.

7.5 Impacts of waves and tidal currents on the bed level changes and their combined impact on seedling establishment.

Waves affect bed level changes and seedlings establishment. Especially during low water levels, waves affect bed level changes. Seedlings are again most affected by bed level changes, but are not correlated with waves. The number of seedlings can be modelled well using the vegetation module and the empirical formula describing the number of seedlings as a function of bed level changes. Modelling the seedlings results in high R^2 values compared with the observed number of seedlings. An increase of the wave height results in an increase of erosion. As bed level changes are calculated by subtracting the maximum weekly bed level with the minimum weekly bed level, the change is not significantly. The modelled number of seedlings, with time-dependent and or increased wave heights, do not show any significant differences.

Chapter 8

Recommendations

The used model consists of only one transect. Interesting would be to see if seedlings can be modelled for a larger part of the Sungei Buloh mangroves. A starting point would be the Mandai model (Willemsen et al., 2016). This model could be upgraded to Delft-FM. Combining this with an update of the bathymetry and correct structures as the stop bank and the row of poles, can make an interesting model. Field observations can be based on this research, but an update of the sediment characteristics would be useful. It would be interesting to see what happens at other parts of the mangrove regarding bed level changes and seedling establishment. Then a comparison can be made with the already found observations to see if there are certain locations that are more suitable for seedling establishment. Additionally, tagging seedlings at each measuring moment can give a more precise pattern of the growth of seedlings.

The model currently only has been ran for approximately 3 months. Additionally, the number of seedlings mainly decreased during this period. Including a growing season would be interesting to research. Currently, the initial number of seedlings is implemented as a random initial field, based on observations. It is however unclear what the results would be if a season growth season is applied in the model.

As mentioned in the introduction of this research, the gap between short- and long-term bed level changes is unknown. In the Sungei Buloh mangroves, RSETs are placed. The gap can be closed by combining the measurements of the RSETs and continue monitoring the short-term bed level changes.

In relation with nature based flood defences, it would be interesting to see what the long-term development of the mangrove would be. This would require longer model runs. Seedlings might not affect the hydrodynamics in mangroves that much, but on the long-term (years) they potentially can grow until the become an established tree. Then, hydrodynamics do get affected by this vegetation. This would require to model the grow of seedlings, which is possible by the observed seedling growth rates and literature.

Bibliography

Anthony, E. J. and Gratiot, N. (2012). Coastal engineering and large-scale mangrove destruction in Guyana, South America: Averting an environmental catastrophe in the making. *Ecological Engineering*, 47:268–273.

Balke, T., Bouma, T. J., Horstman, E. M., Webb, E. L., Erftemeijer, P. L. A., and Herman, P. M. J. (2011). Windows of opportunity : thresholds to mangrove seedling establishment on tidal flats. *Marine Ecology Progress Series*, 440:1–9. doi: 10.3354/meps09364.

Balke, T., Swales, A., Lovelock, C. E., Herman, P. M. J., and Bouma, T. J. (2015). Limits to seaward expansion of mangroves: Translating physical disturbance mechanisms into seedling survival gradients. *Journal of Experimental Marine Biology and Ecology*, 467:16–25. doi: 10.1016/j.jembe.2015.02.015.

Balke, T., Webb, E., Elzen, E., Galli, D., Herman, P., and Bouma, T. (2013). Seedling establishment in a dynamic sedimentary environment: A conceptual framework using mangroves. *The Journal of applied ecology*, 50:740–747. doi: 10.1111/1365-2664.12067.

Broekema, Y. (2013). Hydrodynamic modelling of a mangrove system in Singapore. Master's thesis, TU Delft. url: http://resolver.tudelft.nl/uuid:c334b017-4c4c-4a70-b28c-dceca6e04131.

CERC (1984). Shore Protection Manual. U.S. Army Corps of Engineers, Washington DC. Technical Report 4, U.S. Army Corps for Engineers. http://resolver.tudelft.nl/uuid:98791127-e7ae-40a1-b850-67d575fa1289.

Codiga, D. L. (2011). Unified Tidal Analysis and Prediction Using the UTide Matlab Functions. *Graduate School of Oceanography. University of Rhode Island, Narragansett, RI, USA*, page 60. doi: 10.13140/RG.2.1.3761.2008.

de Swart, H. and Zimmerman, J. (2009). Morphodynamics of Tidal Inlet Systems. *Annual Review of Fluid Mechanics*, 41(1):203–229.

Deltares (2019a). D-Flow Flexible Mesh. D-Flow FM in Delta Shell User Manual. Technical Report 1.5.0, Deltares. url: https://content.oss.deltares.nl/delft3d/manuals/D-Flow_FM_User_Manual.pdf.

Deltares (2019b). D-Morphology, 1D/2D/3D D-Morphology in Delta Shell User Manual. Technical Report 1.5, Deltares, Delft. url: https://content.oss.deltares.nl/delft3d/manuals/D-Morphology_User_Manual.pdf.

Deltares (2020). D-Waves Simulation of short-crested waves with SWAN User Manual. Technical Report 1.2, Deltares. url: https://content.oss.deltares.nl/delft3d/manuals/D-Waves_User_Manual.pdf.

Friedrichs, C. T. (2012). *Tidal Flat Morphodynamics: A Synthesis*, volume 3. Elsevier Inc.

Friedrichs, C. T. and Perry, J. E. (2001). Tidal Salt Marsh Morphodynamics: A Synthesis. *Journal of Coastal Research*, (27):7–37.

Friess, D. A., Krauss, K. W., Horstman, E. M., Balke, T., Tjeerd, J., Galli, D., and Webb, E. L. (2012). Are all intertidal wetlands naturally created equal ? Bottlenecks , thresholds and knowledge gaps to mangrove and saltmarsh ecosystems. *Biological Reviews*, 87:346–366. doi: 10.1111/j.1469-185X.2011.00198.x.

Furukawa, K. and Wolanski, E. (1996). Sedimentation in mangrove forests. *Mangroves and Salt Marches*, 1:3–10. doi: 10.1023/A:1025973426404.

Furukawa, K., Wolanski, E., and Mueller, H. (1997). Currents and Sediment Transport in Mangrove. *Estuarine, Coastal and Shelf Science*, pages 301–310. doi: 10.1006/ecss.1996.0120.

Hasan, G. M., Van Maren, D. S., and Cheong, H. F. (2012). Improving hydrodynamic modeling of an estuary in a mixed tidal regime by grid refining and aligning. *Ocean Dynamics*, 62(3):395–409. doi: 10.1007/s10236-011-0506-4.

Hasselmann, K., Barnett, T. P., Bouws, E., Carlson, H., Cartwright, D. E., Enke, K., Ewing, J. A., Gienapp, H., Hasselmann, D., Kruseman, P., Meerburg, A., Müller, P., Olbers, D. J., Richter, K., Sell, W., and Walden, H. (1973). Measurements of Wind-Wave Growth and Swell Decay during the Joint North Sea Wave Project (JONSWAP). *Ergänzungsheft zur Deutschen Hydrographischen Zeitschrift*, 12:93.

Hegge, B. J. and Masselink, G. (1996). Spectral analysis of geomorphic time series: Auto-spectrum. *Earth Surface Processes and Landforms*, 21(11):1021–1040.

Herman, P. M. and Dijkstra, J. (2020). Python manual for Delft-FM. Technical report, Deltares, Delft.

Horstman, E. M. (2019). Coastal wetland dynamics. *University of Twente - Cource: Morphology*, 1:45.

Horstman, E. M., Dohmen-Janssen, C. M., Bouma, T. J., and Hulscher, S. J. (2015). Tidal-scale flow routing and sedimentation in mangrove forests: Combining field data and numerical modelling. *Geomorphology*, 228:244–262.

Horstman, E. M., Dohmen-Janssen, C. M., Narra, P. M., van den Berg, N. J., Siemerink, M., and Hulscher, S. J. (2014). Wave attenuation in mangroves: A quantitative approach to field observations. *Coastal Engineering*, 94:47–62.

Horstman, E. M. and Willemsen, P. W. J. M. (2018). Coastal wetland dynamics introduction. *University of Twente - Course: Morphology*, 1:45.

Kernkamp, H. W. J., Petit, H. A. H., Gerritsen, H., and de Goede, E. D. (2005). A unified formulation for the three-dimensional shallow water equations using orthogonal co-ordinates: theory and application. *Ocean Dynamics*, 55(3-4):351–369.

Kurniawan, A., Hasan, G. J., Ooi, S. K., Kit, L. W., Loh, L. L., and Bayen, S. (2014). Understanding Hydrodynamic Flow Characteristics in a Model Mangrove Ecosystem in Singapore. *APCBEE Procedia*, 10:286–291.

Kurniawan, A., Ooi, S. K., Hummel, S., and Gerritsen, H. (2011). Sensitivity analysis of the tidal representation in Singapore Regional Waters in a data assimilation environment. *Ocean Dynamics*, 61(8):1121–1136.

Le Minor, M., Bartzke, G., Zimmer, M., Gillis, L., Helfer, V., and Huhn, K. (2019). Numerical modelling of hydraulics and sediment dynamics around mangrove seedlings: Implications for mangrove establishment and reforestation. *Estuarine, Coastal and Shelf Science*, 217(September 2018):81–95.

Lesser, G. R., Roelvink, J. A., van Kester, J. A. T. M., and Stelling, G. S. (2004). Development and validation of a three-dimensional morphological model. *Coastal Engineering*, 51:883–915.

Luijendijk, A. P., Ranasinghe, R., Schipper, M. A. D., Huisman, B. A., Swinkels, C. M., Walstra, D. J. R., and Stive, M. J. F. (2017). crossmark. *Coastal Engineering*, 119(January):1–14.

Massel, S. R., Furukawa, K., and Brinkman, R. M. (1999). Surface wave propagation in mangrove forests. *Fluid Dynamics Research*, 24(4):219–249.

Mazda, Y., Kanazawa, N., and Wolanski, E. (1995). Tidal asymmetry in mangrove creeks. *Hydrobiologica*, 295:51–58.

Mazda, Y., Magi, M., Kogo, M., and Nguyen Hong, P. (1997). Mangroves as a coastal protection from waves in the Tong King delta, Vietnam. *Mangroves and Salt Marches*, 1:127–135.

Mcivor, A., Spencer, T., Möller, I., and Spalding, M. D. (2013). The response of mangrove soil surface elevation to sea level rise Natural Coastal Protection Series: Report 3. *Natural Coastal Protection Series*.

Mullarney, J. C., Henderson, S. M., Reyns, J. A., Norris, B. K., and Bryan, K. R. (2017). Spatially varying drag within a wave-exposed mangrove forest and on the adjacent tidal flat. *Continental Shelf Research*, 147(October 2016):102–113. doi: 10.1016/j.csr.2017.06.019.

Odink, S. J. (2019). Long-term marsh growth and retreat in an online coupled hydrodynamic, morphodynamic and ecological model. Master's thesis, University of Twente.

Ribberink, J. S. (2011). *River Dynamics: II Transport Processes and Morphology*. University of Twente.

Roelvink, J. A. (2006). Coastal morphodynamic evolution techniques. *Coastal Engineering*, 53(2-3):277–287.

Samson, M. S. and Rollon, R. N. (2008). Growth Performance of Planted Mangroves in the Philippines : Revisiting Forest Management Strategies. *Ambio*, 37(4):234–240. doi: 10.1579/0044-7447(2008)37[234:GPOPMI]2.0.CO;2.

Siemes, R. W. A., Borsje, B. W., Daggenvoorde, R. J., and Hulscher, S. J. M. H. (2020). Artificial Structures Steer Morphological Development of Salt Marshes : A Model Study. *Journal of Marine Science and Engineering*, 8:22.

Swales, A., Bentley, S. J., Lovelock, C., and Bell, R. G. (2007). Sediment processes and mangrove-habitat expansion on a rapidly-prograding muddy coast, new zealand. *Coastal Sediments*, 7:1441–1454.

Tan, T. T. W., Choong, M. F., Chua, K. S., Loo, A. H. B., Ahmad., S., Seah, E. E. L., Turner, I. M. I. M., and Yong, J. W. H. J. W. H. (1997). A botanical survey of sungei buloh nature park, singapore. *The Gardens' bulletin, Singapore.*, 49:15–35.

Temmerman, S., Bouma, T. J., Van de Koppel, J., Van der Wal, D., De Vries, M. B., and Herman, P. M. (2007). Vegetation causes channel erosion in a tidal landscape. *Geology*, 35(7):631–634.

Temmerman, S., Meire, P., Bouma, T. J., and Herman, P. M. J. (2013). in the face of global change. *Nature*, 504(December).

Tran, T. T. (2011). *MORPHODYNAMICS OF SEASONALLY CLOSED: Coastal inlets at the central coast of Vietnam*. PhD thesis, UNESCO-IHE Delft.

Van den Broek, J. (2020). Numerical modelling of the biophysical feedbacks of Salicornia at the constructed Marconi salt marsh. Master's thesis, University of Twente.

van Loon, A. F., Dijksma, R., and van Mensvoort, M. E. F. (2007). Hydrological classification in mangrove areas: A case study in Can Gio, Vietnam. *Aquatic Botany*, 87(1):80–82.

van Maanen, B., Coco, G., and Bryan, K. R. (2015). On the ecogeomorphological feedbacks that control tidal channel network evolution in a sandy mangrove setting. *Proceedings of the Royal Society A: Mathematical, Physical and Engineering Sciences*, 471(2180). doi: 10.1098/rspa.2015.0115.

Van Santen, P., Augustinus, P. G. E. F., Janssen-Stelder, B. M., Quartel, S., and Tri, N. H. (2007). Sedimentation in an estuarine mangrove system. *Journal of Asian Earth Sciences*, 29(4):566–575.

Ward, R. D., Friess, D. A., Day, R. H., and Mackenzie, R. A. (2016). Impacts of climate change on mangrove ecosystems: a region by region overview. *Ecosystem Health and Sustainability*, 2(4):25.

Willemsen, P. W., Horstman, E. M., Borsje, B. W., Friess, D. A., and Dohmen-Janssen, C. M. (2016). Sensitivity of the sediment trapping capacity of an estuarine mangrove forest. *Geomorphology*, 273:189–201. doi: 10.1016/j.geomorph.2016.07.038.

Winterwerp, J. C., Erftemeijer, P. L., Suryadiputra, N., Van Eijk, P., and Zhang, L. (2013). Defining eco-morphodynamic requirements for rehabilitating eroding mangrove-mud coasts. *Wetlands*, 33(3):515–526.

Wright, L. W. (1995). *Morphodynamics of Inner Continental Shelves*. CRC Press, Baco Raton.

Zhang, K., Liu, H., Li, Y., Xu, H., Shen, J., Rhome, J., and Smith, T. J. (2012). The role of mangroves in attenuating storm surges. *Estuarine, Coastal and Shelf Science*, 102-103:11–23.

Appendices

Appendix A

Tidal constituents

Table A.1: Derived tidal constituents

Tidal constituent	**Amplitude**	**Phase ϕ**	**Angular frequency ω**	Period
[-]	[m]	[degr]	[degr/hour]	[h]
M2	1.1	107	28.9841042	12.42060122
S2	0.545	137	30	12
K1	0.358	28.4	15.0410686	23.93446966
O1	0.244	6.13	13.9430356	25.81934166
N2	0.226	76.3	28.4397295	12.65834824
M4	0.158	151	57.9682084	6.21030061
MSF	0.141	182	1.0158958	354.3670522
L2	0.117	84.4	29.5284789	12.19162021
MK3	0.0942	85.6	44.0251728	8.177139966
MM	0.0923	242	0.5543747	649.3802838
M6	0.0711	109	86.9523126	4.140200407
MS4	0.0572	81.4	58.9841042	6.103339279
MO3	0.0549	51.3	42.9271398	8.38630297
SN4	0.052	37.8	58.4397295	6.160192785
MU2	0.0507	164	27.9682084	12.87175763
Q1	0.0437	316	13.3986609	26.86835667
S4	0.0388	116	60	6
2MK5	0.035	32	73.009277	4.930880222
2MS6	0.0345	243	87.9682084	4.09238754
OO1	0.0318	75.6	16.1391017	22.3060742
2Q1	0.0286	294	12.8542862	28.00622255
J1	0.0274	13.9	15.5854433	23.09847677
SK3	0.0229	292	45.0410686	7.992705573
UPS1	0.0218	95.3	16.6834764	21.57823654
2MN6	0.0192	128	86.4079379	4.166283894
M8	0.0188	6.72	115.9364168	3.105150305
ETA2	0.0188	144	30.626512	11.7545217
EPS2	0.0179	176	27.4238338	13.12726742
NO1	0.0178	278	14.4966939	24.83324836
2SM6	0.0171	336	88.9841042	4.045666394
M3	0.011	101	43.4761563	8.280400814
2SK5	0.0102	290	75.0410686	4.797373048
ALP1	0.00982	89.8	14.4715188	24.87644904
3MK7	0.00446	223	101.9333814	3.531718413
MN4	0.00376	334	57.4238337	6.269173909

Appendix B

Inundation periods

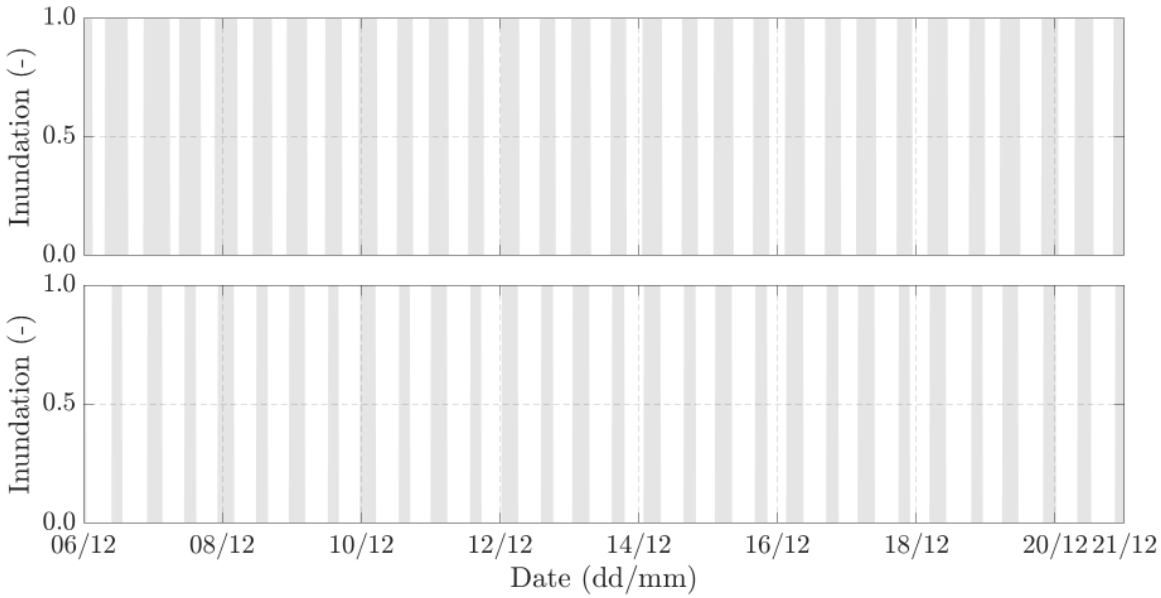

Figure B.1: Inundation periods fieldwork period 1. Top plot represents the forest fringe location. Bottom plot represents the inland location.

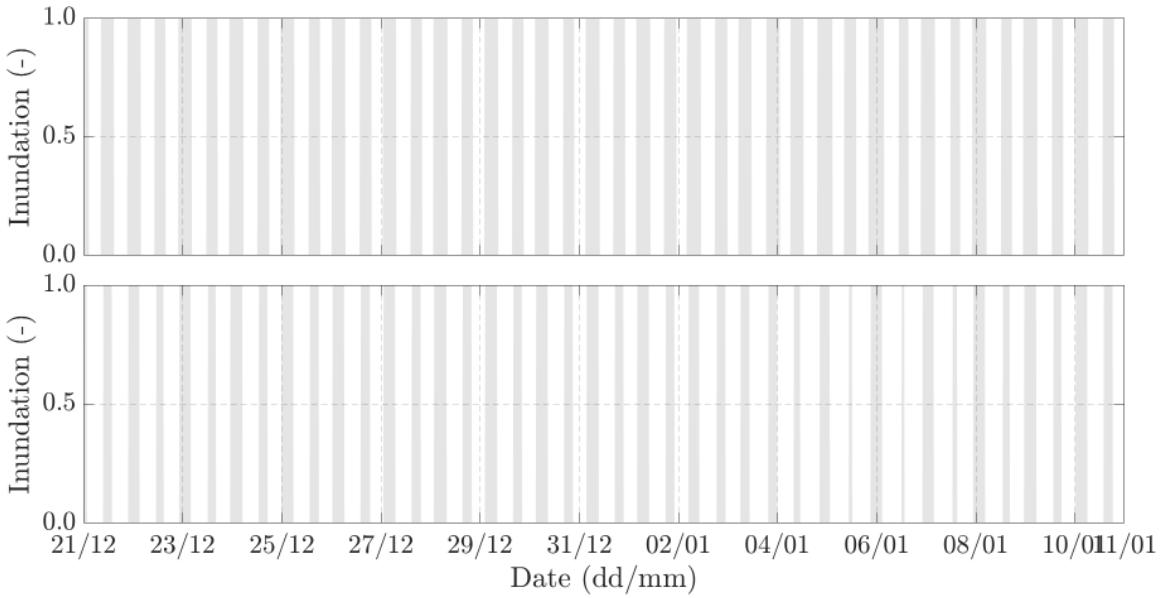

Figure B.2: Inundation periods fieldwork period 2. Top plot represents the forest fringe location. Bottom plot represents the inland location.

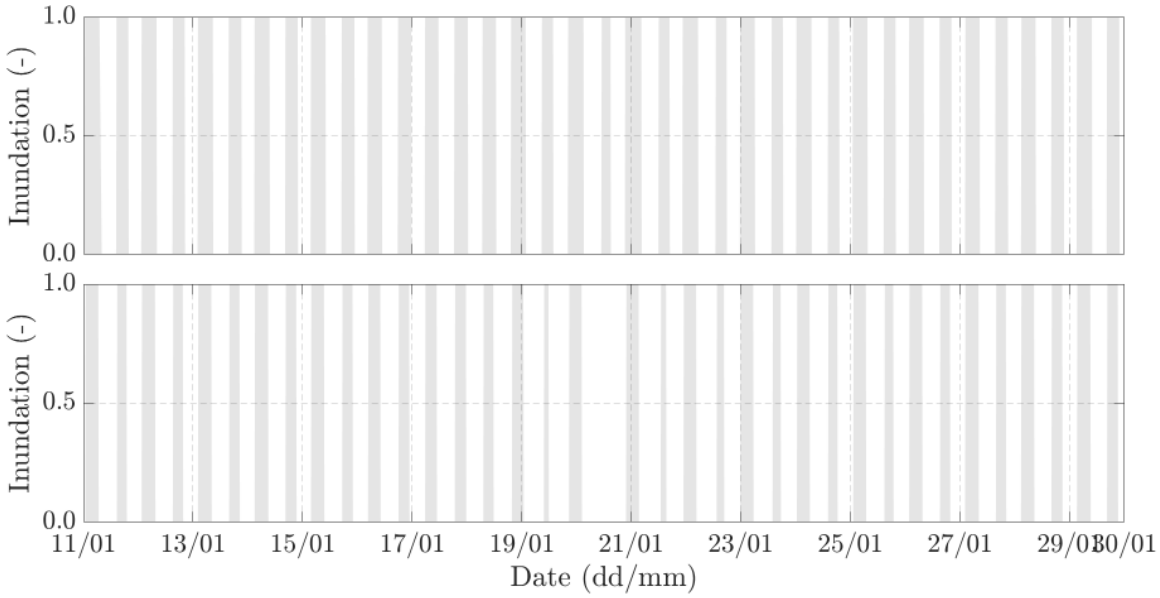

Figure B.3: Inundation periods fieldwork period 3. Top plot represents the forest fringe location. Bottom plot represents the inland location.

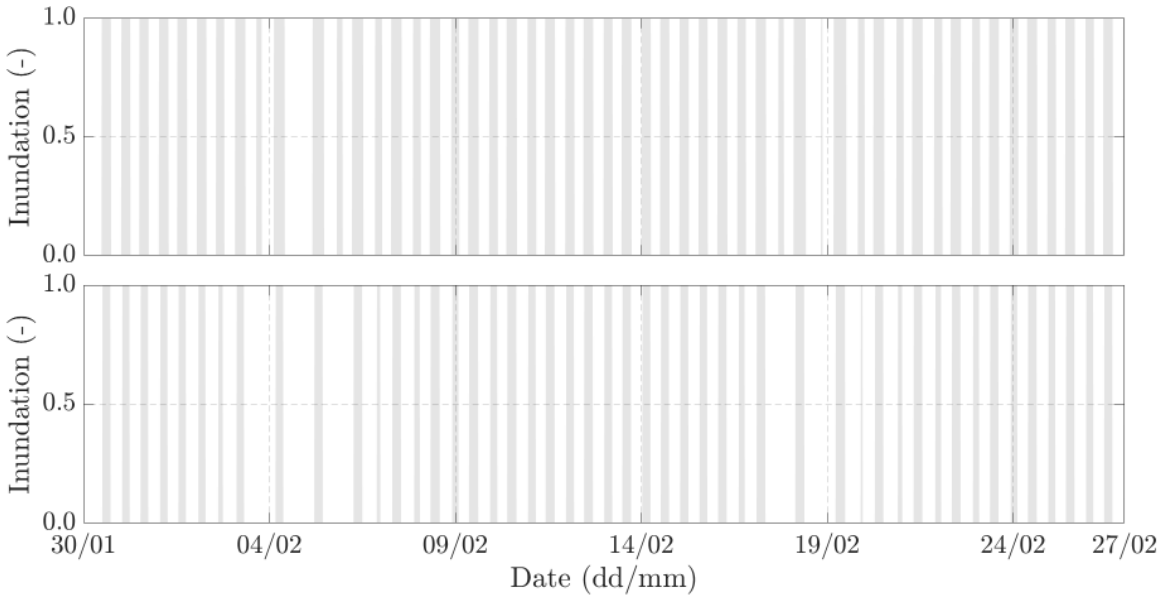

Figure B.4: Inundation periods fieldwork period 4. Top plot represents the forest fringe location. Bottom plot represents the inland location.

Appendix C

Seedling data

Table C.1: Seedling data transect A, 06-12-2019

Transect A seedling data: 06 - 12 - 2019

Plot	4.00	[-]	Plot	3.00	[-]	Plot	2.00	[-]	Plot	1.00	[-]	Plot	0.00	[-]
N	124.00	[#]	N	11.00	[#]	N	7.00	[#]	N	5.00	[#]	N	3.00	[#]
Height [cm]	**Diam. [mm]**	**Leaves [#]**	**Height [cm]**	**Diam. [mm]**	**Leaves [#]**	**Height [cm]**	**Diam. [mm]**	**Leaves [#]**	**Height [cm]**	**Diam. [mm]**	**Leaves [#]**	**Height [cm]**	**Diam. [mm]**	**Leaves [#]**
10.50	3.00	4.00	12.00	3.00	3.00	5.00	3.00	2.00	11.00	3.00	2.00	43.50	8.00	32.00
3.00	4.00	4.00	8.50	2.00	1.00	12.00	3.00	3.00	7.00	3.00	2.00	9.00	3.00	4.00
8.00	3.00	2.00	10.00	4.00	4.00	6.50	3.00	2.00	13.50	4.00	4.00	6.50	2.00	3.00
8.50	3.00	4.00	7.00	3.00	4.00	17.00	6.00	6.00	5.00	4.00	3.00			
6.55	2.00	1.00	11.50	3.00	2.00	13.00	4.00	5.00	8.00	3.00	2.00			
10.00	3.00	3.00	12.00	3.50	1.00	7.50	5.00	2.00						
8.50	3.00	2.00	10.50	3.50	4.00	7.00	4.00	2.00						
6.00	3.00	2.00	12.00	3.00	2.00									
7.00	3.00	4.00	12.00	2.50	2.00									
11.00	3.00	4.00	8.00	3.00	2.00									
12.50	3.00	4.00	9.00	3.00	0.00									
15.50	4.00	4.00												
17.00	3.00	5.00												
11.00	3.00	5.00												
12.00	3.00	5.00												
13.50	3.00	2.00												
9.50	3.00	3.00												
3.50	2.00	2.00												
7.50	3.00	3.00												
10.00	3.00	4.00												
Avg	**Avg**	**Avg**	**Avg**	**Avg**	**Avg**	**Avg**	**Avg**	**Avg**	**Avg**	**Avg**	**Avg**	**Avg**	**Avg**	**Avg**
9.55	3.00	3.35	10.23	3.05	2.27	9.71	4.00	3.14	8.90	3.40	2.60	19.67	4.33	13.00

Table C.2: Seedling data transect B, 06-12-2019

Transect B seedling data: 06 - 12 - 2019

Plot	4.00	[-]	Plot	3.00	[-]	Plot	2.00	[-]	Plot	1.00	[-]	Plot	0.00	[-]
N	124.00	[#]	N	11.00	[#]	N	7.00	[#]	N	5.00	[#]	N	3.00	[#]
Height [cm]	**Diam. [mm]**	**Leaves [#]**	**Height [cm]**	**Diam. [mm]**	**Leaves [#]**	**Height [cm]**	**Diam. [mm]**	**Leaves [#]**	**Height [cm]**	**Diam. [mm]**	**Leaves [#]**	**Height [cm]**	**Diam. [mm]**	**Leaves [#]**
12.00	2.00	3.00	13.00	3.00	3.00	22.50	6.00	24.00	45.00	5.00	30.00	41.00	8.00	44.00
13.50	4.00	4.00	15.00	3.00	4.00	24.00	4.50	6.00	7.50	3.00	2.00	7.00	2.00	2.00
4.50	2.00	1.00	13.00	3.00	6.00	17.00	3.00	3.00	3.50	3.00	2.00	9.50	2.00	2.00
7.50	3.00	2.00	9.00	3.00	4.00	27.00	6.00	22.00	5.00	2.00	4.00	9.50	2.00	2.00
7.00	1.00	2.00	7.50	3.00	2.00	20.00	4.50	4.00	6.50	3.00	2.00	8.00	2.00	2.00
11.00	3.00	4.00	9.00	3.00	1.00	19.50	4.00	3.00	14.00	3.00	2.00	10.00	3.00	2.00
15.50	3.00	5.00	6.50	3.00	1.00	18.50	4.00	2.00	8.00	4.00	2.00	9.00	3.00	2.00
15.50	3.00	3.00	11.00	3.00	4.00	9.50	3.00	3.00	10.00	3.00	2.00	11.00	3.00	2.00
11.50	3.00	4.00	9.50	3.00	2.00	20.00	5.00	21.00	4.50	2.00	2.00	13.50	3.00	4.00
			13.00	3.00	1.00	41.00	6.50	33.00	11.00	3.00	2.00	31.00	7.00	18.00
			11.50	4.00	6.00	18.50	3.00	16.00				14.00	3.00	2.00
			11.50	4.00	4.00	12.00	3.00	7.00				5.50	2.00	2.00
						13.00	2.50	4.00				8.50	2.00	2.00
						9.00	3.50	4.00				9.50	2.00	2.00
						12.00	3.00	5.00				17.00	6.00	3.00
						21.00	5.00	6.00				11.00	2.00	2.00
						9.00	2.50	2.00				14.00	3.00	2.00
						17.00	4.00	6.00				37.00	6.00	6.00
						26.00	5.00	45.00						
Avg	**Avg**	**Avg**	**Avg**	**Avg**	**Avg**	**Avg**	**Avg**	**Avg**	**Avg**	**Avg**	**Avg**	**Avg**	**Avg**	**Avg**
10.89	2.67	3.11	10.79	3.17	3.17	18.76	4.11	11.37	11.50	3.10	5.00	14.78	3.39	5.61

Table C.3: Seedling data transect A, 21-12-2019

Transect A seedling data: 21 - 12 - 2019

Plot	4.00	[-]	Plot	3.00	[-]	Plot	2.00	[-]	Plot	1.00	[-]	Plot	0.00	[-]
N	124.00	[#]	N	11.00	[#]	N	7.00	[#]	N	5.00	[#]	N	3.00	[#]
Height [cm]	**Diam. [mm]**	**Leaves [#]**	**Height [cm]**	**Diam. [mm]**	**Leaves [#]**	**Height [cm]**	**Diam. [mm]**	**Leaves [#]**	**Height [cm]**	**Diam. [mm]**	**Leaves [#]**	**Height [cm]**	**Diam. [mm]**	**Leaves [#]**
13.50	3.00	1.00	11.00	3.00	2.00	17.00	4.00	5.00	13.00	4.00	1.00	4.00	3.00	0.00
9.50	3.00	5.00	7.50	3.00	1.00	3.00	3.00	0.00	3.00	3.00	0.00	5.00	3.00	0.00
7.60	3.00	4.00	11.50	3.00	3.00	8.50	3.00	2.00	3.00	3.00	0.00	10.00	5.00	2.00
10.50	3.00	2.00	10.00	3.50	4.00	9.00	4.00	4.00	4.00	3.00	3.00	10.00	3.00	2.00
6.00	3.50	3.00	8.00	3.00	2.00	4.00	3.00	0.00				4.00	3.00	0.00
7.00	4.00	4.00	19.00	5.00	5.00	4.50	3.00	0.00				45.20	8.50	30.00
7.00	3.00	4.00				3.50	3.50	0.00						
16.00	3.00	4.00												
10.00	4.00	4.00												
12.00	3.00	3.00												
10.50	3.00	4.00												
6.00	3.00	2.00												
5.50	3.00	3.00												
12.00	3.00	6.00												
10.50	4.00	2.00												
12.00	4.00	5.00												
11.50	3.00	4.00												
12.00	4.00	5.00												
11.00	3.00	5.00												
8.80	2.00	2.00												
Avg	**Avg**	**Avg**	**Avg**	**Avg**	**Avg**	**Avg**	**Avg**	**Avg**	**Avg**	**Avg**	**Avg**	**Avg**	**Avg**	**Avg**
9.95	3.23	3.60	11.17	3.42	2.83	7.07	3.36	1.57	5.75	3.25	1.00	13.03	4.25	5.67

Table C.4: Seedling data transect B, 21-12-2019

Transect B seedling data: 21 - 12 - 2019

Plot	4.00	[-]	Plot	3.00	[-]	Plot	2.00	[-]	Plot	1.00	[-]	Plot	0.00	[-]
N	124.00	[#]	N	11.00	[#]	N	7.00	[#]	N	5.00	[#]	N	3.00	[#]
Height [cm]	**Diam. [mm]**	**Leaves [#]**	**Height [cm]**	**Diam. [mm]**	**Leaves [#]**	**Height [cm]**	**Diam. [mm]**	**Leaves [#]**	**Height [cm]**	**Diam. [mm]**	**Leaves [#]**	**Height [cm]**	**Diam. [mm]**	**Leaves [#]**
16.00	3.00	5.00	9.00	4.00	1.00	41.00	6.50	30.00	47.00	5.50	39.00	5.00	3.00	0.00
12.00	3.00	4.00	15.00	3.00	6.00	12.50	4.00	6.00	11.50	3.00	2.00	4.00	3.00	0.00
5.00	2.00	1.00	13.50	4.00	3.00	8.50	3.00	3.00	6.00	3.00	2.00	5.00	3.00	0.00
8.00	3.00	3.00	10.00	3.00	4.00	21.00	5.00	3.00	5.00	3.00	0.00	33.00	11.00	14.00
15.00	4.00	5.00	9.00	3.00	2.00	30.50	4.00	24.00	9.00	3.00	2.00	12.00	4.00	2.00
11.00	3.50	4.00	4.50	4.00	1.00	19.00	4.00	20.00	9.00	3.50	1.00	11.00	3.00	2.00
			10.50	5.00	3.00	10.00	4.00	4.00	11.00	3.50	2.00	10.00	3.00	3.00
			5.00	3.00	0.00	22.00	5.00	7.00	5.50	3.00	0.00	10.00	3.00	2.00
			12.00	4.50	2.00	20.50	5.00	5.00	3.00	3.00	0.00	40.00	9.50	49.00
			4.00	3.00	0.00	28.00	4.00	18.00	6.00	3.00	2.00	10.00	3.00	2.00
						10.00	4.00	2.00				5.00	3.00	0.00
						25.00	5.00	4.00				12.50	2.00	2.00
						27.00	6.00	23.00				9.00	4.00	1.00
						3.00	3.00	0.00				14.00	5.00	3.00
						13.00	3.00	1.00				3.00	3.00	0.00
						31.00	5.00	52.00				6.00	3.00	0.00
						18.00	4.00	4.00				33.00	7.00	9.00
												4.00	3.00	0.00
												3.00	3.00	0.00
												9.50	3.00	2.00
Avg	**Avg**	**Avg**	**Avg**	**Avg**	**Avg**	**Avg**	**Avg**	**Avg**	**Avg**	**Avg**	**Avg**	**Avg**	**Avg**	**Avg**
11.17	3.08	3.67	9.25	3.65	2.20	20.00	4.38	12.12	11.30	3.35	5.00	11.95	4.08	4.55

Table C.5: Seedling data transect A, 11-01-2020

Transect A seedling data: 11 - 01 - 2020

Plot	4.00	[-]	Plot	3.00	[-]	Plot	2.00	[-]	Plot	1.00	[-]	Plot	0.00	[-]
N	124.00	[#]	N	11.00	[#]	N	7.00	[#]	N	5.00	[#]	N	3.00	[#]
Height [cm]	**Diam. [mm]**	**Leaves [#]**	**Height [cm]**	**Diam. [mm]**	**Leaves [#]**	**Height [cm]**	**Diam. [mm]**	**Leaves [#]**	**Height [cm]**	**Diam. [mm]**	**Leaves [#]**	**Height [cm]**	**Diam. [mm]**	**Leaves [#]**
10.50	4.00	3.00	8.00	4.00	5.00	13.50	3.00	2.00	5.90	2.00	2.00	47.20	9.00	27.00
8.00	3.00	1.00	10.00	3.00	3.00	9.60	3.00	3.00				9.50	6.00	3.00
7.00	3.00	2.00	7.50	2.00	2.00	18.40	3.00	4.00						
12.50	3.00	6.00	9.00	3.00	2.00									
6.90	3.00	3.00												
12.30	4.00	6.00												
14.00	3.00	3.00												
15.50	4.00	4.00												
17.50	4.00	4.00												
11.50	3.00	3.00												
9.10	3.00	2.00												
16.20	3.00	1.00												
7.60	3.00	2.00												
11.50	3.00	6.00												
10.50	4.00	3.00												
13.70	3.00	2.00												
7.00	3.00	1.00												
9.10	3.00	4.00												
8.20	3.00	4.00												
9.90	3.00	2.00												
Avg	**Avg**	**Avg**	**Avg**	**Avg**	**Avg**	**Avg**	**Avg**	**Avg**	**Avg**	**Avg**	**Avg**	**Avg**	**Avg**	**Avg**
10.93	3.25	3.10	8.63	3.00	3.00	13.83	3.00	3.00	5.90	2.00	2.00	28.35	7.50	15.00

Table C.6: Seedling data transect B, 11-01-2020

Transect B seedling data: 11 - 01 - 2020

Plot	4.00	[-]	Plot	3.00	[-]	Plot	2.00	[-]	Plot	1.00	[-]	Plot	0.00	[-]
N	124.00	[#]	N	11.00	[#]	N	7.00	[#]	N	5.00	[#]	N	3.00	[#]
Height [cm]	**Diam. [mm]**	**Leaves [#]**	**Height [cm]**	**Diam. [mm]**	**Leaves [#]**	**Height [cm]**	**Diam. [mm]**	**Leaves [#]**	**Height [cm]**	**Diam. [mm]**	**Leaves [#]**	**Height [cm]**	**Diam. [mm]**	**Leaves [#]**
16.60	3.00	3.00	15.30	3.00	3.00	13.40	3.00	4.00				43.00	6.00	53.00
11.70	4.00	4.00	12.00	3.00	1.00	9.20	4.00	2.00				2.50	3.00	0.00
10.30	3.00	3.00				21.00	5.00	10.00				7.70	3.00	2.00
11.30	3.00	6.00				19.00	3.00	15.00				15.80	5.00	4.00
15.80	3.00	3.00				31.50	5.00	40.00				3.50	3.00	0.00
						19.80	4.00	1.00				2.20	3.00	2.00
						30.30	5.00	17.00				4.50	3.00	2.00
						20.70	4.00	3.00				32.50	9.00	20.00
						20.50	4.00	15.00				39.00	7.00	14.00
						25.90	4.00	6.00						
						27.00	5.00	21.00						
Avg	**Avg**	**Avg**	**Avg**	**Avg**	**Avg**	**Avg**	**Avg**	**Avg**	**Avg**	**Avg**	**Avg**	**Avg**	**Avg**	**Avg**
13.14	3.20	3.80	13.65	3.00	2.00	21.66	4.18	12.18	NaN	NaN	NaN	16.74	4.67	10.78

Table C.7: Seedling data transect A, 30-01-2020

Transect A seedling data: 30 - 01 - 2020

Plot	4.00	[-]	Plot	3.00	[-]	Plot	2.00	[-]	Plot	1.00	[-]	Plot	0.00	[-]
N	124.00	[#]	N	11.00	[#]	N	7.00	[#]	N	5.00	[#]	N	3.00	[#]
Height [cm]	**Diam. [mm]**	**Leaves [#]**	**Height [cm]**	**Diam. [mm]**	**Leaves [#]**	**Height [cm]**	**Diam. [mm]**	**Leaves [#]**	**Height [cm]**	**Diam. [mm]**	**Leaves [#]**	**Height [cm]**	**Diam. [mm]**	**Leaves [#]**
13.40	4.50	2.00	18.00	3.70	5.00	9.50	3.90	3.00	7.00	3.40	2.00	47.00	11.60	15.00
9.00	3.70	4.00				5.00	3.20	2.00						
9.00	4.20	5.00												
10.00	5.50	3.00												
9.50	3.90	2.00												
10.00	3.90	5.00												
11.50	3.00	1.00												
8.00	3.60	6.00												
8.50	4.00	5.00												
9.00	3.80	3.00												
12.50	4.20	1.00												
11.50	3.70	3.00												
6.50	4.40	2.00												
15.50	3.70	2.00												
10.50	4.30	4.00												
13.00	4.80	4.00												
15.00	4.30	6.00												
13.50	4.20	4.00												
12.00	3.70	4.00												
13.50	3.90	6.00												
Avg	**Avg**	**Avg**	**Avg**	**Avg**	**Avg**	**Avg**	**Avg**	**Avg**	**Avg**	**Avg**	**Avg**	**Avg**	**Avg**	**Avg**
11.07	4.07	3.60	18.00	3.70	5.00	7.25	3.55	2.50	7.00	3.40	2.00	47.00	11.60	15.00

Table C.8: Seedling data transect B, 30-01-2020

Transect B seedling data: 30 - 01 - 2020

Plot	4.00	[-]	Plot	3.00	[-]	Plot	2.00	[-]	Plot	1.00	[-]	Plot	0.00	[-]
N	124.00	[#]	N	11.00	[#]	N	7.00	[#]	N	5.00	[#]	N	3.00	[#]
Height [cm]	**Diam. [mm]**	**Leaves [#]**	**Height [cm]**	**Diam. [mm]**	**Leaves [#]**	**Height [cm]**	**Diam. [mm]**	**Leaves [#]**	**Height [cm]**	**Diam. [mm]**	**Leaves [#]**	**Height [cm]**	**Diam. [mm]**	**Leaves [#]**
16.00	4.30	4.00				22.50	7.00	7.00				39.00	7.00	11.00
11.00	4.70	5.00				9.00	4.00	2.00				6.50	3.20	2.00
8.50	3.30	2.00				26.50	4.60	4.00				33.50	10.70	54.00
12.00	4.70	4.00				19.00	6.40	15.00				7.50	2.60	2.00
						11.00	3.60	2.00				16.50	7.60	4.00
						13.50	3.60	2.00						
						41.50	7.70	24.00						
						31.50	6.80	43.00						
						31.00	5.00	13.00						
						7.50	3.40	2.00						
						21.00	5.80	2.00						
						28.00	6.80	16.00						
Avg	**Avg**	**Avg**	**Avg**	**Avg**	**Avg**	**Avg**	**Avg**	**Avg**	**Avg**	**Avg**	**Avg**	**Avg**	**Avg**	**Avg**
11.88	4.25	3.75	NaN	NaN	NaN	21.83	5.39	11.00	NaN	NaN	NaN	20.60	6.22	14.60

Table C.9: Seedling data transect A, 27-02-2020

Transect A seedling data: 30 - 01 - 2020

Plot	4.00	[-]	Plot	3.00	[-]	Plot	2.00	[-]	Plot	1.00	[-]	Plot	0.00	[-]
N	124.00	[#]	N	11.00	[#]	N	7.00	[#]	N	5.00	[#]	N	3.00	[#]
Height [cm]	**Diam. [mm]**	**Leaves [#]**	**Height [cm]**	**Diam. [mm]**	**Leaves [#]**	**Height [cm]**	**Diam. [mm]**	**Leaves [#]**	**Height [cm]**	**Diam. [mm]**	**Leaves [#]**	**Height [cm]**	**Diam. [mm]**	**Leaves [#]**
8.00	3.10	4.00	19.00	2.80	2.00	8.40	2.30	2.00	8.90	2.40	4.00	7.00	2.80	2.00
7.20	3.20	3.00				2.50	2.50	2.00				33.00	8.10	21.00
8.80	3.00	2.00				7.20	2.00	2.00				3.30	1.30	2.00
8.80	3.20	6.00				2.50	1.10	2.00						
11.80	3.60	4.00				18.10	3.90	1.00						
14.10	3.60	5.00				9.30	2.60	2.00						
10.20	3.50	3.00				1.90	0.90	2.00						
13.00	3.60	3.00												
10.10	2.70	5.00												
12.10	2.90	4.00												
12.50	3.40	6.00												
9.00	2.90	2.00												
10.90	2.80	3.00												
10.70	3.10	4.00												
8.90	2.60	4.00												
9.60	3.40	4.00												
8.40	2.80	4.00												
10.40	2.70	4.00												
11.00	2.70	5.00												
5.90	2.10	2.00												
Avg	**Avg**	**Avg**	**Avg**	**Avg**	**Avg**	**Avg**	**Avg**	**Avg**	**Avg**	**Avg**	**Avg**	**Avg**	**Avg**	**Avg**
10.07	3.05	3.85	19.00	2.80	2.00	7.13	2.19	1.86	8.90	2.40	4.00	14.43	4.07	8.33

Table C.10: Seedling data transect B, 27-02-2020

Transect B seedling data: 27 - 02 - 2020

Plot	4.00	[-]	Plot	3.00	[-]	Plot	2.00	[-]	Plot	1.00	[-]	Plot	0.00	[-]
N	124.00	[#]	N	11.00	[#]	N	7.00	[#]	N	5.00	[#]	N	3.00	[#]
Height [cm]	**Diam. [mm]**	**Leaves [#]**	**Height [cm]**	**Diam. [mm]**	**Leaves [#]**	**Height [cm]**	**Diam. [mm]**	**Leaves [#]**	**Height [cm]**	**Diam. [mm]**	**Leaves [#]**	**Height [cm]**	**Diam. [mm]**	**Leaves [#]**
9.20	2.50	4.00	13.50	3.40	2.00	6.20	2.00	2.00	24.50	4.20	4.00	32.50	6.80	16.00
14.20	3.10	4.00				41.00	5.00	30.00				34.50	6.60	11.00
9.40	2.40	3.00				12.60	2.60	4.00				4.00	1.10	2.00
						8.50	2.90	1.00				34.00	8.10	59.00
						17.90	5.90	17.00				17.00	4.10	2.00
						4.00	2.10	2.00						
						23.00	5.90	11.00						
						31.60	4.30	19.00						
						7.90	2.80	4.00						
						29.00	4.10	21.00						
						26.50	3.20	6.00						
						28.70	5.40	17.00						
						32.00	4.80	58.00						
Avg	**Avg**	**Avg**	**Avg**	**Avg**	**Avg**	**Avg**	**Avg**	**Avg**	**Avg**	**Avg**	**Avg**	**Avg**	**Avg**	**Avg**
10.93	2.67	3.67	13.50	3.40	2.00	20.68	3.92	14.77	24.50	4.20	4.00	24.40	5.34	18.00

Appendix D

Pneumatophores

Table D.1: Pneumatophores properties transect A

Transect A

Plot	4	[-]	3	[-]	2	[-]	1	[-]	0	[-]
Number	67	[#]	203	[#]	262	[#]	213	[#]	226	[#]
Property	**Heigth**	**Diameter**	**Heigth**	**Diameter**	**Heigth**	**Diameter**	**Heigth**	**Diameter**	**Heigth**	**Diameter**
Unit	**[cm]**	**[mm]**	**[cm]**	**[mm]**	**[cm]**	**[mm]**	**[cm]**	**[mm]**	**[cm]**	**[mm]**
	2.70	6.00	2.00	5.00	5.00	6.00	7.80	6.00	7.00	5.00
	9.00	5.00	6.50	5.00	7.00	4.00	4.50	4.00	8.20	5.00
	7.00	5.00	12.10	5.00	2.20	3.00	1.80	4.00	4.30	4.00
	9.00	5.00	2.00	6.00	8.20	5.00	4.10	5.00	6.20	5.00
	3.50	4.00	2.00	5.50	2.50	4.00	6.00	4.00	5.70	3.00
	1.20	5.00	2.10	4.00	7.00	6.00	17.10	24.00	2.60	3.00
	7.50	7.00	2.50	6.00	5.50	4.00	7.50	14.00	5.80	6.00
	0.50	9.00	2.30	5.00	14.80	7.00	4.20	7.00	12.00	10.00
	3.00	6.00	10.90	4.00	3.00	5.00	7.40	5.00	10.20	6.00
	1.50	5.00	1.00	4.00	2.10	4.00	5.00	7.00	7.20	8.00
	1.30	4.00	8.60	5.00	3.70	7.00	6.80	6.00	5.70	6.00
	2.10	6.00	2.50	4.00	15.10	5.00	11.50	13.00	10.70	7.00
	3.40	5.00	2.60	5.00	1.20	4.00	3.20	8.00	17.80	9.00
	2.60	5.00	1.60	6.00	4.50	7.00	3.50	7.00	6.10	4.00
	1.30	6.00	2.30	4.00	3.20	5.00	3.00	9.00	4.80	5.00
	2.10	6.00	9.20	5.00	10.20	6.00	19.20	8.00	9.10	4.00
	4.90	6.00	3.50	5.00	9.50	7.00	12.00	10.00	11.50	6.00
	3.50	6.00	1.70	4.00	6.80	6.00	12.80	17.00	12.40	4.00
	4.80	7.00	2.70	5.00	3.20	4.00	10.40	6.00	12.80	4.00
	6.50	4.00	1.00	3.00	4.00	4.00	5.00	5.00	2.50	3.00
Average	**3.87**	**5.60**	**3.96**	**4.78**	**5.94**	**5.15**	**7.64**	**8.45**	**8.13**	**5.35**

Appendix E

Representative tree diameters

Table E.1: Representative tree diameters at different heights

	Transect A Tree diameters		**Transect B Tree diameters**	
Tree	**0 - 10 mm**		**0 - 10 mm**	
Height [m]	**Diameter [mm]**	**Circumference [cm]**	**Diameter [mm]**	**Circumference [cm]**
0.10	14.00	4.40	19.00	5.97
0.50	3.80	1.19	15.00	4.71
Mean	8.90		17.00	
Tree	**10 - 25 mm**		**10 - 25 mm**	
0.10	59.00	18.54	31.00	9.74
0.50	15.00	4.71	12.00	3.77
1.00	12.00	3.77	11.00	3.46
1.50	10.00	3.14	NA	NA
2.00	6.00	1.88	NA	NA
Mean	20.40		18.00	
Tree	**25 - 100 mm**		**10 - 25 mm**	
0.10	74.00	23.25	82.00	25.76
0.50	64.00	20.11	84.00	26.39
1.00	53.00	16.65	68.00	21.36
1.50	55.00	17.28	58.00	18.22
2.00	53.00	16.65	114.00	35.81
Mean	59.80		81.20	
Tree	**100 - 200 mm**	**100 - 200 mm**	**100 - 200 mm**	
0.10	200.85	63.10	NA	NA
0.50	171.89	54.00	NA	NA
1.00	143.88	45.20	NA	NA
1.50	130.51	41.00	NA	NA
2.00	130.51	41.00	NA	NA
Mean	155.53		NA	
Tree	**200 - 300 mm**		**200 - 300 mm**	
0.10	NA	NA	114.59	36.00
0.50	NA	NA	321.49	101.00
1.00	NA	NA	276.93	87.00
1.50	NA	NA	254.65	80.00
2.00	NA	NA	248.28	78.00
Mean	NA		243.19	
Tree	**>300 mm**		**>300 mm**	
0.10	541.13	170.00	697.10	219.00
0.50	171.89	54.00	452.00	142.00
1.00	143.88	45.20	404.25	127.00
1.50	130.51	41.00	448.82	141.00
2.00	130.51	41.00	884.90	278.00
Mean	223.58		577.41	

Appendix F

Seedling figures

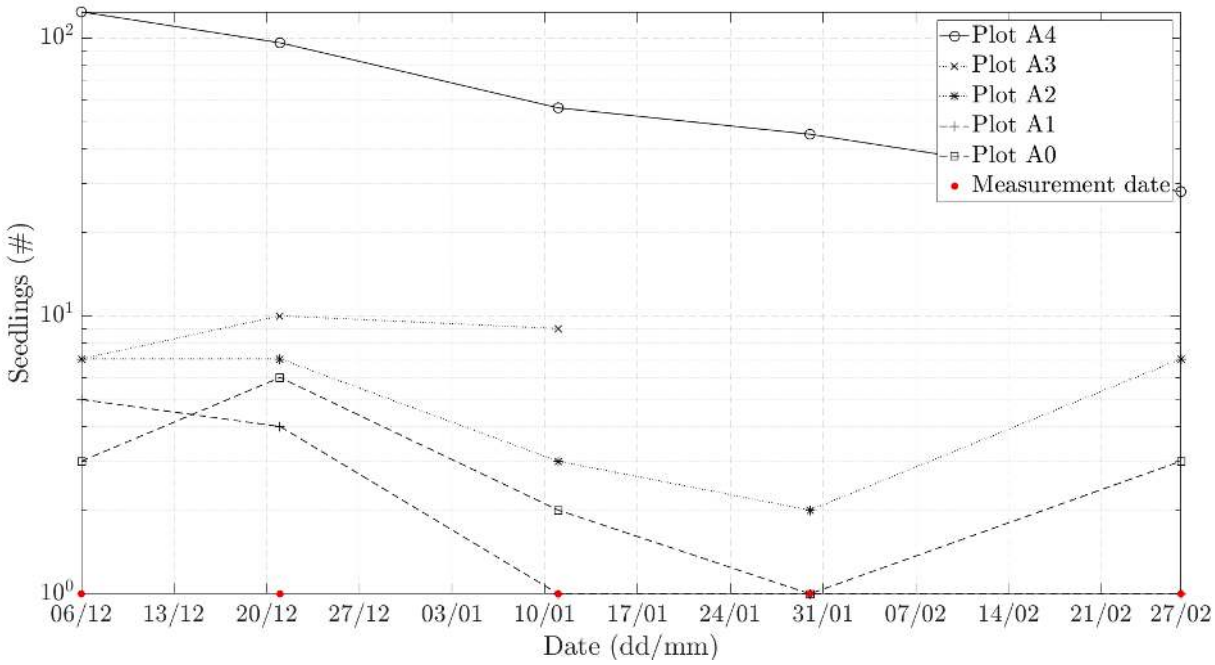

Figure F.1: Number of seedlings per plot at transect A

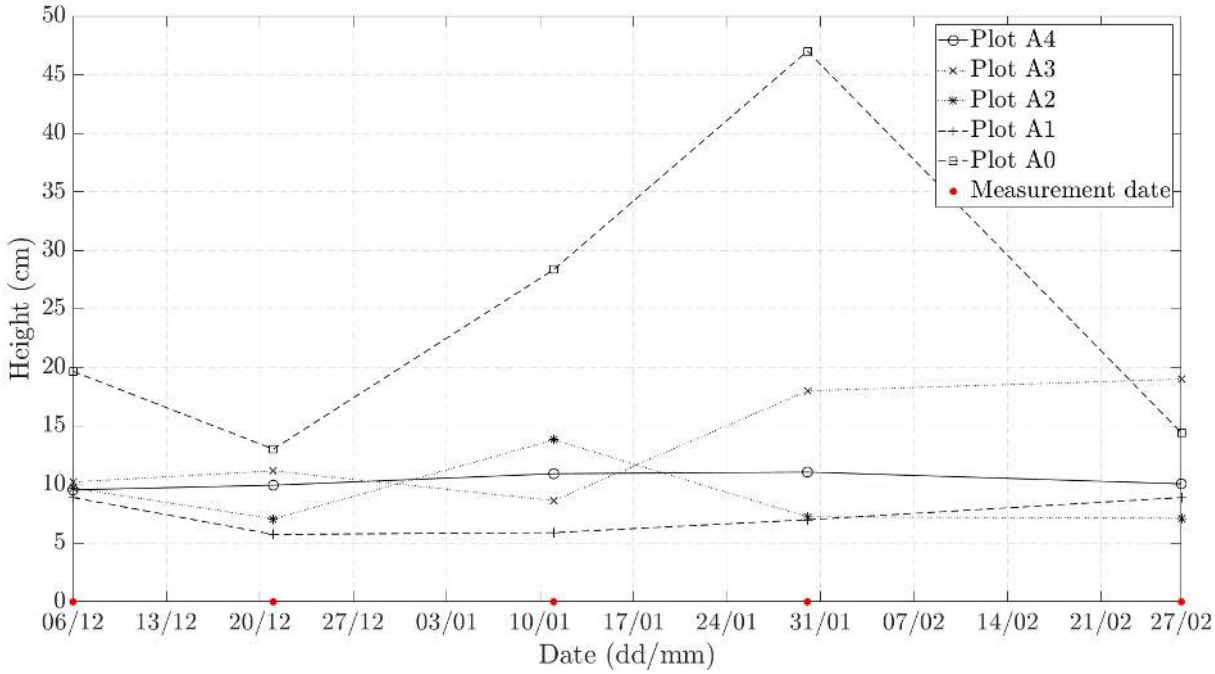

Figure F.2: Average seedling height per plot at transect A

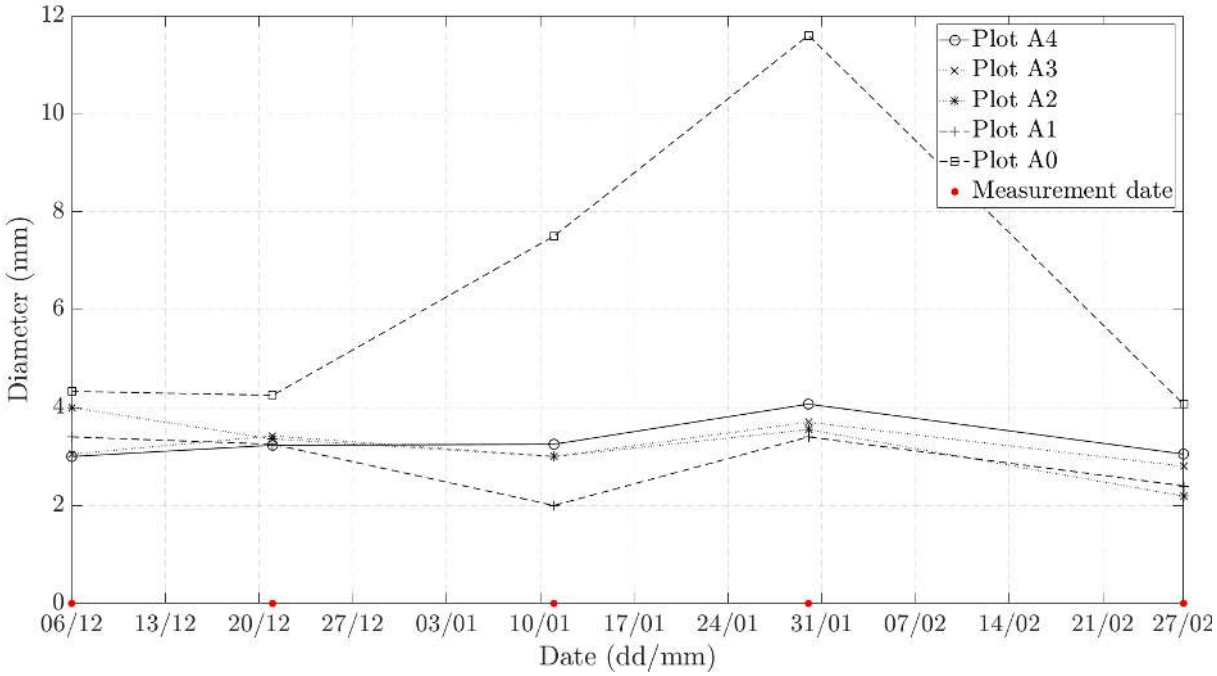

Figure F.3: Average seedling diameter per plot at transect A

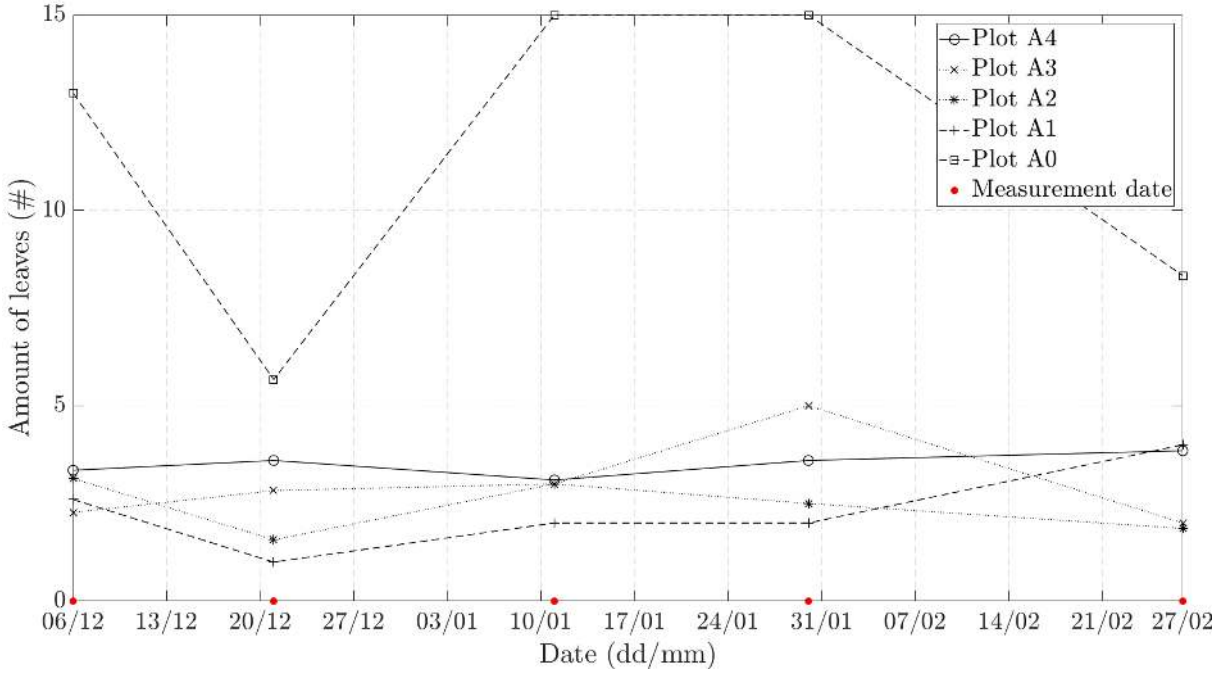

Figure F.4: Average number of leaves per seedling per plot at transect A

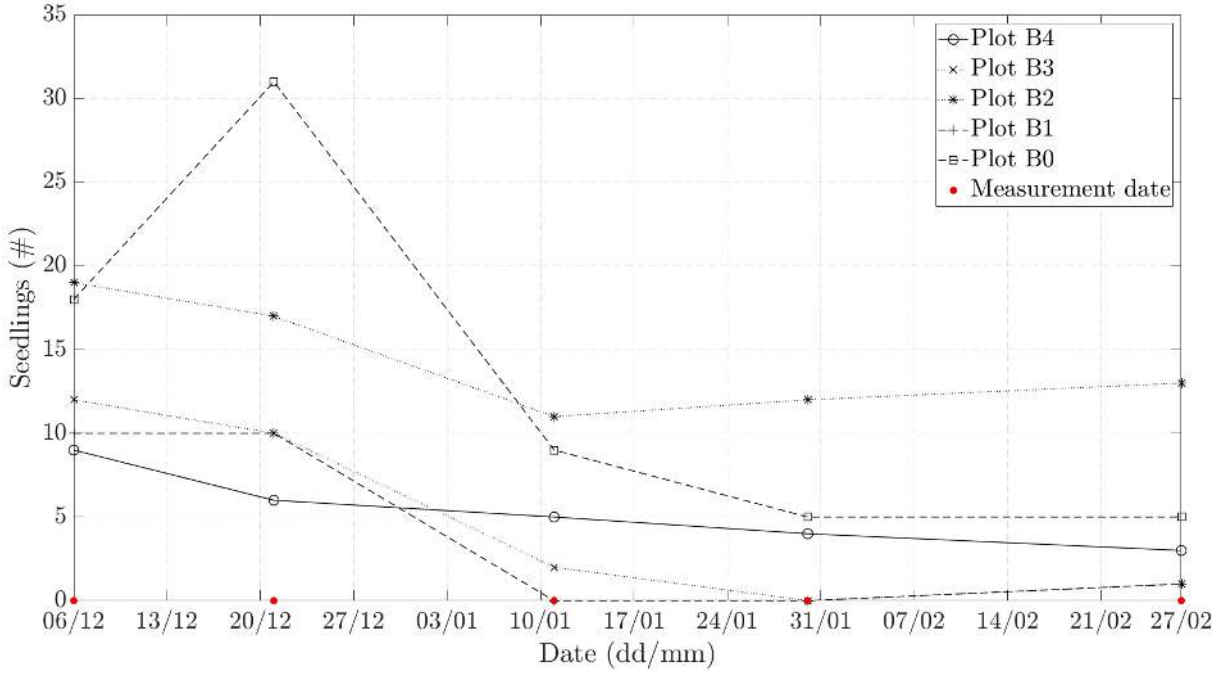

Figure F.5: Number of seedlings per plot at transect B

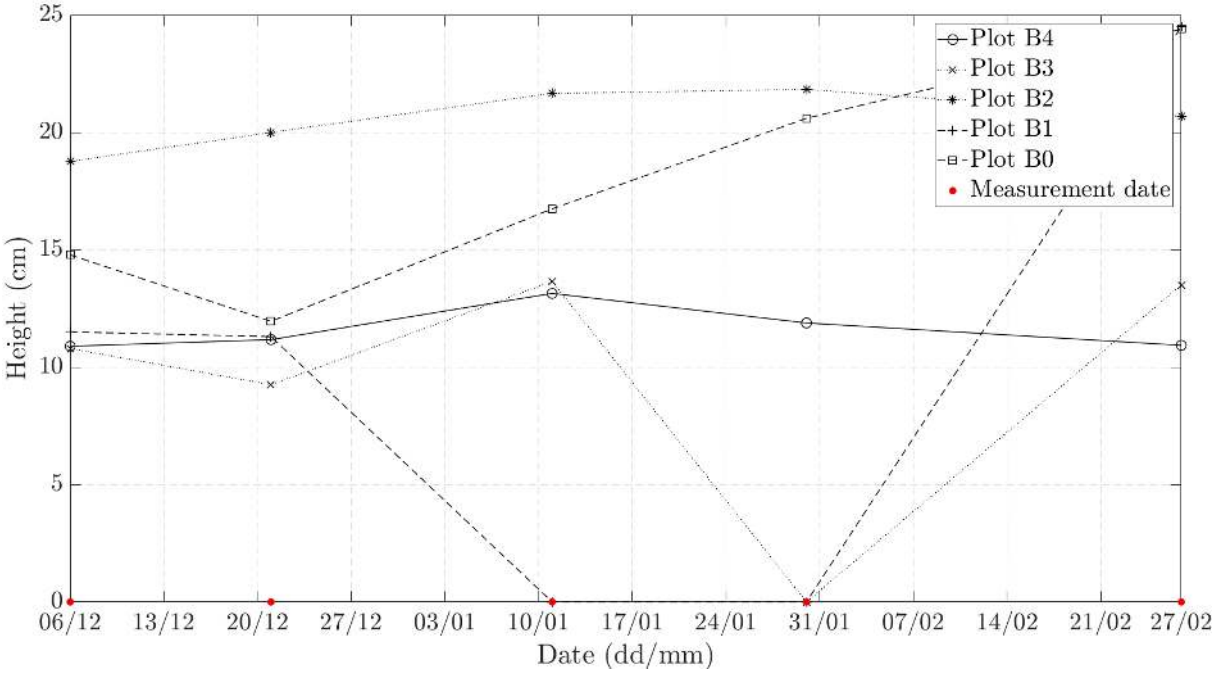

Figure F.6: Average seedling height per plot at transect B

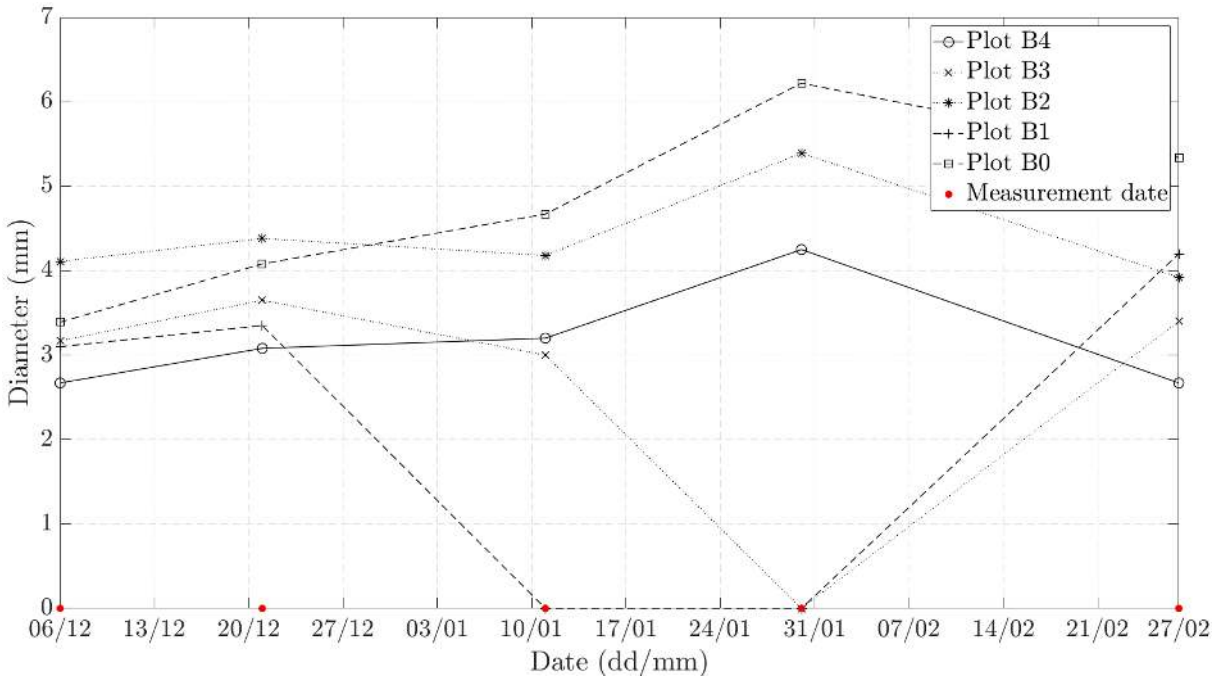

Figure F.7: Average seedling diameter per plot at transect B

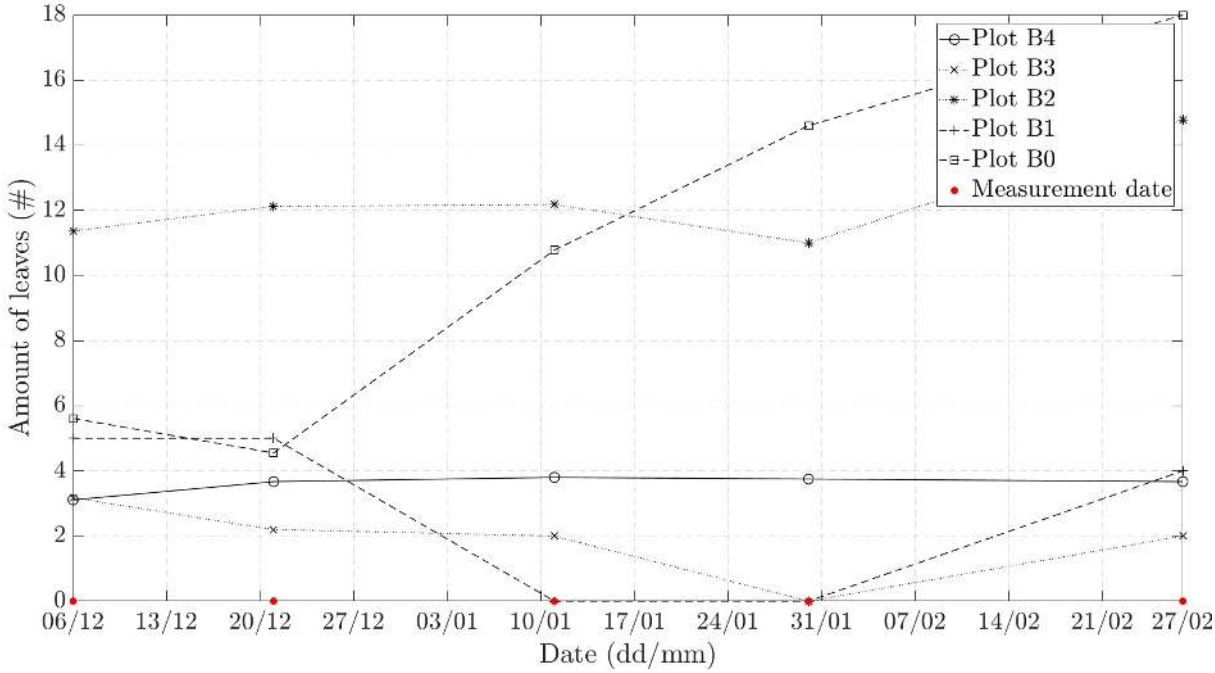

Figure F.8: Average number of leaves per seedling per plot at transect B

Appendix G

Spectral Analysis

In order to retrieve wave properties from the RBR-Solo instruments, a spectral analysis is needed to extract wave data from the measured pressure. The first step of the spectral is the detrending of the signal. This removes the trend in the series. Secondly, a Hann-taper w window is used. This to prevent leakage of the spectral density from large peaks, (Horstman et al., 2014). This window can be formulated as:

$$w(n) = 0.5\left(1 - \cos\frac{2\pi n}{N-1}\right) \qquad \text{for } n = 1, 2 \ldots, N \tag{G.1}$$

In Equation G.1, N is the length of the time series. Next, the Fourier coefficients $X(m)$ of the time series of the water depth $x(n)$ can be determined. This is calculated using the next formulas:

$$X(m) = \sum_{n=1}^{N} x(n) \exp(-2\pi i(m-1)(n-1)/N \qquad \text{for } m = 1, \ldots, N \tag{G.2}$$

$$f(m) = mf_s/N \qquad \text{for } m = 1, \ldots, N. \tag{G.3}$$

When the Fourier coefficients have been calculated, the pressure response factor K_p can be calculated. This factor depends on the water depth and keeps attenuation into account. The dynamic pressure magnitude decreases from the water level till the bottom level. This is why pressure response factor is needed to account for that. It is calculated with the next formula,(CERC, 1984):

$$K_p(m) = \frac{\cosh\left(k(m) \cdot z\right)}{\cosh\left(k(m) \cdot d\right)} \qquad \text{for } m = 1, \ldots, N. \tag{G.4}$$

In Equation G.4 the wave number, k is calculated as: $k = 2\pi/L$. The wave number is calculated for each frequency interval. The water depth d and the elevation of the sensor above the bed z is assumed to be constant, (Horstman et al., 2014).

When the previous step is executed, the periodogram P can be calculated. This is calculated using:

$$P(m) = \frac{\|X(m) \cdot K_p(m)^{-1}\|^2}{f_s N} \qquad \text{for } m = 1, \frac{N}{2} + 1$$

$$P(m) = \frac{2 \cdot \|X(m) \cdot K_p(m)^{-1}\|^2}{f_s N} \qquad \text{for } m = 2, \ldots, \frac{N}{2}$$

Then an additional correction factor C to take the effect of the Hann-taper into account is calculated.

$$C = \frac{N}{\sum_{n-1}^{N} w(n)^2} \tag{G.5}$$

$$S(f(m)) = C \cdot P(m) \qquad \text{with } m = 1, \ldots, \frac{N}{2}. \tag{G.6}$$

Now the energy density spectrum S is calculated. The energy density spectrum can than be used to calculated the wave properties.

$$E_{tot} = \sum_{m=1}^{N/2} S(f_m) \cdot \Delta f \cdot \rho g \tag{G.7}$$

$$H_s = 4\sqrt{m_0} \tag{G.8}$$

$$H_{rms} = 2\sqrt{2 \cdot m_0} \tag{G.9}$$

$$T_m = m_0/m_1 \tag{G.10}$$

Appendix H

Modelled seedlings

H.1 Standard run, wave height = 0.02 m

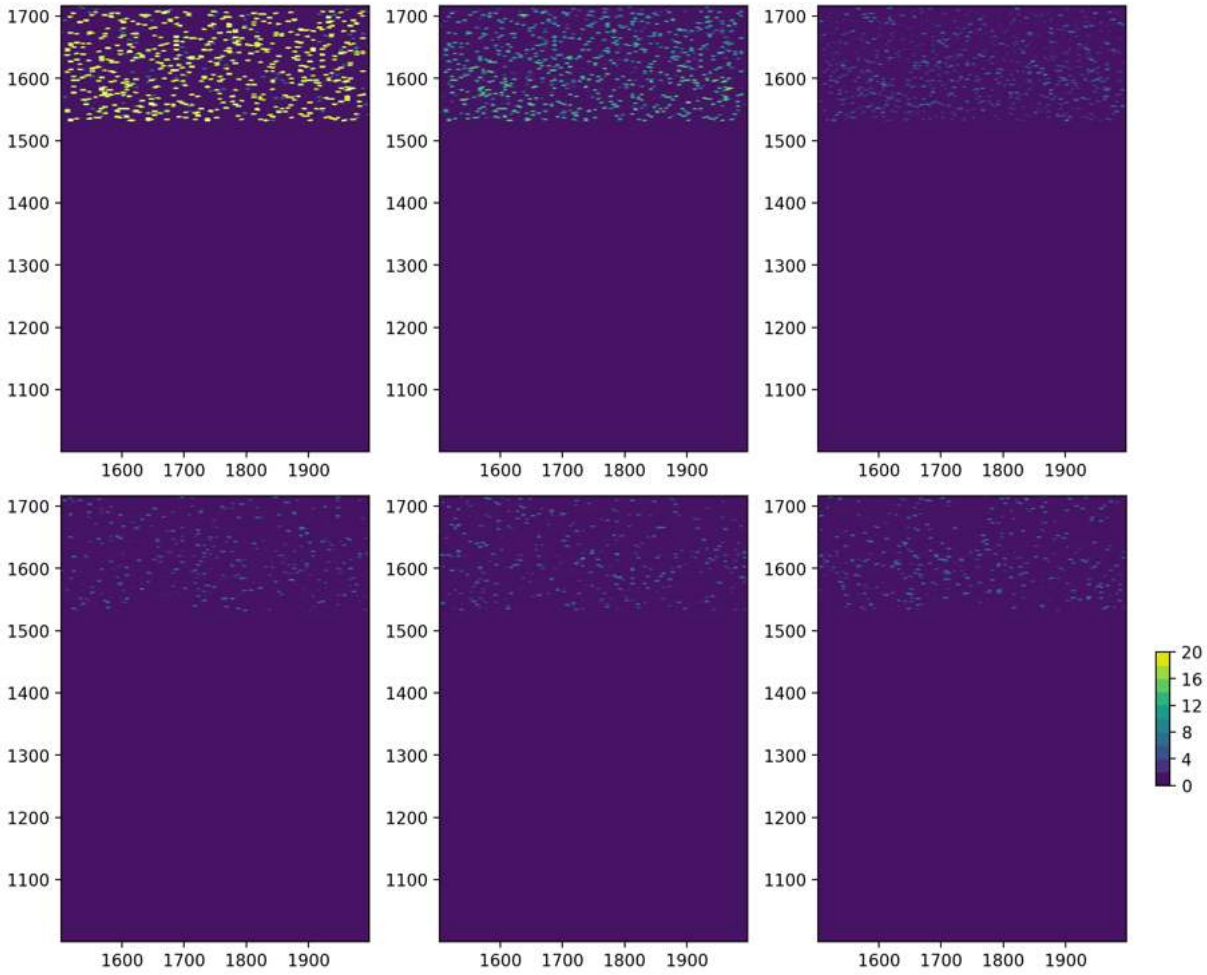

Figure H.1: Modelled number of seedlings per cell (#). Top-left, top-middle and top-right represent the number of seedlings per cell in week 1, 3 and 5. Bottom-left, bottom-middle and bottom-right represent the number of seedlings per cell in week 7,9 and 12.

H.2 Increased wave heights run, wave height = 0.10 m

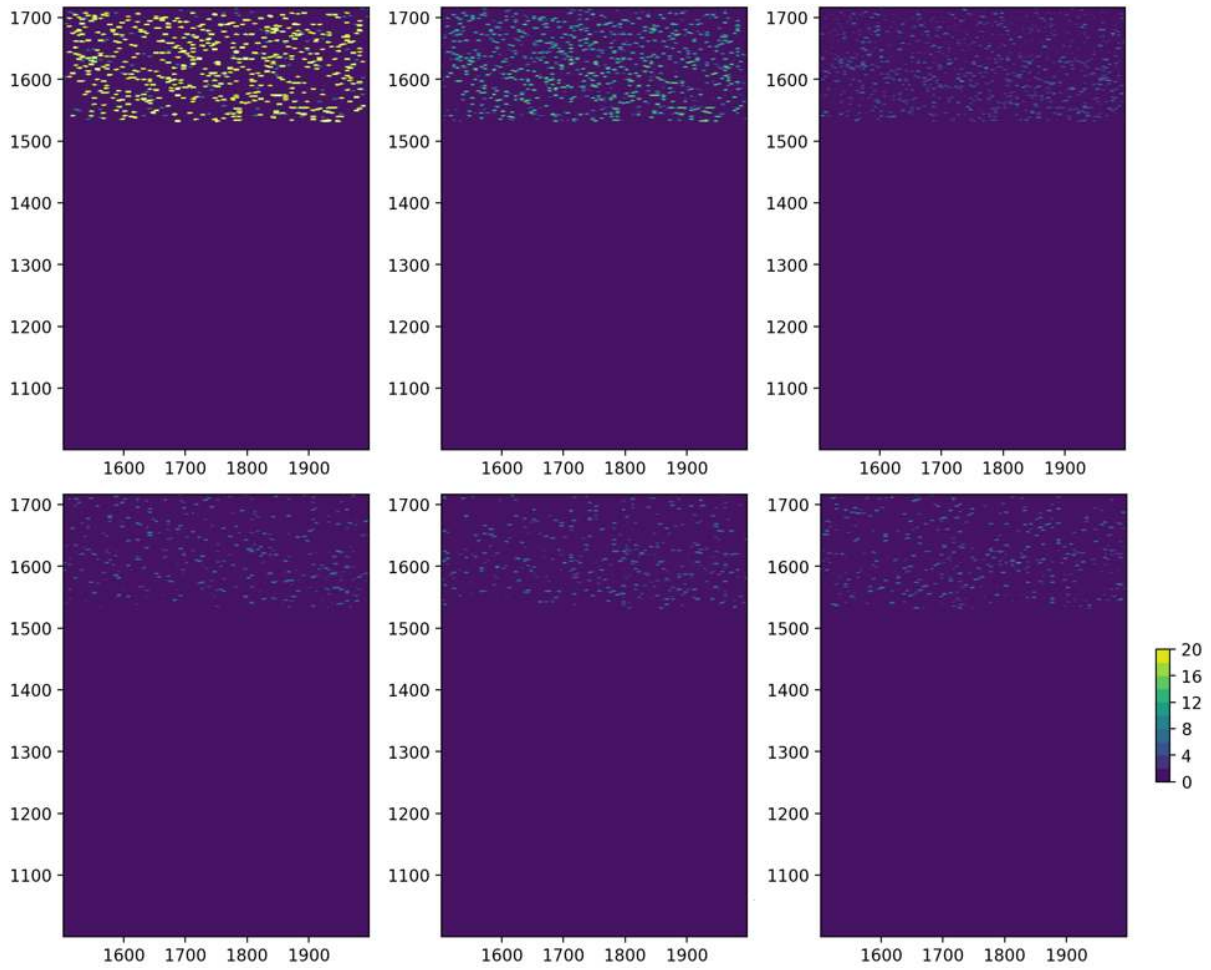

Figure H.2: Modelled number of seedlings per cell (#) for the increased wave height = 0.10 m run. Top-left, top-middle and top-right represent the number of seedlings per cell in week 1, 3 and 5. Bottom-left, bottom-middle and bottom-right represent the number of seedlings per cell in week 7,9 and 12.

H.3 Increased wave heights run, wave height = 0.20 m

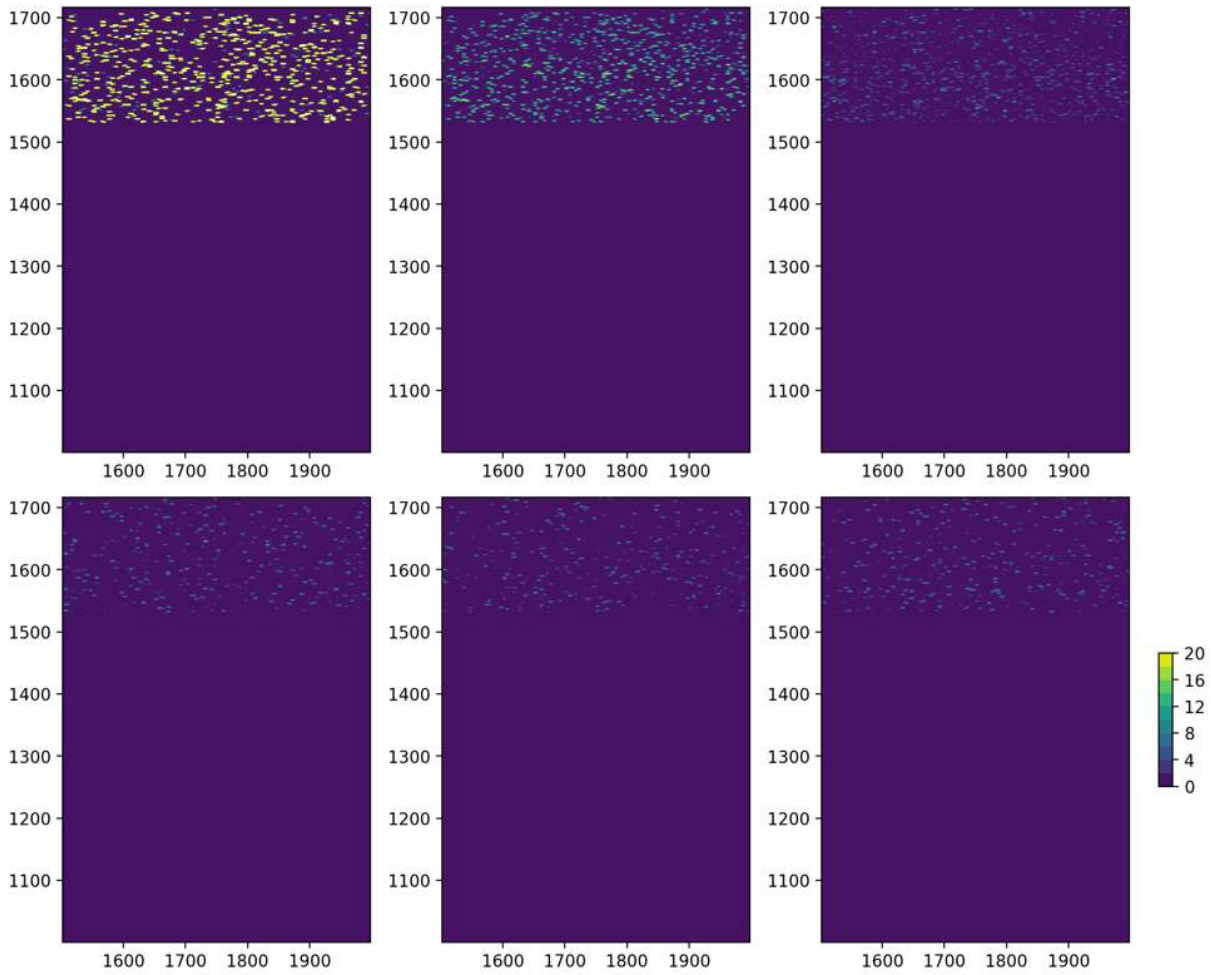

Figure H.3: Modelled number of seedlings per cell (#) for the increased wave height = 0.20 m run. Top-left, top-middle and top-right represent the number of seedlings per cell in week 1, 3 and 5. Bottom-left, bottom-middle and bottom-right represent the number of seedlings per cell in week 7,9 and 12.

Appendix I

Modelled bed level changes

I.1 Standard run, wave height = 0.02 m

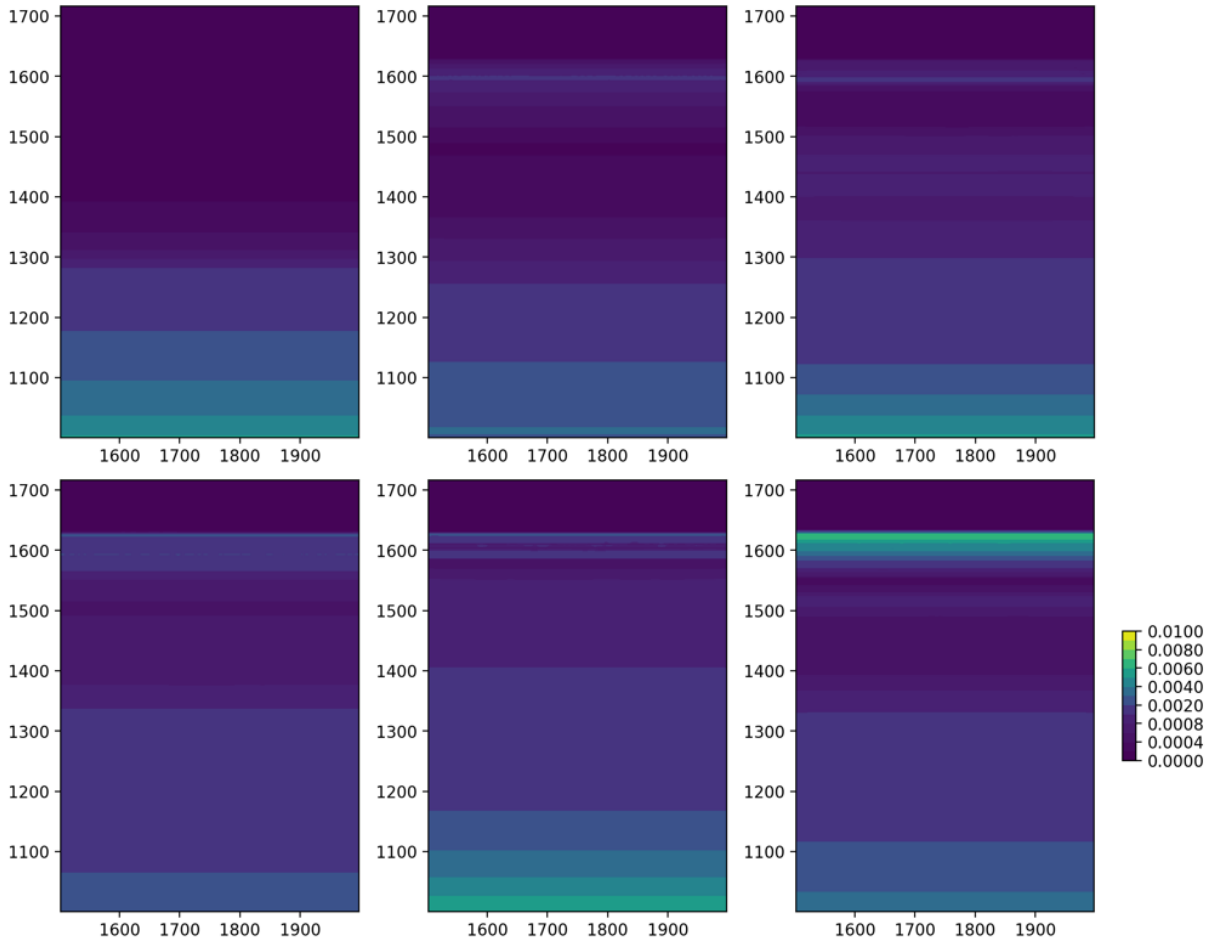

Figure I.1: Modelled weekly bed level changes per cell (m). Top-left, top-middle and top-right represent the weekly bed level changes cell in week 1, 3 and 5. Bottom-left, bottom-middle and bottom-right represent the weekly bed level changer per cell in week 7,9 and 12.

I.2 Increased wave heights run, wave height = 0.10 m

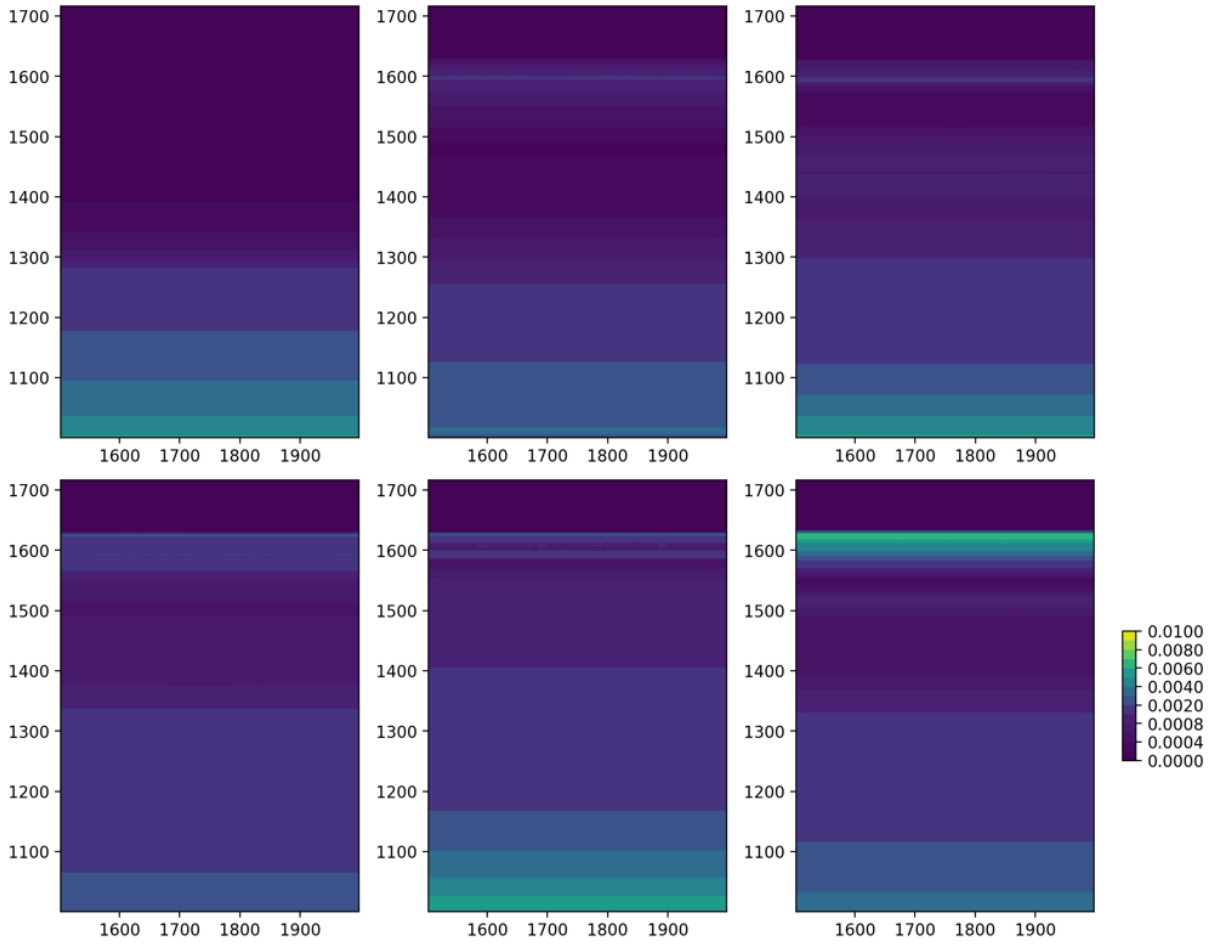

Figure I.2: Modelled weekly bed level changes per cell (m) for the increased wave height = 0.10 m run. Top-left, top-middle and top-right represent the weekly bed level changes cell in week 1, 3 and 5. Bottom-left, bottom-middle and bottom-right represent the weekly bed level changer per cell in week 7,9 and 12.

I.3 Increased wave heights run, wave height = 0.20 m

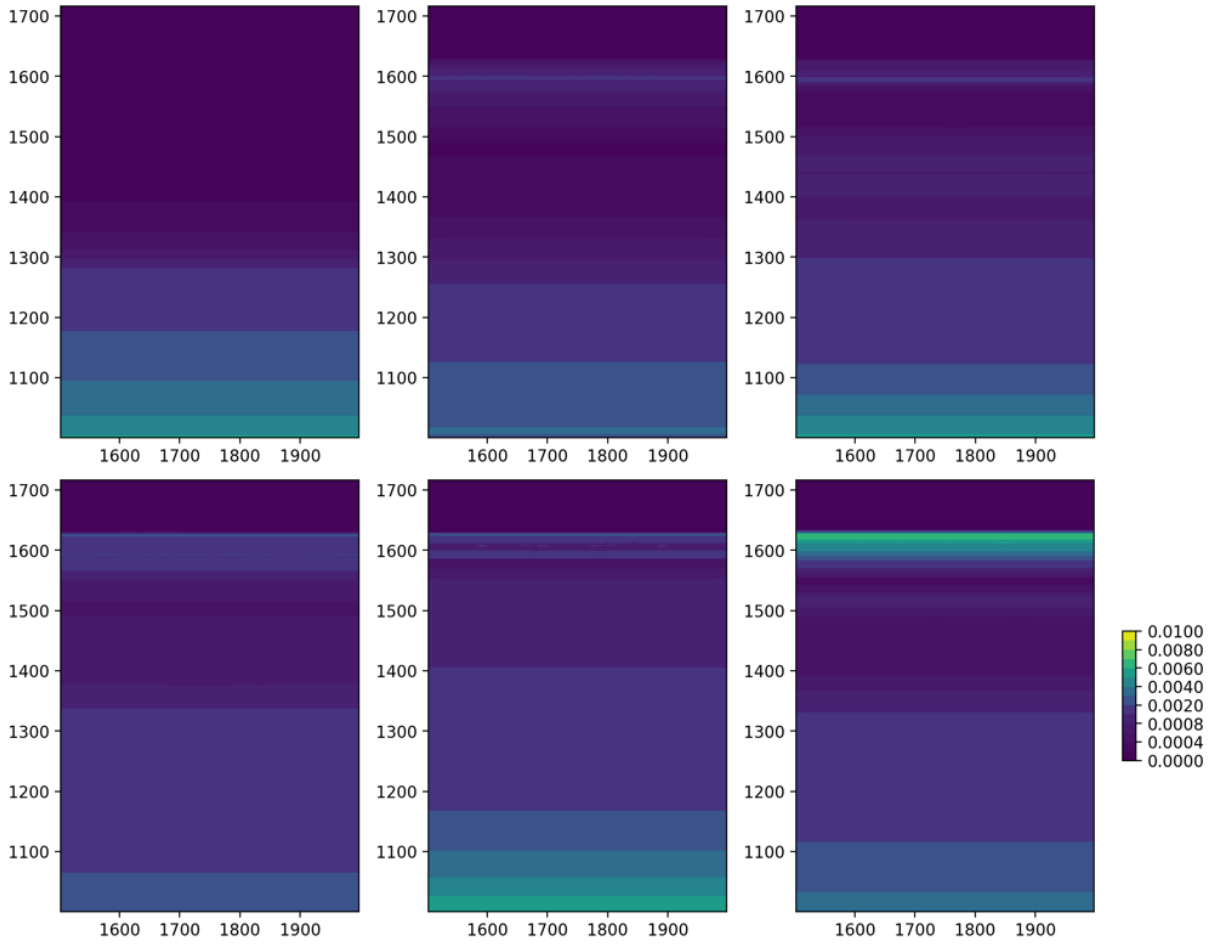

Figure I.3: Modelled weekly bed level changes per cell (m) for the increased wave height = 0.20 m run. Top-left, top-middle and top-right represent the weekly bed level changes cell in week 1, 3 and 5. Bottom-left, bottom-middle and bottom-right represent the weekly bed level changer per cell in week 7,9 and 12.